DESIGN AND SIMULATION OF SUGARCANE LOADER STRUCTURE

KANTAPIT MEETAM

A THESIS REPORT SUBMITTED IN PARTIAL FULFILLMENT
OF THE REQUIREMENTS FOR THE DEGREE OF
MASTER OF ENGINEERING IN AUTOMOTIVE ENGINEERING
INTERNATIONAL COLLEGE
KING MONGKUT'S INSTITUTE OF TECHNOLOGY LADKRABANG
ACADEMIC YEAR 2016
KMITL-2016-IC-M-004-04

THESIS TITLE	DESIGN AND SIMULATION OF SUGARCANE LOADER STRUCTURE
STUDENT NAME	Mr. Kantapit Meetam
STUDENT ID	55600904
DEGREE	Master of Engineering
PROGRAME	Automotive Engineering
ADVISOR	Asst. Prof. Dr. Preechar Karin
CO-ADVISOR	Dr. Chi-na Benyajati
CO-ADVISOR	Prof. Dr. Masaaki Okuma

ABSTRACT

The Entrepreneurs in small and medium size enterprises (SME) have an experience in sugarcane loader structure fabrication for a long time but it has not been developed with sufficient and appropriate engineering technologies. Thus, the purpose of this research is to design and analyze the strength of the sugarcane loader structure bases on engineering. The sugarcane loader structure was designed by Computer Aided Design (CAD) and Computer Aided Engineering (CAE), for the 45 horsepower KUBOTA ZL-1 Reverse tractor, which can install grab equipment to lift 300 kilogram of sugarcane mass up to 5 meters from ground, that total weight is approximately 3.5 tons. Using finite element method (FEM) to simulate stress contour to occurs on the part with the sufficient structural strength to operate on the farm. The knowledge is gained from design and development of sugarcane loader structure bases on engineering which can be transferred to the entrepreneur for sugarcane loader structure proceeding. The model of sugarcane loader structure was designed and analyzed under static condition with maximum hydraulic force. Moreover, the stress result of Finite Element Analysis is verified by using classical theory.

ACKNOWLEDGEMENT

This thesis has been accomplished with the very best support from many people. Firstly, I would like to express my deep gratefulness to Asst. Prof. Dr. Preechar Karin, my major advisor for his guidance and kind supporting throughout my research and also giving special opportunity to do the research with industrial company.

I would like to express my gratitude to my co-advisors, Dr. Chi-na Benyajati, head of Automotive Laboratory, National Metal and Materials Technology Center (MTEC), Thailand, and Prof. Dr. Masaaki Okuma, department of Mechanical and Aerospace Engineering, Tokyo Institute of Technology, Japan, for his kind advice and suggestions. I would like to express my thankfulness to Asst. Prof. Dr. Chinda Charoenphonphanich and Asst. Prof. Dr. Monsak Pimsarn, department of Mechanical Engineering, King Mongkut's Institute of Technology Ladkrabang (KMITL), Thailand, for the good guidance and suggestions. I am very grateful to Mr. Sutee Petchlohakul, Mr. Thanapol Luckanawat and his team, TSP METAL WORK CO., LTD. for their special supporting in research budget, equipment, facilities and technical data. I would like to thank to my seniors, my friends and my juniors; Miss Sutthichit Pimchan, Mr. Isara Promsorn, Mr. Teerapan Uttaragara, Mr. Panuwat Kangkaya, Mr. Komkla Siricholathum, Mr. Chockchai Jantang, Mr. Songchai Saenkam-Ouan and Mr. Tanawat Wongmaneethad for their technical supporting and friendship.

Finally, I would like to express my great appreciation to my parents and relatives for their true love, warm care and extreme encouragement.

Kantapit Meetam

TABLE OF CONTENTS

Chapter **Page**

TABLE OF CONTENTS

(Continued)

Chapter **Page**

TABLE OF CONTENTS

(Continued)

Chapter **Page**

LIST OF TABLES

Table **Page**

LIST OF FIGURES

Figure **Page**

LIST OF FIGURES

(Continued)

Figure **Page**

LIST OF FIGURES

(Continued)

Figure **Page**

LIST OF FIGURES

(Continued)

Figure **Page**

LIST OF FIGURES

(Continued)

Figure **Page**

LIST OF FIGURES

(Continued)

Figure **Page**

LIST OF FIGURES

(Continued)

Figure **Page**

LIST OF FIGURES

(Continued)

Figure **Page**

CHAPTER 1

INTRODUCTION

1.1 Research Background

Thailand is one of the top leads of ASEAN in exporting sugar and sugarcane, there were 2.73 million tons had been exported to the region. As the market requires around 2.9 million tons of importing products including the announcement of AEC, these could be great opportunities for Thailand to expand the market within the region. In order to be competitive in the market, Thailand must focus on quality development as well as increasing the efficiency in producing as to decrease the costing. And as to succeed in those targets, many entrepreneurs have imported machines from overseas such as sugarcane loader to decrease transferring time of harvested sugarcanes to the factory and also decreasing the costing of permanent labors. But the prices of imported machines are quite high as well as the allowance for maintenance which are responsibilities for the entrepreneurs, therefore, there are some entrepreneurs have tried to developed the sugarcane loader by themselves by modifying the existing tractors with extra parts and material that can be found within the country as to be able to attach sugarcane loader structure as shows in Figure1.1. Generally, the sugarcane loader structure is consisted of 5 main components: 1) the loader structure that supports all of the load; grabber mouthing parts, grabber arm, and sugarcane bundle, as well as being the attach points with the tractor, 2) the loader arm that supports the loads from grabber weight and sugarcane bundle, 3) grabber that opens and close to collects and release sugarcane bundle, 4) hydraulic cylinders that transfer the hydraulic pressure as to move the loader arm and grabber, 5) the counter weight that keeps the balance of the tractor due to the installation of the grabber attachment which causes the unbalancing character which possibly leads to roll over when parking or operating as shows in the figure below:

Thai entrepreneurs have experienced in sugarcane loader structure development for a long time but they have not been developed with sufficient and appropriate engineering technologies. Sugarcane loader structure is often failed when it is operated in farm. This means the equipment is not safe and also very dangerous for farmers. Therefore, the purpose of this research is to design and development sugarcane loader structure that bases on engineering knowledge which can withstand

the load on severe condition, to study on Static Finite Element Analysis (FEA) of sugarcane loader structure, and to provide design procedure for Thai entrepreneurs.

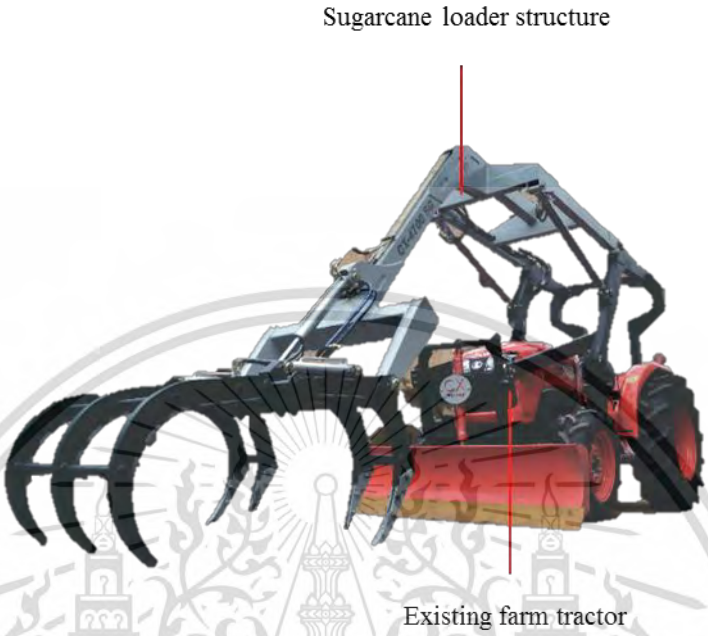

Figure 1.1 Sugarcane loader structure on existing farm tractor

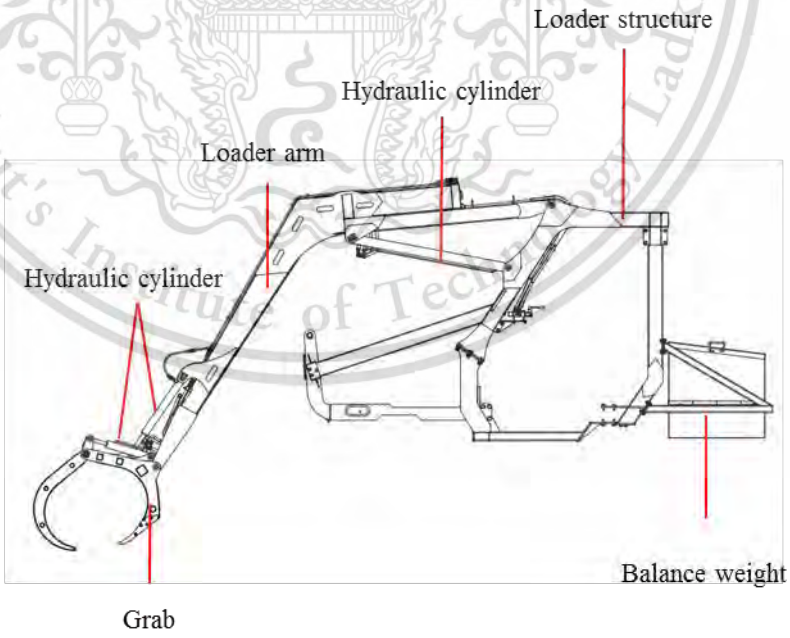

Figure 1.2 Components of sugarcane loader structure

1.2 Objective

1. To design and develop sugarcane loader structure that can withstand static load in severe condition.
2. To study on Static Analysis of sugarcane loader structure using FEA approach.
3. To provide a designed and development of sugarcane loader structure proceeding base on engineering knowledge for Thai entrepreneurs.

1.3 Scope of Work

1. To analyze strength of sugarcane loader structure in static loading condition by using Finite Element Method.
2. To verify stress analysis of FEA by classical theory.
3. Data, material and tooling of sugarcane loader structure are supported by TSP METAL WORK Co., Ltd.

1.4 Research Methodology

1. Collect data and indicate design concept of the sugarcane loader structure.
2. Create 3D geometry of the sugarcane loader structure by CAD software.
3. Analyze the static force acting on the sugarcane loader structure.
4. Analyze the strength of the sugarcane loader structure in static load condition by Finite Element Analysis approach with Von Mises Failure Theory.
5. Improve the strength of sugarcane loader structure in critical points.
6. Verify stress result of FEA by using classical theory.
7. Create 2D drawing and Bill of Material (BOM) of sugarcane loader structure for prototype fabrication.
8. Fabricate the prototype of sugarcane loader structure (Full scale).

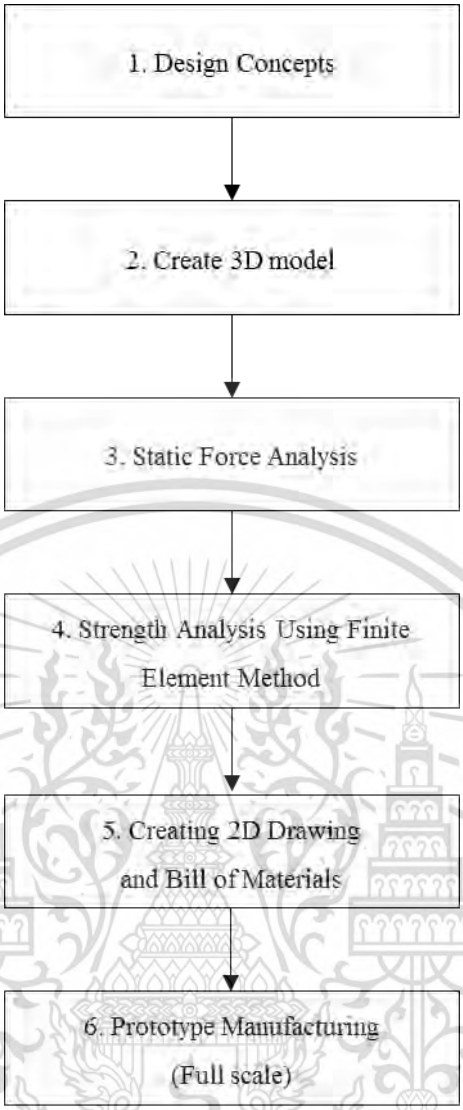

Figure 1.3 Research methodology flow chart

CHAPTER 2

THEORY AND LITERATURE REVIEWS

2.1 Finite Element Method

Finite element method (FEM) is considered as one of numerical methods that use to examine for the approximate solution for different fields of engineering or science. Most of finite element methods are consisted of differential equations describing the reality of problems under different boundary conditions which the domain geometries can be complex that stated by Sakkarin Choodoung (2006).

There are 5 main steps of finite element method.

1) Mesh the domain geometry into discretization.

For example, if the tensile load analysis of steel plate is required, meshing the steel plate in to small element is the first step. This first step is normally consuming a lot of practical time, because it is necessary to create the correct domain geometry model which can be in different shape and consist of complex curves.

2) Choose the type of element.

The element of the steel plate can be in the form of unknown tetrahedral or cubic. If the type of element is chosen as tetrahedral, the point at each corner of the element is called node. The type of element is related to the gradient of solution value on each element. The characteristic of the gradient solution value is assumed as the flat plane, etc. If the chosen element type is cubic, the gradient of solution value might not be flat but in curves. Therefore, the type of element is directly effect to the solution of gradient.

3) Create the finite element equations for each element from partial differential equations relating to the domain geometry.

The particle differential equations relating to the interested domain geometry will be simplified into algebra equations which is called finite element equations. These finite element equations are created for each element due to the differences of the dimensions of the elements. The methodology of creating the differential equations is the core of the studying of finite element.

For the general 3D object, finite element equations can be created for tetrahedral element as follow

Assume the deformation value in 3 directions. The deformation value in each direction can be written into numerical function inside each element, and the deformation value at each node as follow;

$$\begin{aligned} u(x,y,z) &= [N\ (x,y,z)]\{u\} \\ v(x,y,z) &= [N\ (x,y,z)]\{v\} \\ w(x,y,z) &= [N\ (x,y,z)]\{w\} \end{aligned} \tag{2.1}$$

Or can be written as;

$$[\bar{\delta}] = [N(x,y,z)][\delta] \tag{2.2}$$

By;

$$[\bar{\delta}]^T = [\,u\ \ v\ \ w]$$

$$[\bar{\delta}]^T = [\,u_1\ \ v_1\ \ w_1\ u_2\ \ v_2\ \ w_2 \ldots\ u_n\ \ v_n\ \ w_n]$$

Vector of Strain equation can be written in the form of deformation equation as;

$$\{\varepsilon\} = \begin{Bmatrix} \varepsilon_x \\ \varepsilon_y \\ \varepsilon_z \\ \gamma_{xy} \\ \gamma_{yz} \\ \gamma_{xz} \end{Bmatrix} = \begin{Bmatrix} \dfrac{\partial u}{\partial x} \\ \dfrac{\partial v}{\partial y} \\ \dfrac{\partial w}{\partial z} \\ \dfrac{\partial u}{\partial y} + \dfrac{\partial v}{\partial x} \\ \dfrac{\partial v}{\partial z} + \dfrac{\partial w}{\partial y} \\ \dfrac{\partial u}{\partial z} + \dfrac{\partial w}{\partial x} \end{Bmatrix} = [B(x,y,z)]\{\delta\} \tag{2.3}$$

When $[B(x,y,z)]$ represents the matrix of relation between stress and deformation as;

$$J = \frac{1}{2}\int_v\ [\delta][B]^T\,[C][B]\{\delta\}dv - \int_v\ [\delta][B]^T\,[C]\{\varepsilon_0\}dv + \frac{1}{2}\int_v\ [\varepsilon_0]\,[C]\{\varepsilon_0\}dv -$$

$$\int_v\ [\delta][N]^T\{F\}dv - \int_s\ [\delta][N]^T\{T\}ds$$

Or to write in a shorter term as;

$$J = \frac{1}{2}[\delta][K]\{\delta\}dv - [\delta]\{F_0\} + \frac{1}{2}\int_v [\varepsilon_0][C]\{\varepsilon_0\}dv - [\delta]\{F_B\} - [\delta]\{F_t\} \qquad (2.4)$$

By

$$[K] = \int_v [B]^T[C][B]dv$$

$$\{F_0\} = \int_v [B]^T[C]\{\varepsilon_0\}dv$$

$$\{F_B\} = \int_v [N]^T\{F\}dv$$

$$\{F_t\} = \int_v [N]^T\{T\}ds$$

Matrix [K] is the stiffness of element $\{F_0\}$, $\{F_B\}$, $\{F_t\}$ which are the loads of vectors due to original stress, body force, and external load, respectively. Finite Element equation can be created by calculating the minimal summation of potential force in equation (2.4) which is;

$$\frac{\partial J}{\partial\{\delta\}} = 0 \qquad (2.5)$$

4) Combine the finite element equations together of element

Combine the finite element equations together of element which create set of simultaneous equation that explain the overview states of each problem, and then apply the boundary conditions before solving the set of simultaneous equation to examine approximate solution at each node in all the domain geometry.

$$[K]\{\delta\} = \{F_0\} + \{F_B\} + \{F_t\} \qquad (2.6)$$

5) Calculate others value as require.

This step is to analyze to rest of other required values apart from the main desired values, such as temperature at each node, then the flux density, etc.

2.2 Failure Criterion Theory

In engineering design of static models, the model will receive many loads at the same time, such as tensile stress, compressive stress, and shear stress. Therefore, the testing model is brought to test in tensile, bending, and torsion including collecting the result data of the experiment for studying the idea of strain in the work piece. The relation between the stress-strain and elastic limit, then create the theories, which those value come from the testing by pulling the test piece in an axle or one dimension, and these theories are called Failure Criterion Theory.

According to the ductile material and Brittle material have different failure, Ductile material will fail when the stress value reaches the Yield point which is undesired, because when the stress reaches that point, the material will be permanently deform and will not reshape back to the original state. When talking about ductile material, the Yield stress must be mentioned which is the stress at the Yield point. Brittle material does not have the Yield point, the failure will occur when the material receive the stress value exceed the brittleness or brake point of the material, therefore, when talking about the failure of the brittle material, the Ultimate stress must be mentioned which is the stress value that causes the failure of the material.

Because of used material in this work is ductile material, therefore in this chapter will focus on failure criterion theory of ductile material. There are 2 favorable failure theories for ductile material, Maximum shear stress theory and Maximum distortion energy theory.

2.2.1 Maximum Shear Stress Theory

Maximum shear stress theory or Tresca theory indicates that yielding will occur when the maximum shear stress at one point of the material is equal maximum shear stress from the tensile testing for the stress in multi-axle. The maximum stress will be as the equation (2.7) below.

$$\tau_{max} = \frac{1}{2}(\sigma_{max} - \sigma_{min}) \tag{2.7}$$

When σ_{max} and σ_{min} are the main maximum value and minimum value respectively, if considering single axle shear stress $\sigma_1 = \sigma_y,\ \sigma_2 = \sigma_3 = 0$ will get

$$\tau_{max} = \frac{\sigma_y}{2} \tag{2.8}$$

This maximum shear stress theory is considering the yield point of the material on the slip plan when the maximum shear stress value reaches the specified maximum value as to mention in equation (2.7). Therefore, from the equation (2.8) above will get

$$\sigma_y = \sigma_{max} - \sigma_{min} \tag{2.9}$$

For the dual axle tress state of one material, when display in Figure 2.1 as to follow the maximum shear stress theory will specify the un damage area in the hexagonal area of Tresca. This theory will deliver the results that really accord to some type of the ductile material which this part can be considered when the basic of the yield point of steel is considered, because of the permanent deformation of the steel will occur on a plan called slip plan which this plan is a related phenomenon with the shear force.

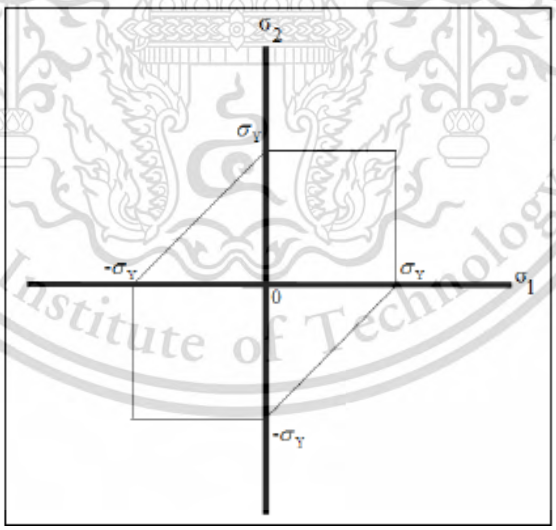

Figure 2.1 Stress limit of maximum shear stress theory

Source: Natchaya Murachai (2013). *Design and strength analysis of the seat anchorages for large passenger vehicles using Finite Element Method* (Master's thesis). Suranaree University of Technology, Thailand, p. 37.

Considering the possibility in the of main stress occur

Case 1: If $\sigma_1 > \sigma_2 > 0$, and $\sigma_3 = 0$ (which $\sigma_{max} = \sigma_1$ and $\sigma_{min} = \sigma_3 = 0$) the failure will occur at the material when $\sigma_y - 0 = \sigma_1 = \sigma_y$

Case 2: If $\sigma_1 > 0 > \sigma_2$, the failure will occur when $\sigma_1 - \sigma_2 = \sigma_y$

Case 3: If $\sigma_1 < \sigma_2 < 0$, the failure will occur when $\sigma_2 = \sigma_y$

2.2.2 Maximum Distortion Energy Theory

Maximum distortion energy theory of Von Mises theory is indicates the theory that the yielding will occur when the energy of the deformation per unit volume under the stress summation is over or equal the energy of deformation from the occurred yielding of the tensile testing. The simple energy value that causes the failure under the tensile force is;

$$U = \frac{1}{2}\sigma_x\varepsilon_x + \frac{1}{2}\sigma_y\varepsilon_y + \frac{1}{2}\sigma_z\varepsilon_z \tag{2.10}$$

From the relation between stress, strain and Poisson's ratio;

$$\begin{aligned} \varepsilon_x &= \frac{\sigma_x}{E} - v\frac{\sigma_y}{E} - v\frac{\sigma_z}{E} \\ \varepsilon_y &= -v\frac{\sigma_x}{E} + \frac{\sigma_y}{E} - v\frac{\sigma_z}{E} \\ \varepsilon_z &= -v\frac{\sigma_x}{E} - v\frac{\sigma_y}{E} + v\frac{\sigma_z}{E} \end{aligned} \tag{2.11}$$

When place the strain value from equation (2.11) into equation (2.12), it will get the strain energy equation per unit volume under 3 axles stress value in 3 dimensions as;

$$U = \frac{1}{2E}(\sigma_1^2 + \sigma_2^2 + \sigma_3^2 - 2v(\sigma_1\sigma_2 + \sigma_2\sigma_3 + \sigma_3\sigma_1)) \tag{2.12}$$

Strain energy that causes the specific volume changes (U_v) can be defined by placing σ_{av} for σ_1, σ_2, and σ_3 into equation (2.12)

$$U_v = \frac{3(1-2v)}{2E}\sigma_{av}^2 \tag{2.13}$$

Which

$$U_v = \frac{1-2v}{6E}(\sigma_1 + \sigma_2 + \sigma_3)^2 \tag{2.14}$$

Therefore, the distortion energy (U_D) can be defined by minus the equation (2.12) with equation (2.14)

$$U_D = U - U_v = \frac{1+v}{3E}\left[\frac{(\sigma_1-\sigma_2)^2 + (\sigma_2-\sigma_3)^2 + (\sigma_3-\sigma_1)^2}{2}\right] \tag{2.15}$$

For this testing, the first step is to consider the load under the single axle stress which is $\sigma_1 = \sigma_y, \sigma_2 = \sigma_3 = 0$ and it will get;

$$U_D = \frac{1+v}{3E}\sigma_y^2 \tag{2.16}$$

For only the shear stress$\sigma_1 = -\sigma_2 = \sigma, \sigma_3 = 0$, it will get;

$$U_D = \frac{1+v}{3E}(\sigma_1^2 - \sigma_1\sigma_2 + \sigma_2^2) \tag{2.17}$$

Therefore, the yielding value is equal;

$$\sigma_y^2 = (\sigma_1^2 - \sigma_1\sigma_2 + \sigma_2^2) \tag{2.18}$$

The area of oval in Figure 2.2 will follow equation (2.18) which the boundary curve will meet σ_1 at $\pm\sigma_y$ and meet σ_2 at $\pm\sigma_y$ as well. When rearrange the equation (2.18) again, the Von Mises stress value will be;

$$\sigma_y = \sqrt{\sigma_1^2 - \sigma_1\sigma_2 + \sigma_2^2} \tag{2.19}$$

Which considering the stress in a form of the shear stress, it shows $\tau_{max} = \sigma_1 = -\sigma_2$ when placing the value into equation (2.19), The Von Mises stress value can be defined from equation (2.20)

$$\sigma_y = \sqrt{3\tau_{max}^2} = \sqrt{3} = \tau_{max} \tag{2.20}$$

The failure will occur when;

$$\tau_{max} = 0.577\sigma_y \tag{2.21}$$

When comparing between the Tresca theory at the same stress value, Tresca theory will approximate the yielding by the maximum shear stress only $\tau_{max} = 0.5\sigma_y$, which make the Von Mises theory has more value than Tresca theory at 15%.

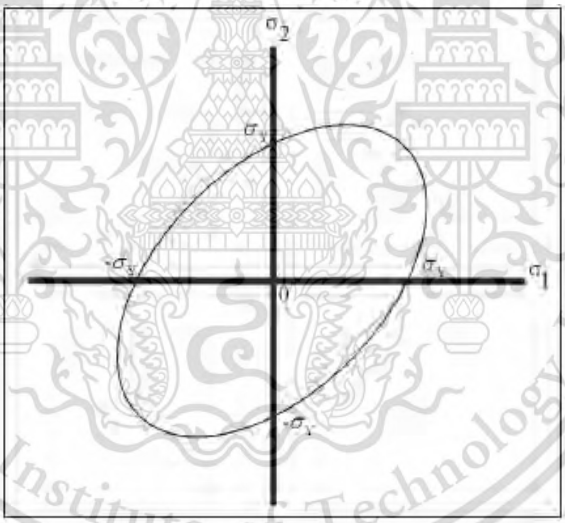

Figure 2.2 Stress limit of Von Mises theory

Source: Natchaya Murachai (2013). *Design and strength analysis of the seat anchorages for large passenger vehicles using Finite Element Method* (Master's thesis). Suranaree University of Technology, Thailand, p. 40.

The usage of Tresca theory is more comfort and easier to predict than the von Mises theory. However, due to the yielding function of Tresca is not connected function, but the Von Mises theory will give continuing yielding function. Therefore, the derivative at each point can be defined. Therefore, the von Mises stress theory is more favorable for permanent deformation studies.

2.3 Meshing Density and Mesh Sensitivity

Basically, finer order element delivers more structural simulation accuracy than the first-drought order element. Meaning, the higher of mesh density gives the higher accuracy of stress result, but at the same time, it means more computation time consuming. Therefore, it is necessary to choose between work-efficiency and unnecessary time consumable simulation accuracy.

In order to ensure convergence of the results and the quality of the mesh, the mesh sensitivity analysis is the selected method that uses to optimize the mesh density. Mesh sensitivity is mesh refinement method by iterative procedures to refine the size of element as in random percentage (from 1-100%). If the result of stress is slightly changed between the previous iteration and the last iteration, the value of difference is acceptable, and the simulation result is convergence. Moreover, there are interesting researches about mesh density as below,

Naren Chaithanee et al. (2014) studied 3D Structural Analysis of an Electric Tree-Wheeled Vehicle Integrating with a Battery Switching System. The Strength Analysis of Electric Tuk-Tuk chassis was carried out by using Finite Element Method (FEM) on ANSYS software under different condition of inclining angles of the ground plane (0-30°). This work suggested the mesh sensitivity method to ensure the quality of computational mesh. 2 points around the area of maximum stress were randomly picked to perform the mesh sensitivity and the acceptable error range of stress was ±5%.

Natchaya Murachai (2013) studied Design and Strength Analysis of the Seat Anchorages for Large Passenger Vehicles Using Finite Element Method. The strength analysis of the seat anchorages with following ECE regulation No.80 was carried out by using Finite Element Method. This work suggested the mesh sensitivity to ensure the accuracy of simulation result. The mesh refinement of each iteration was decreased by 1 mm (the element size of first iteration was set 17 mm and the element size of second iteration was decreased to16 mm), and then, compare the maximum Von Mises stress of the previous iteration with the last iteration. The result of mesh refinement showed the maximum difference of maximum Von Mises stress of element size 10 mm and 9 mm was 3.81%. The 10 mm of element size was selected because the maximum Von Mises stress of element size 10 mm was approached to the maximum Von Mises stress of element size 9 mm but used less CPU time and the comparison of the stress in variants of element size is shown in Figure 2.3.

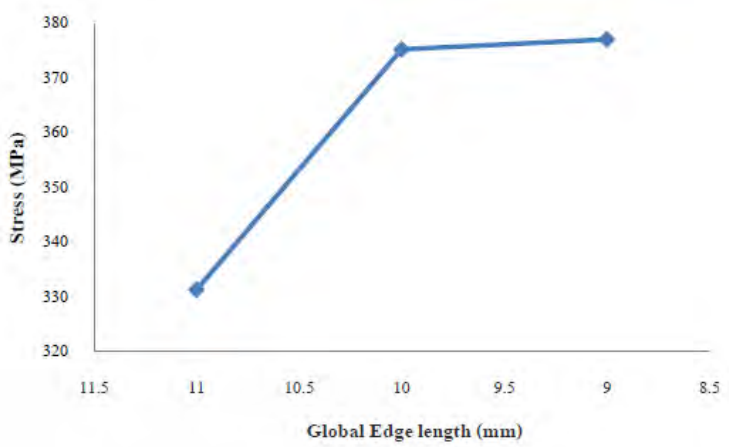

Figure 2.3 Von Mises stress in variants of element size

Source: Natchaya Murachai (2013). *Design and strength analysis of the seat anchorages for large passenger vehicles using Finite Element Method* (Master's thesis). Suranaree University of Technology, Thailand, p. 64.

Martinez (2013) suggested the method that could help to check the simulation result is divergence or convergence and optimize the mesh density by using manual mesh refinement. The first step, choose several sizes of elements, the second step is to perform as many simulations as number of sizes, the third step is to plot the graph between the variant number of the element and stress. If the difference between the previous iteration and the last iteration is less than 5%, which means the stress is convergence (simulation result is correct) and the number of element is acceptable. In case of divergent result, it can be assumed that it is occurred from stress singularity. A method that avoids the stress singularity is to add the tangent fillet at the edge or corner of geometry.

2.4 Stress Singularity

Andy (2010) and Patel (2017) stated that the Stress singularity is a function of divergence of stress into infinity. In terms of stress equation, stress is equal to the force per area as shown in equation (2.22).

$$\sigma = \frac{F}{A} \tag{2.22}$$

When the load applies in a very small area (area approach to zero), Stress tends to get to infinity. This phenomenon is called stress singularity. Stress

singularities are usually seen at points, edges, or reentrant corners. Normally, the stress singularity does not occur in real life, it occurs in software only because the corner of geometry in software is perfectly sharp, but there will be slightly bend in real life. In order to check stress singularity and determine the divergent simulation result, the mesh sensitivity is suggested to use. (For more detail is shown in previous chapter 2.3; mesh density and mesh sensitivity). Moreover, there are many way to avoid the stress singularity by Patel (2017), First way is always added fillet or chamfer in sharp edge and corner as shown in Figure 2.4. The fillet and chamfer provide a large surface area to distribute load. Second way is should not apply fixture at a point or edge but should apply to face, and stress divergence due to fixture on edge is shown in Figure 2.5, and third way is should not apply load at a point or edge but should apply to face (as same as second way) as shown in Figure 2.6. If a thin loading area is required, create split lines and apply force to the area between them, this will allow convergence.

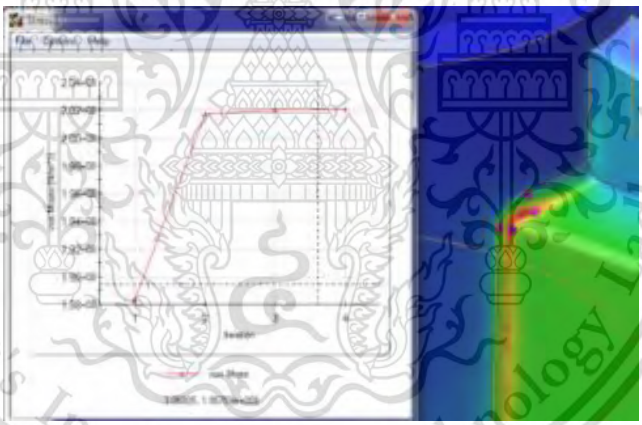

Figure 2.4 Stress convergence due to fillet

Source: Patel, S. (2017). SolidWorks 2017 simulation – avoiding singularities [Blog post]. Retrieved from http://www.goengineer.com/2016/12/02/solidworks-2017-simulation-avoiding-singularities/blog/

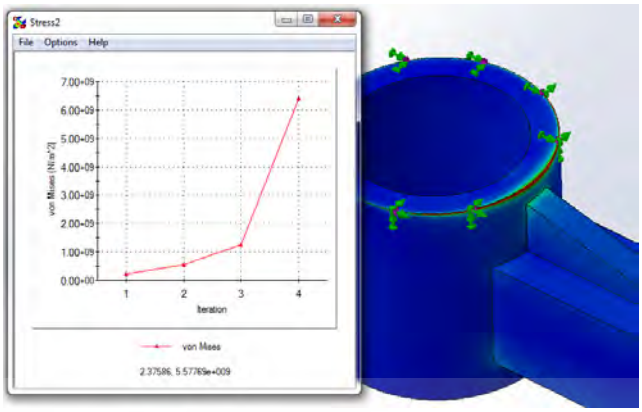

Figure 2.5 Stress divergence due to fixture on edge

Source: Patel, S. (2017). SolidWorks 2017 simulation – avoiding singularities [Blog post]. Retrieved from http://www.goengineer.com/2016/12/02/solidworks-2017-simulation-avoiding-singularities/blog/

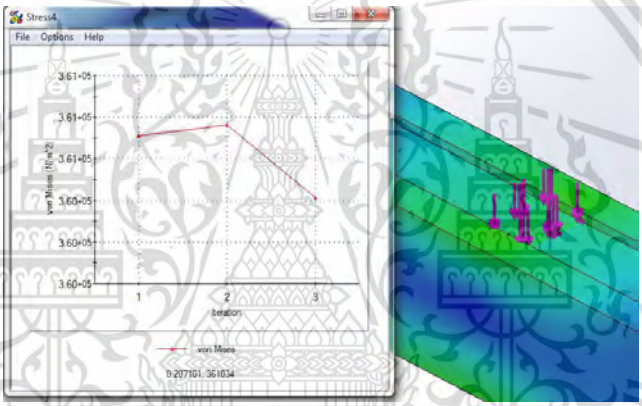

Figure 2.6 Stress convergence due to load applying on face

Source: Patel, S. (2017). SolidWorks 2017 simulation – avoiding singularities [Blog post]. Retrieved from http://www.goengineer.com/2016/12/02/solidworks-2017-simulation-avoiding-singularities/blog/

2.5 Safety Factor

Juvinall and Marshek (2006) suggested the selection of an appropriate value of safety factor should base primarily on the following five factors.

1) Degree of uncertainty about loading.
2) Degree of uncertainty about material strength.
3) Uncertainties in relating applied loading to material strength via stress analysis.
4) Consequences of failure - human safety and economics.
5) Cost of providing a large factor of safety.

Moreover, there are the recommended values for safety factor which are based on yield strength of material as shown in Table 2.1. These safety factors can be used as guide for designer at least.

Table 2.1 Recommend values for a safety factor

Design factor	Application
1.25 - 1.5	For exceptionally reliable materials used under controllable condition and subjected to load and stress that can be determined with certainly.
1.5 - 2.0	For well-known materials, under reasonably constant environmental, subjected to load and stress that can be determined readily.
2.0 - 2.5	For average materials operated in ordinary environments and subjected to load and stress that can be determined.
2.5 - 3.0	For less tried materials or for brittle materials under average conditions of environment, load, and stress.
3.0 - 4.0	For untried materials used under average conditions of environmental, load, and stress. Moreover, safety factor 3.0 - 4.0 should also be used with well-known materials that are to be used in uncertain environments or subjected to uncertain stresses.

Source: Juvinall, R. C., & Marshek, K. M. (2006). *Fundamentals of Machine Component Design* (4th ed).John Wiley & Sons.

2.6 Previous Work Related to Structural Analysis by FEA

Rahmen, Tamin, and Kurdi (2008) studied stress analysis of heavy duty truck chassis as a preliminary data for its fatigue life prediction by using FEM. In this work the material of chassis was ASTM Low Alloy A 710 C (class 3) with 552 MPa of yield strength and 620 MPa of tensile strength. The result showed the location of critical point which was at opening point of chassis which contacted with bolt, and the stress magnitude of critical point was 386.9 MPa. In this critical point should be considered for fatigue failure.

Somsak Siwadamrongpong, Supakit Rooppakhun, Natchaya Murachai, and Pakorn Burakorn (2013) studied strength analysis of the seat anchorages for large passenger vehicle using Finite Element Method. According to the seat anchorages for bus was analyzed by following European standard ECE regulation 80, therefore the boundary conditions on the Finite Element model of the seat anchorages of bus were defined according to this regulation. The seat anchorages structure and dimension was simplified from the real bus seat which supported by Cherdchai Industrial Co, Ltd. The Finite Element model of seat anchorages of bus consisted of 6 components; seat-back, base, leg, side anchorages, ground anchorage, test equipment, and floor with combination of shell and solid element. The structural materials were consisted of sheet metals and rectangular steel tubes, the yield strength of sheet metals and rectangular steel tubes were 390 MPa and 470 MPa respectively. For the boundary conditions on Finite Element model, the floor was specified as fully fixed constraint and force F1 and F2 were applied to the test equipment, and the magnitude of force F1 and F2 were 1,250 N and 3,640 N respectively. FEM result showed maximum Von Mises stress on the side anchorage was 1,005.3 MPa which occurred at below corner of the side anchorage, this clearly indicated that the side anchorage was not safe enough under European standard ECE regulation because the maximum stress was higher than the limit of ductile material failure. Therefore this geometry should have been improved to decrease the stress of critical point. In order to reduce the stress on critical point, DOE (Design of Experiment) approach was carried out geometry modification. The thickness and the distance of side anchorage effect to the stress on critical point. Therefore the model should be optimized by changing thickness and distance of the side anchorages.

Thorat and Rao (2013) studied static analysis of backhoe chassis 770 model. Static analysis was carried out in two different load cases. First load case was maximum reach condition and second was maximum torque condition. The design mechanism was produced 4,020.78 kg and 4,254.27 kg of breakout force in maximum reach condition and maximum torque condition respectively. Moreover, there were two different sub cases. For load case 1A, Stabilizer legs were fixed. Maximum stress of load case 1A was 784.39 MPa which generated at stabilizer legs and maximum deformation was 28.19 mm that generated at front side of chassis. For load case 2A, Loader pivot points were fixed. Maximum stress of load case 2A was 192.52 MPa

that generated at stabilizer legs and maximum deformation was 8.53 mm that generated at front end of the chassis.

Erklig and Yeter (2013) studied the improvement of the backhoe-loader arms. The backhoe loader back and front arm had been analyzed with the maximum breakout force condition by using Finite Element Method. The symmetrical and unsymmetrical of loadings were defined as boundary conditions. For the front arm, first improvement was carried out by increasing thickness of left and right side outer of side parts of the arm from 8 to 10 mm and second improvement was carried out by changing shape of the support. After improvement of the front arm, safety factor had increased to 2.18 from 1.94 and strength had been increased by 12.37 % at symmetrical loading while loader hydraulic cylinder was active. Safety factor had been increased to 1.32 from 1.10 and strength had been increased by 20 % at unsymmetrical loading while bucket hydraulic cylinder was active. Moreover, for the back arm, first improvement was carried out by adding circular plate back of outer plates and second improvement was carried out by changing original reinforcement plate at the face of outer plates. After improvement of the back arm, safety factor had been increased to 1.98 from 1.59 and strength has been increased by 24.5%.

Patel and Prajapati (2012) studied evaluation of bucket capacity, digging force calculation and static force analysis of mini hydraulic backhoe excavator. This work focused in the prediction of digging force and could be applied as boundary condition and loading condition. The capacity of the bucket had been calculated following the SAE standard J296 and the magnitude of capacity was 0.028 m^3. The breakout force had been calculated following the SAE standard J1179 and the magnitude of breakout force was 7,626 N. According to the maximum breakout force condition occurred when the bucket dig the soil, therefore, the static force analysis of the backhoe excavator performed by considering the maximum breakout force condition and could be used as a boundary condition for static Finite Element Analysis of backhoe excavator parts.

Patel and Prajapati (2012) studied static analysis of mini hydraulic backhoe excavator attachment using FEA approach. The backhoe excavator attachment consists of 4 linkage components, bucket, arm, boom and swing link which was connected with pined. According to the suggestion in evaluation of bucket capacity, digging force calculation and static force analysis of mini hydraulic backhoe excavator, therefore, in this work, the stress analysis was carried out base on the

maximum break out force condition. In this work, Von Mises theory was used as failure criterion of material because the materials of backhoe excavator attachment components were ductile material (HARDOX 400 steel with 1,000 MPa of yield strength. According to Von Mises failure theory, the Von Mises stress should be less than the yield strength of material by taking safety factor which the required safety factor was 2. Moreover, the design parts will be safe, if the displacement was less than the minimum cross-section of part. The fixed support was defined as constraint of the bucket, the arm, the boom and the swing link in pre-processing of Finite Element Analysis. As the result shows the stress produced on backhoe excavator attachment components were less than the yield strength of HARDOX 400 steel, it was clearly indicated that all component of attachment were not failure and the final safety factor of bucket, arm, boom and swing link were 4.9, 4.1, 4.0 and 8.4 respectively. Moreover it clearly means that the backhoe excavator attachment is over specification, therefore the attachment can perform the structural optimization for weight reduction and the optimization could help to reduce material cost also.

Patel and Prajapati (2013) studied structural optimization of mini hydraulic backhoe excavator attachment using FEA approach. This paper focused on structural weight optimization of backhoe excavator attachment using FEA approached by Trial-Error method (changing thickness) and Shape optimization. The objective of structural optimization was to obtain the lightest structural that could carry load in maximum breakout force condition. The constraint of structural optimization is minimum limit of safety factor of 2. The result of structural weight optimization showed the reducing of total weight by Trial-Error was 70.65 kg (24.96 % of weight reduction) and the reducing of total weight by Shape optimization was 78.98 kg (27.91% of weight reduction). The comparison showed the differences of weight reduction between Trial-Error method and Shape Optimization was only 3.93%, it clearly indicated that the result of structural optimization is performed by Trial-Error method were accurate and acceptable. The final safety factor of the bucket, the arm, the boom and the swing link were 4.4, 4.3, 3.5 and 6.3 respectively. Moreover, Classical theory of stress analysis by internal force was suggested to verify Finite Element stress analysis result. The Von Mises stress on arm by classical theory and FEA were 41.9 MPa and 41.04 MPa respectively (2.04 % of variation). The Von Mises stress on boom by classical theory and FEA were 54.11 MPa and 51.28 MPa respectively (5.23 % of variation). The variation of Von mises stress between classical

theory and FEA were much less, therefore the stress Analysis result by FEA approach could verify by classical theory.

Patel (2012) studied static structural analysis of backhoe loader chassis. Static analysis of backhoe loader chassis in maximum breakout force condition was carried out to obtain the developed stress and deformation. In this work, the material of the backhoe loader chassis was Steel alloy with 200 GPa of modulus of Elasticity and 7,850 kg/m^3 of density. The strength analysis was divided two different load cases. First load case was maximum reach condition and second load case was maximum torque condition. Moreover, there were two sub cases. For Load case 1A, stabilizer legs were fixed. The result of load case 1A showed the maximum stress occurred at stabilizer legs with 784.39 MPa of stress magnitude and maximum deformation occurred at front side of the chassis with 28.194 mm of displacement magnitude. For load case 1B, loader tower points were fixed. The maximum stress of load case 1B occurred at loader tower with 305.67 MPa of stress magnitude and maximum deformation occurred at front side of the chassis with 9.05 mm of displacement magnitude. However, the maximum stress was higher than permissible value due to sharp edges and corners, therefore the stress on critical points could be reduces by smooth sharp edges or fillet.

Naren Chaithanee et al. (2014) studied 3D structural analysis of an electric three-wheeled vehicle integrating with a battery switch system. According to conventional Tuk Tuk was modified to power by an electric generator motor and batteries instead of internal combustion engine (ICE), therefore Finite Element Method (FEM) was used to ensure the frame of Tuk Tuk that had sufficient strength for static load of electric generator and battery components. The frame was analyzed under different conditions of incline angle of ground plane (0-30°). Carbon steel tube with 370 MPa of yield strength was selected for the frame of the electric Tuk Tuk. In pre-processing of FEA, element type is the combination of Tetrahedral and Hexahedral with 352,044 of elements and 700,917 of nodes. The result of FEA showed the maximum stress and maximum deformation of the electric Tuk Tuk chassis that were occurred at front wheel arch around the fixed support when an inclined angle was 30° from around. The magnitude of maximum stress was 190 MPa, the magnitude of maximum deformation was 3 mm and safety factor was 1.93.Although, the static analysis clearly indicates that the Electric Tuk Tuk chassis had sufficient strength but the dynamic analysis should be consider in the future work.

Abril and Gabriel (2013) studied design, analysis and optimization of an orange peel grapple. Stress analysis of orange peel grapple was performed by using Finite Element Analysis (FEA) and optimization was carried out to reduce weight by trial-error method (changing thickness and shape). The orange peel grapple consisted of 3 main components: main body, hydraulic cylinders and peels. Main body function was supporting the external load and the weight of grapple directly. The hydraulic cylinders generated pressure to move the peels. The peel function was to receive the weight of scrap metal and did not let the scrap metal to fall down and the pined was used to join the orange peel grapple together. The static force analysis was carried out to find the severe working conditions which generate the maximum hydraulic cylinder force and this severe condition was defined as the boundary condition in FEA. The result of static force analysis showed the maximum hydraulic force was occurred when the grapple was fully open, while the grapple grabbed the scrap metal. In pre-processing of FEA, Fixed support was applied in joint of each grapple component for constraint. In material of the grapple was S620Q high tensile steel with 620 MPa of yield strength and 724 MPa of tensile strength. The result of FEA showed the maximum Von Mises stress of the peel, the sleeve of hydraulic cylinder, the piston rod of hydraulic cylinder and the main body were under the yield limit of material with 1.96, 5.91, 3.56 and 3.83 of safety factor respectively.

CHAPTER 3

RESEARCH METHODOLOGY

In chapter 3, it was explaining about the methodology of design, simulation and improving the sugarcane loader structure. The first step is to collect the design data of the sugarcane loader structure which including problems, producing recommendation, and the usage of sugarcane loader structure from entrepreneurs and sugarcane loader farmers' experiences which indicate the design concept. With these advices leads to the specification of the design concepts. After that is to create the 3D model on Computer Aided Design software (CAD) to get the overview of the 3D geometry. Then, analyze the static force acting to the sugarcane loader structure to specify load and boundary condition, and analyze the strength of the sugarcane loader structure by Finite Element Method (FEM) on ANASYS software with load and boundary condition from Static Force Analysis. If this process has found the unmatchable of the design model's safety factor conditions, it need re-design the 3D model to improve the strength of the design model to match the design criterion. Then, finalize the 3D model to create the 2D drawings and Bill of Materials as to prepare the fabrication of the sugarcane loader structure prototype (Full scale).

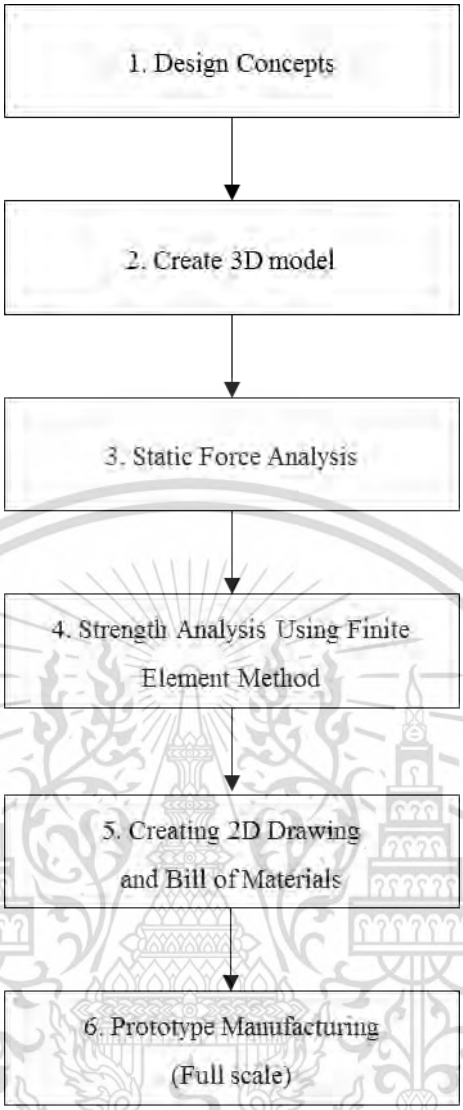

Figure 3.1 Research methodology flow chart

3.1 Concept Designs

Sugarcane loader structure is popular equipment to assemble to existing farm tractor for sugarcane harvesting. The sugarcane loader structure is operated by the driver to grab the harvested sugarcane and place into the loading truck before transfer the sugarcane to the factory. General characteristic are consisted of grabber, loader, loader structure, hydraulic cylinder and counter weight. The grabber and loader arm were moved by pressure from hydraulics cylinder.

Before starting to design the prototype of the sugarcane loader structure, the concept designs was gathered from problems, recommendation about the producing and operating of the sugarcane loader structure. With the employer and the actual

owners of sugarcane farms' experiences, it could define the main design concepts as follow;

1) The sugarcane loader structure could be able to detach and install to the tractor chassis.

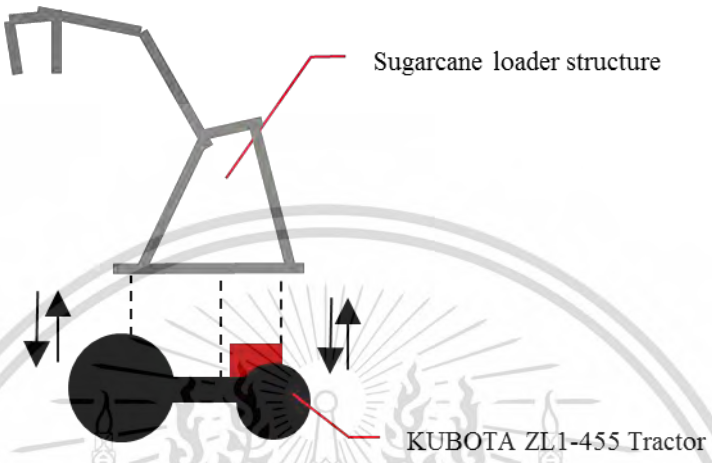

Figure 3.2 Sugarcane loader structure on tractor chassis

2) Use KUBOTA SUNSHINE ZL-1-455 reverse tractor as the base of the sugarcane loader structure which the advantage of this model is the steering wheel and the seat can be swap with each other which the basic details are shown in Table 3.1 and Figure 3.3.

Table 3.1 Vehicle specifications of KUBOTA ZL-1-455 reverse tractor

Component	Specification
Engine	2.4 L Diesel, 5 cylinder , 45.3 HP, liquid cooled
Transmission	Both 4WD- 2WD
Suspension	Rigid suspension
Total weight	1,700 kg
Wheel base	1,980 mm
Wheel track	1,445 mm

Figure 3.3 KUBOTA SUNSHINE ZL-1-455 reverse tractor

3) The requirement of maximum load of sugarcane bundle is 300 kg as shown in Figure 3.4.

4) The requirement of maximum height to lift the sugarcane bundle from the ground is 5 meters as shown in Figure 3.4.

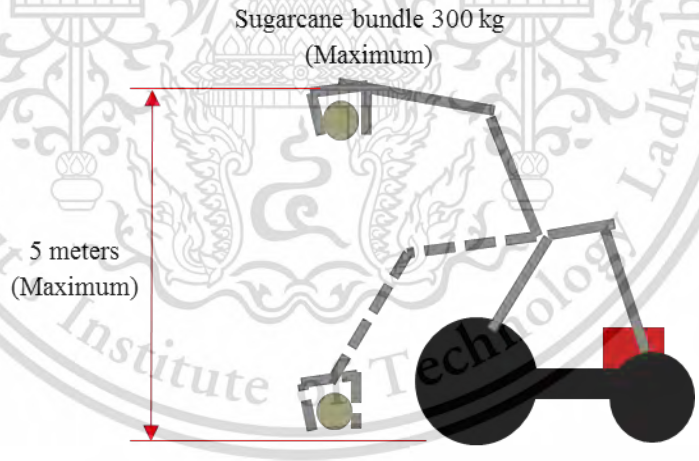

Figure 3.4 Requirement of maximum load of sugarcane bundle and maximum lift height of grabber

5) Use the existing grabber that is designed by TSP METAL WORKS Co., Ltd as shown in Figure 3.5.

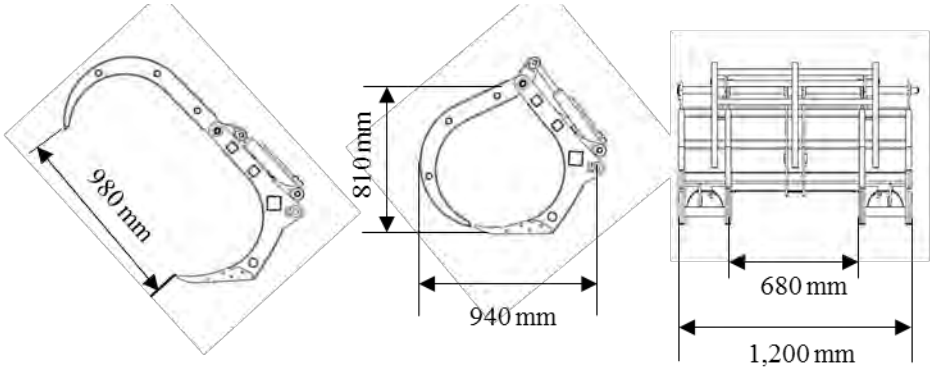

Figure 3.5 Dimension of existing grabber by TSP METAL WORKS Co., Ltd

3.2 Creating 3D Models by Computer Aided Design

3.2.1 Installation Points of Sugarcane Loader Structure

Due to the sugarcane loader structure design concept: the structure must be able to detach and reinstall, before creating the 3D model, the installing position with the tractor must be define first. When the tractor model that mentioned earlier has been investigated, there are possible 7 positions that could be able install the sugarcane loader structure by bolts and nuts: driveshaft area (1 on the left side and 1 on the right side), Gear box area (1 on the left side and 1 on the right side), and the engine area (1 on the left side, 1 on the right side and 1 in the middle) as shown in Figure 3.6.

(a) (b)

Figure 3.6 Installation areas of sugarcane loader structure,
(a) driveshaft, (b) gear box, (c) engine

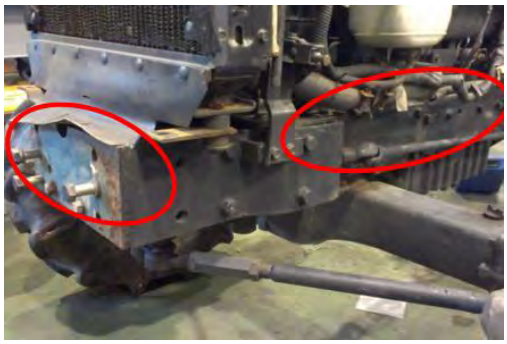

(c)

Figure 3.6 Installation areas of sugarcane loader structure,
(a) driveshaft, (b) gear box, (c) engine (cont.)

Due to the difficulty of using the basic measurement tools to define the positions of installation of the sugarcane loader structure, because there are many bolt holes, and these positions are not exact symmetry, the design team has decided to use CIMCORE ARM - 6 Axis Portable Measuring Arm to measure for more precision in defining the positions and this measurement is shown in Figure 3.7. The principles of using this tool is that the user must install the support program into a computer first, and connect with a computer while using it to measure. To operate the tool, use the end of the measure arm to touch the desire area, the tool will convert the coordinates and positions to the computer, together with saving the electronic file that can also directly link to CAD program (Computer Aided Design) which is easier, faster to draw the 3D geometry on the computer.

Figure 3.7 CIMCORE ARM - 6 Axis Portable Measuring Arm

3.2.2 Components of Sugarcane Loader Structure

After defining the installation of sugarcane loader structure positions, the 3D models are created by SolidWorks program. The 3D models are consisted with 4 main parts: loader structure, loader arm, counter weight and body parts.

1) Loader structure

According to design concepts, the sugarcane loader structure must be able to mount on KUBOTA SUNSHINE ZL1-455 tractor**.** Thus, the loader structure was designed to be 8 components as follow: front cross member, frame, right engine-frame support, left engine-frame support, right transmission-frame support, left transmission-frame support, counter weight belt and counter weight support, as shown in Figure 3.8. Each component was connected by bolts and nuts.

1.1 Front cross member: the front cross member is a bending steel plate which was jointed ladders each side together.

1.2 Frame: the frame are consist of four rectangular steel columns, two rectangular steel ladders and two upper cross member that be fixed on rear axle and lower frame support. Cross section of columns and ladders are 75x100x6 mm and 100x150x6 mm respectively. Both side of loader arm and corresponding lift cylinders supposed to be mounted on frame.

1.3 Right engine-frame support: the right engine-frame support is lower support of frame which mounted to right side of the engine and also connected to counter weight support at rear of frame.

1.4 Left engine-frame support: the left engine-frame support function is similar to right engine-frame support but the shape is not symmetry.

1.5 Right transmission-frame support: the right transmission-frame support is lower support of frame which mounted to right side of the transmission.

1.6 Left transmission-frame support: the left transmission-frame support function is similar to right transmission-frame support but the shape is not symmetry.

1.7 Counterweight belt: Cause of vehicle stability, the counter weight was assembled to sugarcane loader. The belt was designed to mount balance weight with frame together and to make sure balance weight will not translate while loader arm operate in unstable farm ground.

1.8 Counter weight support: Counter weight support was designed to support counter weight around 1,100 kg that mounted to left and right engine -frame supports and engine.

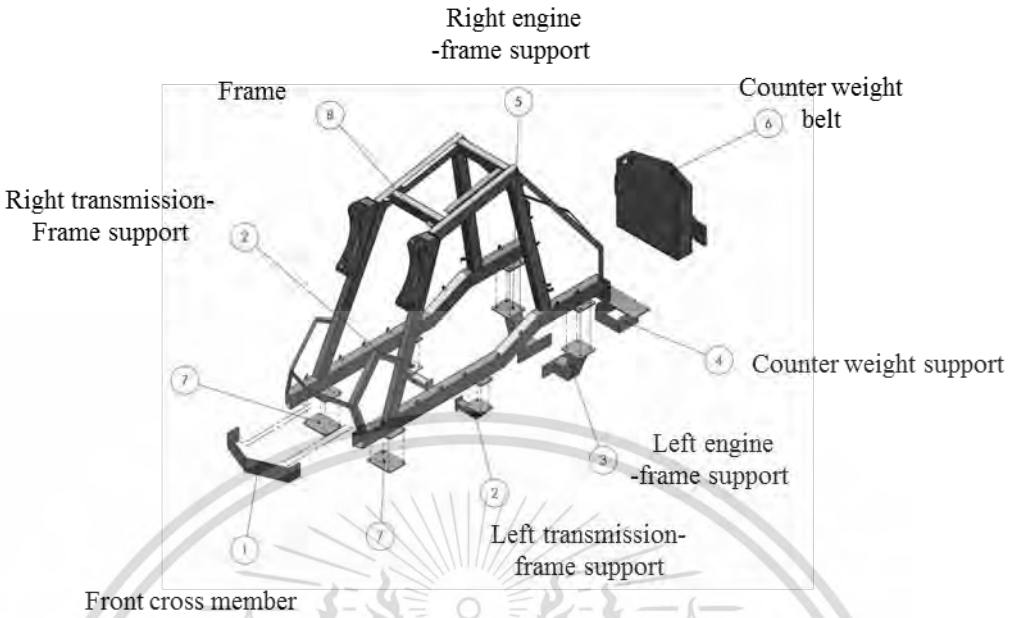

Figure 3.8 Components of loader structure (Explosion view)

2) Loader arm

Loader arm is symmetry geometry and is shown in Figure 3.9.

3) Counter weight

The design of the counter weight is to be the most harmonize with the chassis body design, able to installed with the tractor chassis by bolts and nuts, and closed to the vehicle which leads to the calculation of the weight and the suitable volume of the new counter weight to keep the balance of the vehicle to prevent the rollover characteristic when operating in the sugarcane farm. As the result, the weight of the counter weight is 1,000 kg, and the inside of the counter weight contains steel ball for the easiness to fill and refill the weight material as shown in Figure 3.10.

4) Body parts

Body parts are consist of many part of shell body, roof, front metal net, Rear metal net, front bodies and side bodies as shown in Figure 3.11.

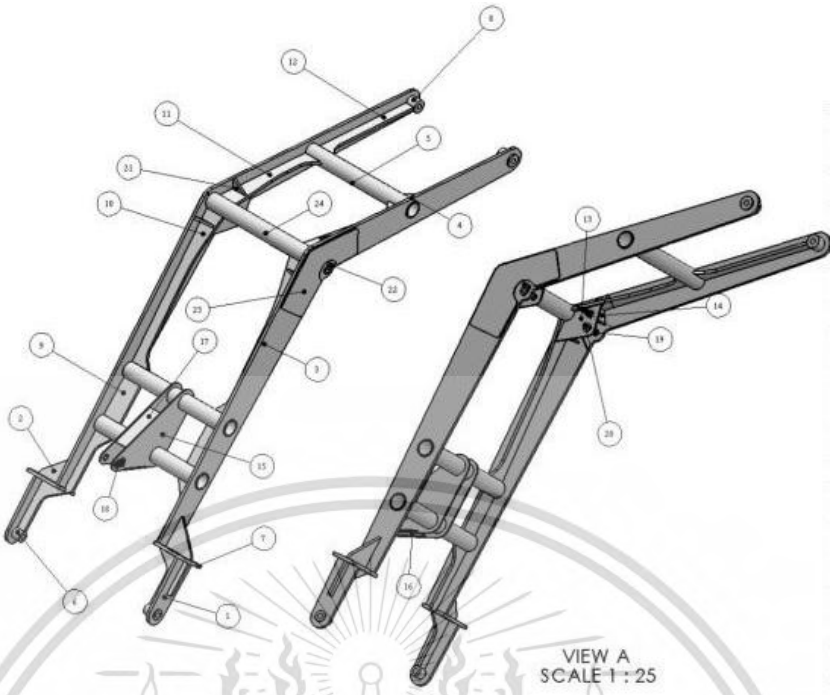

Figure 3.9 Loader arm

(a) (b)

Figure 3.10 Counter weight, (a) Counter weight (b) Steel ball

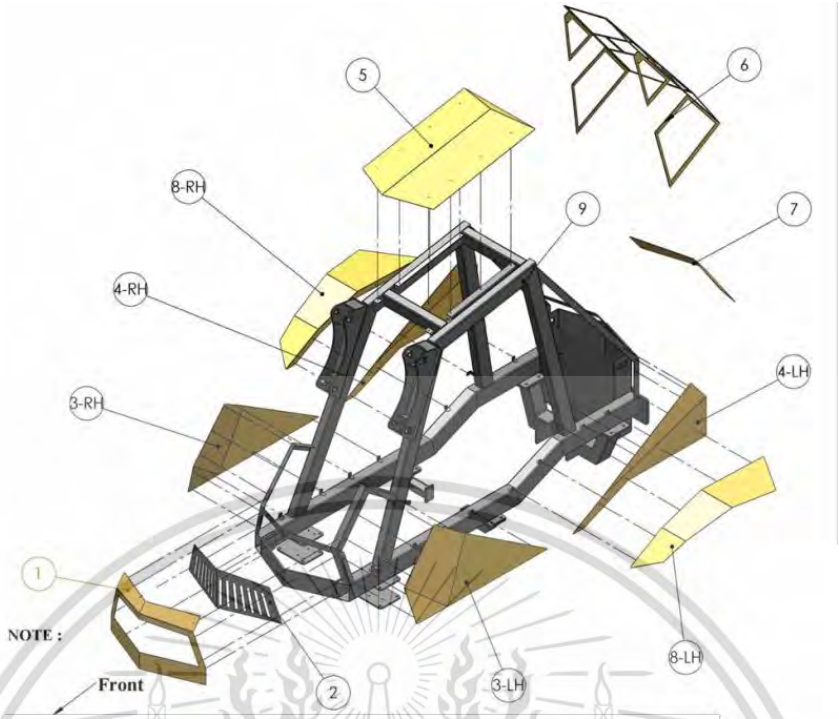

Figure 3.11 Body parts (Explosion view)

3.3 Static Force Analysis of Sugarcane Loader Structure

After the 3D geometry parts are designed by SolidWorks software, the next step is to analyze the strength of designed parts. In general, the strength can be calculated by Mechanic of Solids and Machine Design Theory. However, to obtain the most accurate analysis results, this research has applied Finite Element Method (FEM) to analyze strength of sugarcane loader structure. Before study on structural analysis of sugarcane loader structure by FEM, the maximum force that acts to the structure must be determined first, which these load will be defined as boundary condition in Finite Element Analysis (FEA). This chapter is only focus on Static Force Analysis of the loader structure and loader arm because these parts are main components that withstand the loads.

3.3.1 Static Force Analysis of Loader Arm

Considering to the free body diagram as shown in Figure 3.12, there are 3 main forces that act to the loader arm;

1) The force acting to the loader arm which comes from the summation of weight of loader arm and grabber (W_D). The magnitude is 675 kg.

2) The force acting to the loader arm which comes from the weight of sugarcane bundle (W_E). The magnitude is 300 kg.

3) The force acting by the hydraulic cylinder at point B (F_B).

4) The reaction force at the joint between the loader arm and the loader structure, point A (F_A).

The force at point A and point B can be determined by equilibrium equations as follow;

$$F_B = \frac{W_D dW_D + W_E dW_E}{d_A F_B} \quad (3.1)$$

$$F_{A,x} = -F_B cos\theta \quad (3.2)$$

$$F_{A,y} = F_B sin\theta - W_E - W_D \quad (3.3)$$

$$F_A = \sqrt{F_{A,x}{}^2 + F_{A,y}{}^2} \quad (3.4)$$

When

W_E is Force acting on loader arm due to weight of sugarcane bundle, 300 kg

W_D is Force acting on loader arm due to weight summation of loader arm and grabber at center of gravity (C.G.), 675 kg

$d_A W_E$ is Perpendicular distance with W_E from the hinge at point A

$d_A W_D$ is Perpendicular distance with W_D from the hinge at point A

$d_A F_B$ is Perpendicular distance with force acting by the hydraulic cylinders (F_B) from the hinge at point A

$F_{A,x}$ is Horizontal force acting on loader arm at hinge point A

$F_{A,y}$ is Vertical force acting on loader arm at hinge point A

Respecting to the design concept, the maximum vertical lifting distance of the grabber is 5 meters from the ground, it influences the weight of grabber, loader arm and sugarcane bundle acting to the hinge points ($F_{A,x}$ and $F_{A,y}$), and the force from hydraulic cylinder (F_B) will be varied regarding to the angle between hydraulic cylinder and the horizontal plane (θ), from 12.54 degree (at minimum hydraulic

cylinder stroke, 0 mm) to 81.98 degree (at maximum hydraulic cylinder stroke, 699 mm) as shown in Figure 3.13. Therefore, the maximum angle (θ) that creates maximum reaction force must be defined as to be load and boundary condition of Finite Element Analysis.

As the result in Figure 3.13, the maximum angle is 81.98 degree (at maximum hydraulic cylinder stroke, 699 mm) creates maximum reaction force at point A and B and the magnitude of force as shown below;

$F_A = 56{,}373.15$ N

$F_B = 65{,}828.56$ N

$F_{A,x} = -9{,}184.32$ N

$F_{A,y} = 55{,}619.97$ N

$F_{B,x} = F_B \cos\theta = 9{,}184.32$ N

$F_{B,y} = F_B \sin\theta = 65{,}373.15$ N

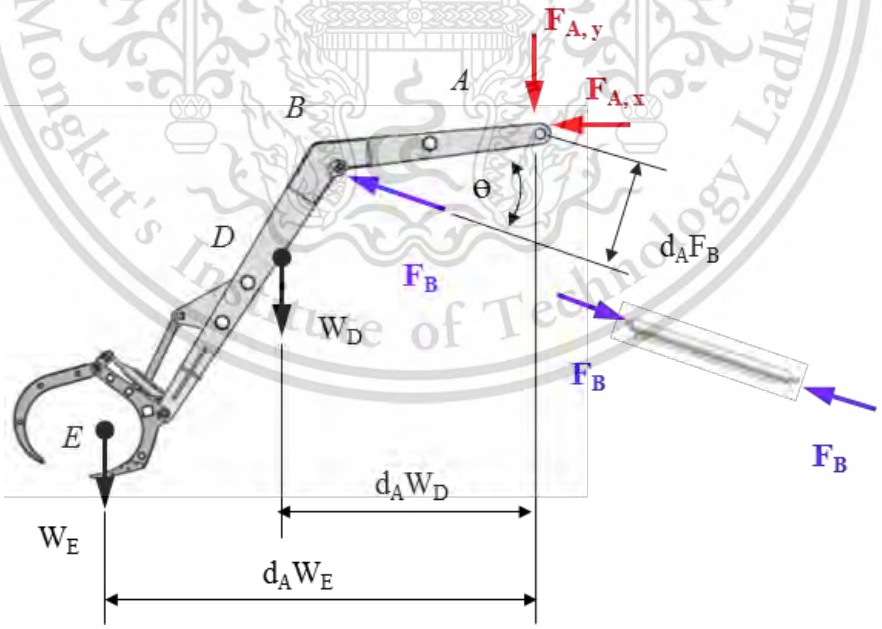

Figure 3.12 Free Body Diagram of loader arm

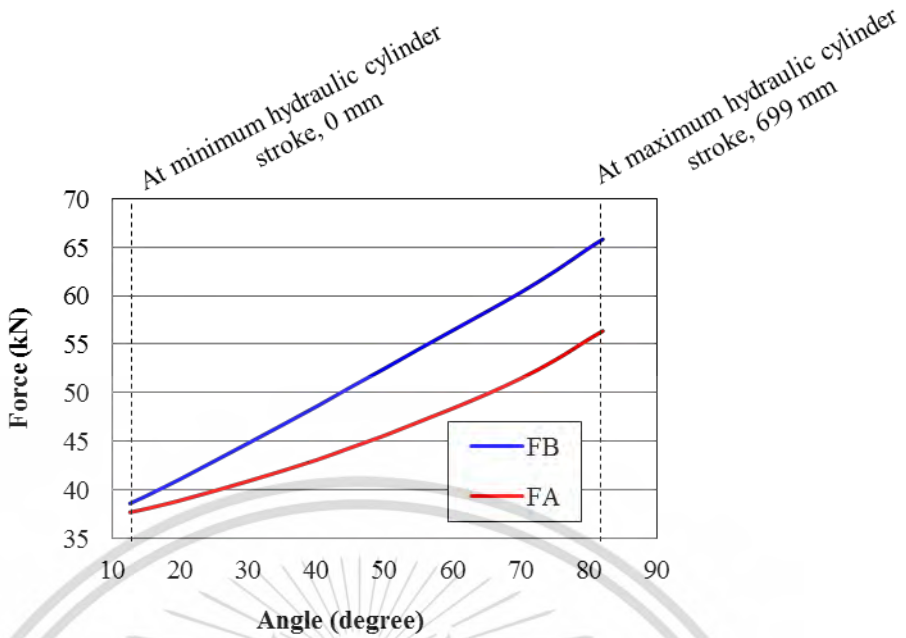

Figure 3.13 Comparison of hydraulic cylinder force in variant angles, $\theta = 12.54° - 81.98°$

3.3.2 Static Force Analysis of Loader Structure

Considering to the free body diagram of loader structure as shown in Figure 3.14, there are 2 main forces that act to the loader structure;

1) The force acting to the hinge point A of the loader arm ($F_{A,x}$ and $F_{A,y}$).
2) The force from the hydraulic cylinder (F_B).

From the equilibrium equation, it can define the reaction force at point A and B as well as static force analysis that act to the loader arm, as to follow equation (3.1), (3.2), (3.3) and (3.4), which are the same values but opposite directions.

$$F_{A,x} = -9{,}184.32 \quad N$$

$$F_{A,y} = 55{,}619.97 \quad N$$

$$F_{B,x} = F_B \cos\theta = 9{,}184.32 \quad N$$

$$F_{B,y} = F_B \sin\theta = 65{,}373.15 \quad N$$

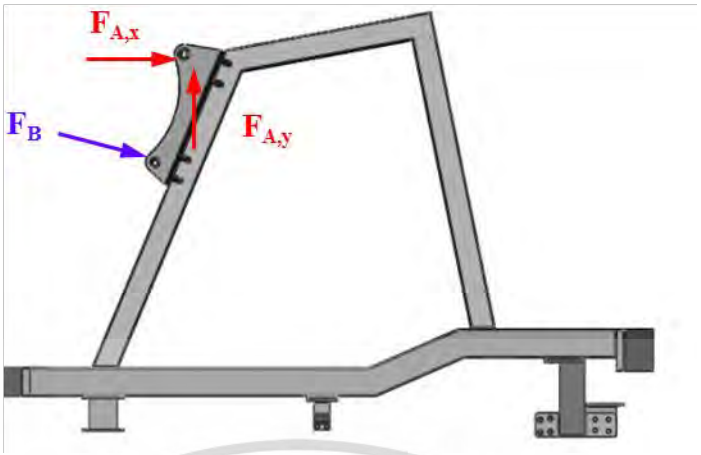

Figure 3.14 Free Body diagram of loader structure

3.4 Strength Analysis of Sugarcane Loader Structure by Finite Element Method

From the analysis of the static force acting to Sugarcane loader structure to find the severe condition, at the highest lifting point of the grabber (or at maximum hydraulic cylinder stroke, 699 mm), it will create maximum static force acting to loader structure and loader arm. Therefore, the next step is to analyze the strength of the designed parts with Finite Element Method by using the highest lifting point state (or at maximum hydraulic cylinder stroke, 699 mm state) to be the load and boundary condition.

Numerical Analysis principle by Finite Element Method begins with creating the part's model, and then divided the model into small elements. After that, specify the element's properties, specify material properties, all of boundary conditions and contact conditions to accord with the real problems. This research is using ductility material; therefore, the main focus will be on Maximum Distortion Energy Failure Theory (Von Mises Yield Criterion) because it is more reliable in results and more popular. After receiving analysis results from Finite Element Method, the designed parts must contain Von Mises stress value smaller than the yield strength of the material divided by safety factor, which in this research, the safety factor, S.F. is 3 (Burr & Cheatham, 1995). If the result does not follow the Von Mises Yield Criterion, the designed parts will fail and need to be improved strength until they pass this criterion (Patel & Prajapati, 2012). The design criterion follow Von Mises Criterion as

shown in equation (3.5) and the flow chart of strength analysis by FEM as shown in Figure 3.15.

$$\sigma_{von} \leq \frac{S_y}{S.F.} \tag{3.5}$$

When

σ_{von} is Von Mises stress (MPa)

S_y is Yield strength of material

S.F. is safety factor (In this work, S.F. =3)

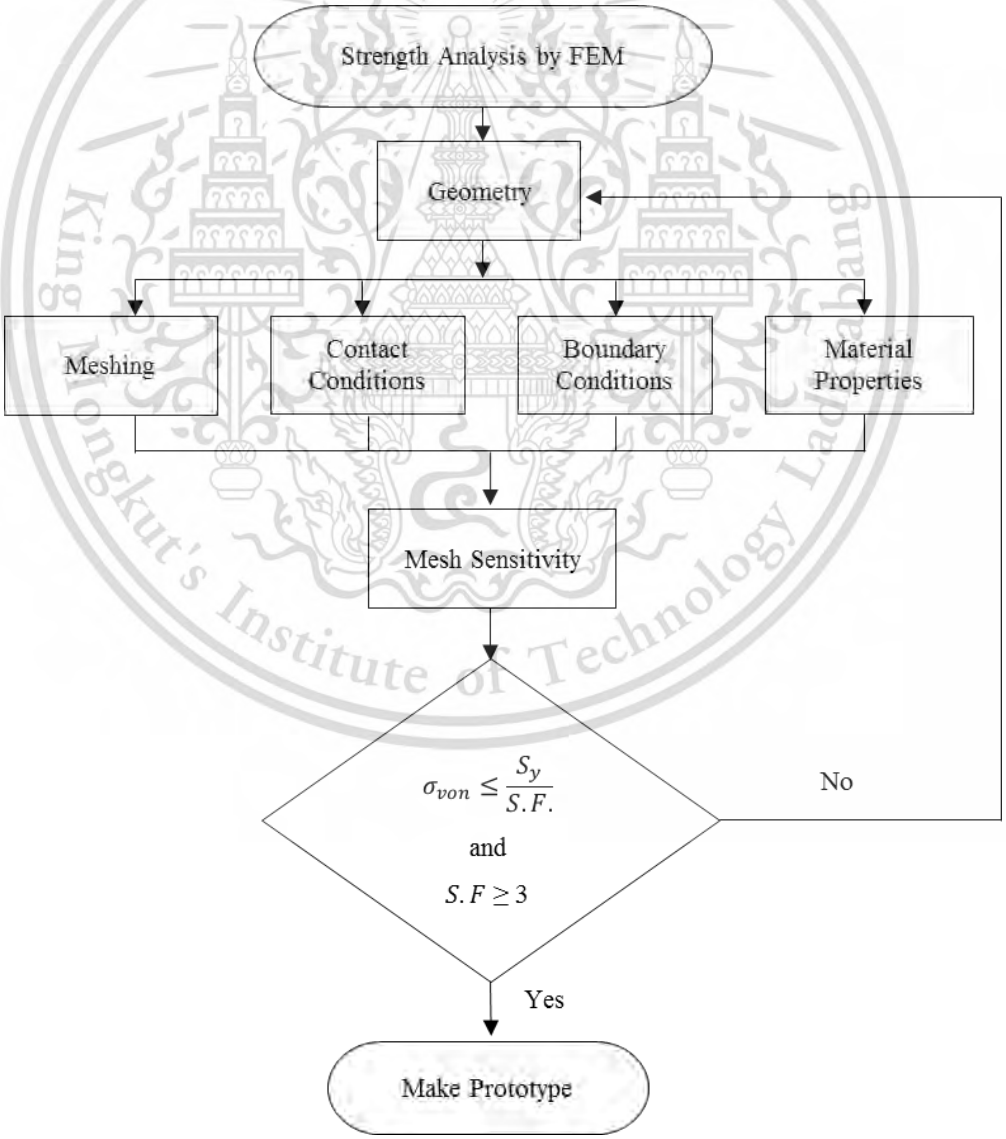

Figure 3.15 Flow chart of strength analysis by FEM

3.4.1 Strength Analysis of Loader Arm

3.4.1.1 Computer Modeling

The loader arm 3D model is created by SolidWorks software. This characteristic is double grabber arms which consist with one single part as shown in Figure 3.16 and Figure 3.17.

Figure 3.16 Geometry of loader arm

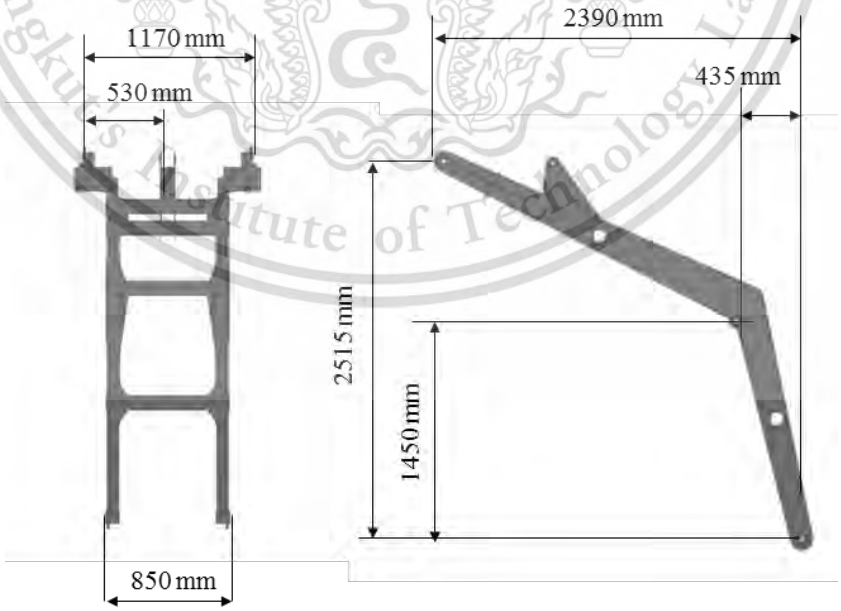

Figure 3.17 Dimensions of loader arm

3.4.1.2 Meshing and Element

When the 3D model of the loader arm is created, and then separated from the 3D model into tetrahedral elements by ANSYS software: Basically, finer order element delivers more strength simulation accuracy than the first-drought order element. Meaning, the higher of mesh density gives the higher accuracy of maximum stress result, but at the same time, it means more computation time consuming. Therefore, it is necessary to choose between work-efficiency and unnecessary time consumable simulation accuracy.

In order to ensure convergence of result and the quality of mesh, the mesh sensitivity analysis is the selected method that uses to optimize the mesh density. Mesh sensitivity is mesh refinement method by iterative procedures to refine the size of element as in random percentage (from 1-100%). If the result of maximum Von Mises stress is changed less than, or equal 5% between the previous iteration and the last iteration, the value of difference is acceptable, and the simulation result is convergence (Martinez, 2013; Natchaya Murachai 2013).

In this research, the selected random refinement percentage is 50%. Therefore, the first iteration, minimum elements size is 10 mm, and second iteration of element size is divided into half of the previous ones (the second order of minimum element size is reduced from 10 mm to 5 mm). The difference of maximum Von Mises stress between the first and the second iteration is 17.91%, which means, the second element density of its size has greater value of stress changing. (Acceptable stress changing is 5% by Martinez, 2013). Therefore, the changing percentage is unacceptable. Then, followed by the difference between maximum Von Mises stress between the second iteration and the third is 6.06% (the 3nd minimum element size is reduced from 5 mm to 2.5 mm), which means, the third element density of its size has greater value of stress changing. (Acceptable stress changing is 5% by Martinez, 2013). Therefore, the changing percentage is unacceptable. Then, followed by the difference between maximum Von Mises stress between the third iteration and the fourth is 0.63% (the 4nd minimum element size is reduced from 2.5 mm to 1.25 mm), which means, the fourth element density of its size has smaller value of stress changing. Therefore, the changing percentage is acceptable and the maximum Von Mises stress is convergence. In this case, minimum element size of 2.5 mm is chosen because the maximum stress value of third order element at 2.5 mm is close to the result from the fourth order element at 1.25 mm (stress changing value is less than 5% of acceptable

value) but it uses less computational time consuming. (CPU time of third order element at 2.5 mm and the fourth order element at 1.25 mm are 354 seconds and 430 seconds respectively). The result of the difference of maximum Von Mises stress in variants of element size and the CPU time in variants of element size are shown in Figure 3.18 and Figure 3.19 respectively.

Therefore, Finite element model of Loader arm with minimum element size 2.5 mm consist of 505,360 nodes and 303,788 elements (element type is Tetrahedral) as shown in Figure 3.20.

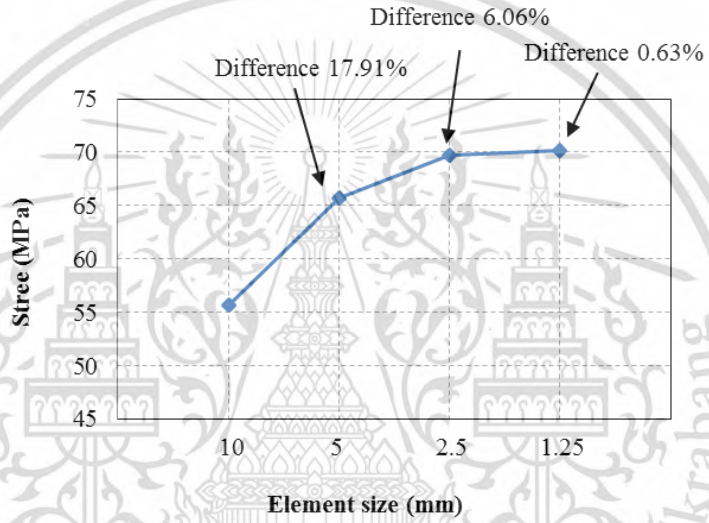

Figure 3.18 Comparison of stress in variants of element size

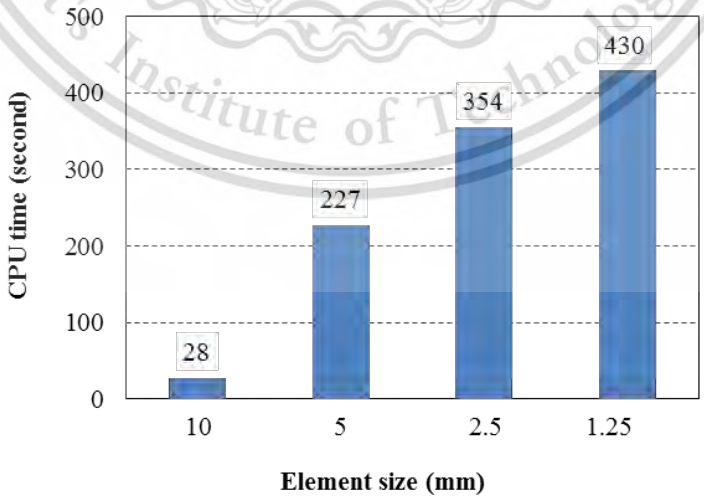

Figure 3.19 Comparison of CPU time in variants of element size

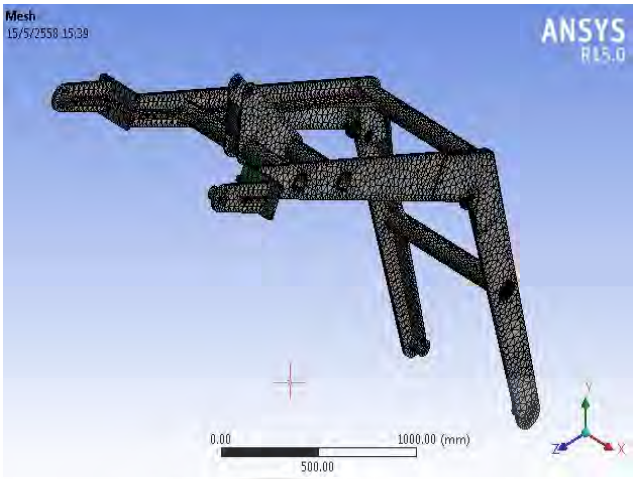

Figure 3.20 Mesh and element of loader arm

3.4.1.3 Boundary Conditions

There are 3 loads and 1 constraint is applied to the FE model of loader arm:

1) The summation weight of the grabber and sugarcane bundle, 483 kg is applied to the pin-hole that attached grabber with loader arm and attached loader arm with hydraulic cylinder of grabber. The weight is specified by Point mass feature in ANSYS software as the red point in Figure 3.21.

2) Hydraulic cylinder force at point B is 65,829N (from chapter 3.3.1; Static force analysis of loader arm). The hydraulic cylinder force at point B is applied at the pin-hole that attached loader arm with hydraulic cylinder by force feature in ANSYS and it is shown as the red area in Figure 3.21.

3) Gravitational acceleration is 9.81 m/s^2, is applied in vertical direction to the whole loader arm model as yellow point in Figure 3.21.

4) Specify the constraint of loader arm model by fixed support around the pin-hole of assemble point of the loader arm and the loader structure. The loader arm will not possible to have any movement in X, Y, and Z axis and it is not able to rotate around X, Y, and Z axis

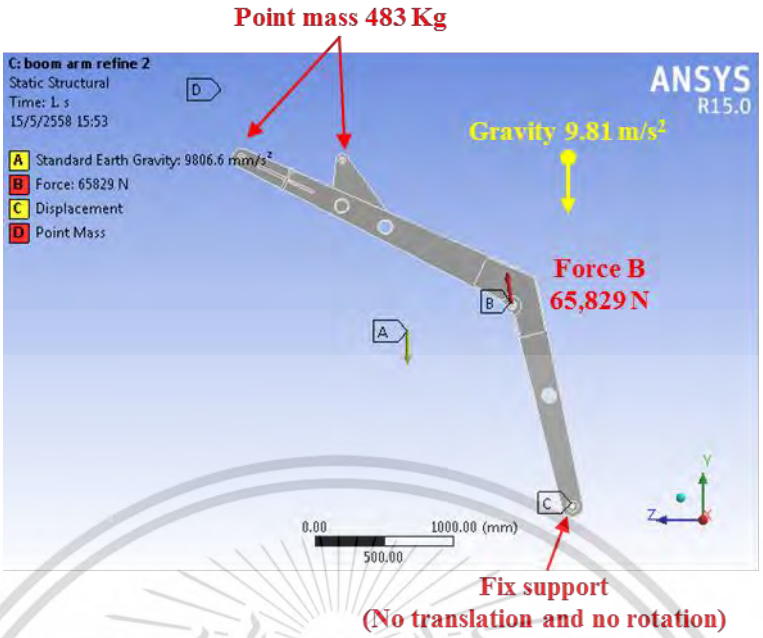

Figure 3.21 Loads and boundary conditions of loader arm

3.4.1.4 Material Properties

The material of the loader arm is ss400 Carbon steel tube which is easy to find in the market and it is popular in usage. The behavior of ss400 steel is linear elastic and contains the mechanical properties as shown in Table 3.2.

Table 3.2 Material properties of ss400 Carbon steel tube

Density (kg/m^3)	Young modulus (GPa)	Poisson's ratio	Yield strength (MPa)
7,850	205	0.29	250

3.4.2 Strength Analysis of Loader Structure

3.4.2.1 Computer Modeling

The loader structure 3D model is created by SolidWorks software. It contains 11 main parts: 1) Front cross member, 2) Rear cross member, 3) Frame, 4) Right engine-frame support, 5) Left engine-frame support, 6) Right transmission-frame support, 7) Left transmission-frame support, 8) Counter weight support, 9) Left Plate, 10) Right Plate, 11) Rigid beam as shown in Figure 3.22 and Figure 3.23.

The rigid beam is acting as the core of rear driveshaft as to support the Loader structure Moreover, the actual producing parts will be assembled by welding. Therefore, the welding lines are created by using fillet feature in SolidWorks software as to make the designed model more complete and to avoid the stress singularity (Patel, 2017). The defined radiuses of fillets are the same value as radius of welding lines in 2D drawing. The sample area of fillet on loader structure is shown in Figure 3.24.

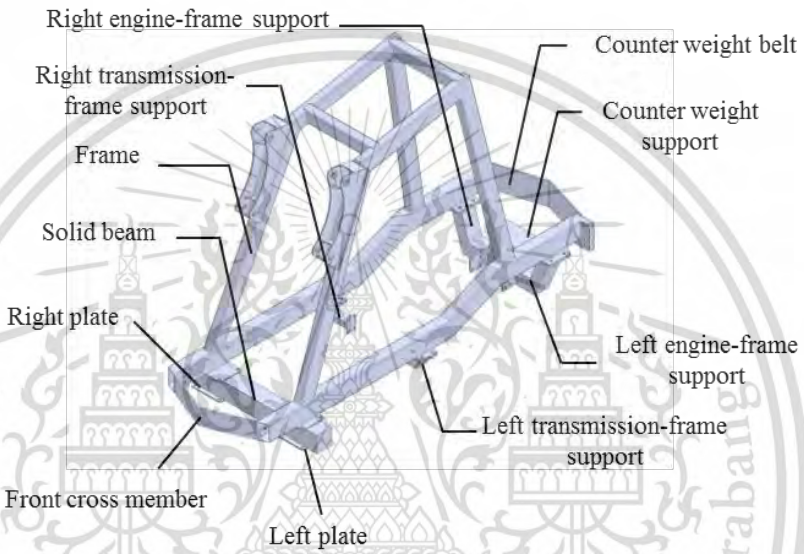

Figure 3.22 3D geometry of loader structure

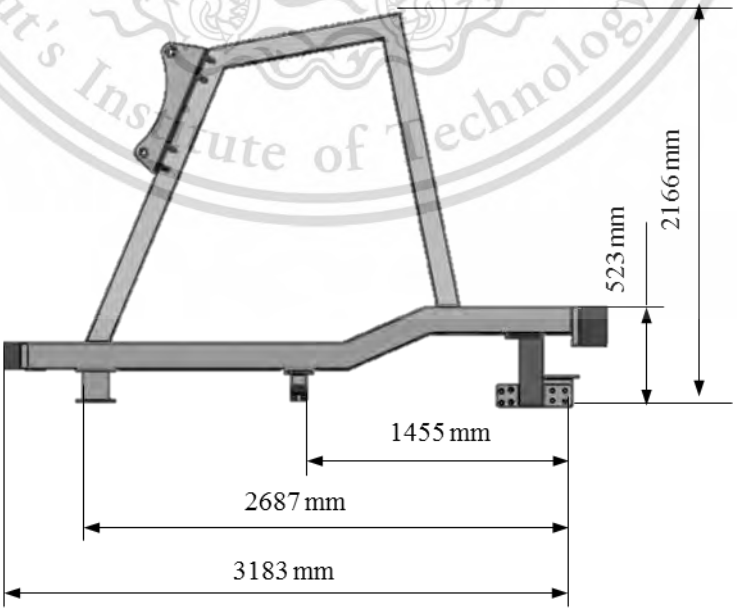

Figure 3.23 Dimensions of loader structure

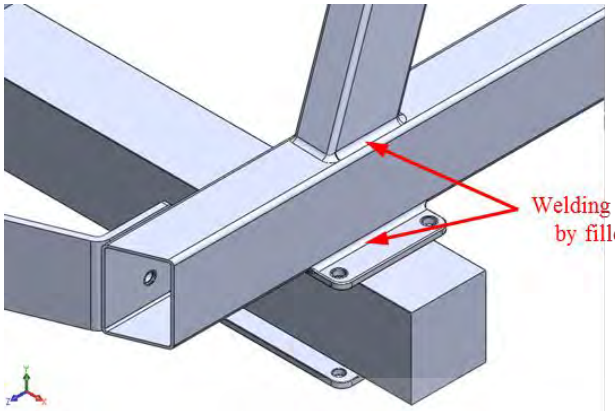

Figure 3.24 Sample areas of fillet on loader structure

3.4.2.2 Meshing and Element

When the 3D model of the loader arm is created, and then separated from the 3D model into tetrahedral elements by ANSYS software: Basically, finer order element delivers more strength simulation accuracy than the first-drought order element. Meaning, the higher of mesh density gives the higher accuracy of maximum stress result, but at the same time, it means more computation time consuming. Therefore, it is necessary to choose between work-efficiency and unnecessary time consumable simulation accuracy.

Respecting to the design objective as to decrease time consuming in computing simulation, mesh sensitivity analysis is the selected method that use to optimize the mesh density. Mesh sensitivity is mesh refinement method by iterative procedures to refine the size of element as in random percentage (from 1-100%). If the result of maximum Von Mises stress is changed less than, or equal 5% between the previous iteration and the last iteration, the value of changes is acceptable, and the simulation result is convergence (Martinez, 2013; Natchaya Murachai, 2013).

In this research, the selected random refinement percentage is 50%. Therefore, the first iteration, minimum elements size is 10 mm, and second iteration of element size is divided into half of the previous ones (the second order of minimum element size is reduced from 10 mm to 5 mm). The difference of maximum Von Mises stress between the first and the second iteration is 27.03%, which means, the second element density of its size has greater value of stress changing (acceptable stress changing is 5% by Martinez, 2013). Therefore, the changing percentage is unacceptable. Then, followed by the difference between maximum Von Mises stress between the second

iteration and the third is 6.35% (the 3nd minimum element size is reduced from 5 mm to 2.5 mm), which means, the third element density of its size has still greater value of stress changing (acceptable stress changing is 5% by Martinez, 2013). Therefore, the changing percentage is unacceptable. Then, followed by the difference between maximum Von Mises stress between the third iteration and the fourth is 0.43% (the 4nd minimum element size is reduced from 2.5 mm to 1.25 mm), which means, the fourth element density of its size has smaller value of stress changing. Therefore, changing percentage is acceptable and the maximum Von Mises stress is convergence. In this case, minimum element size of 2.5 mm is chosen because the maximum stress value of third order element at 2.5 is close to the result of fourth order element at 1.25 mm (stress changing value is less than 5% of acceptable value) but it uses less computational time consuming. (CPU time of third order element at 2.5 mm and fourth order element at 1.25 mm are 6,189 seconds 7,301 seconds respectively). The comparison of the maximum Von Mises stress in variants of element size and the comparison of the CPU time in variants of element size are shown in Figure 3.25 and Figure 3.26 respectively.

Therefore, Finite Element model of loader structure with minimum element 2.5 mm consist of 730,704 nodes and 463,374 elements (element type is Tetrahedral) as shown in Figure 3.27. Moreover, the element of loader structure on fillet is shown in Figure 3.28.

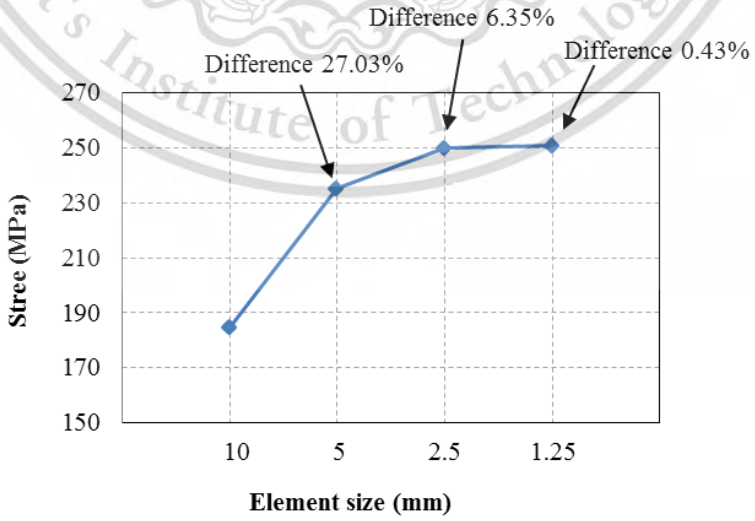

Figure 3.25 Comparison of maximum stress in variants of element size

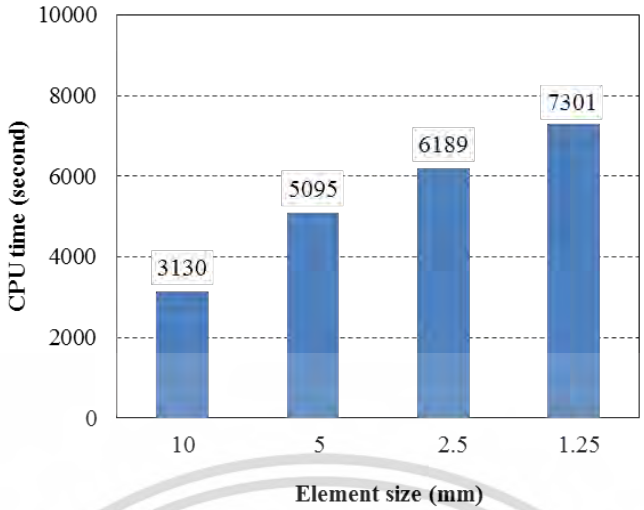

Figure 3.26 Comparison of CPU time in variants of element size

Figure 3.27 Mesh and element of loader structure

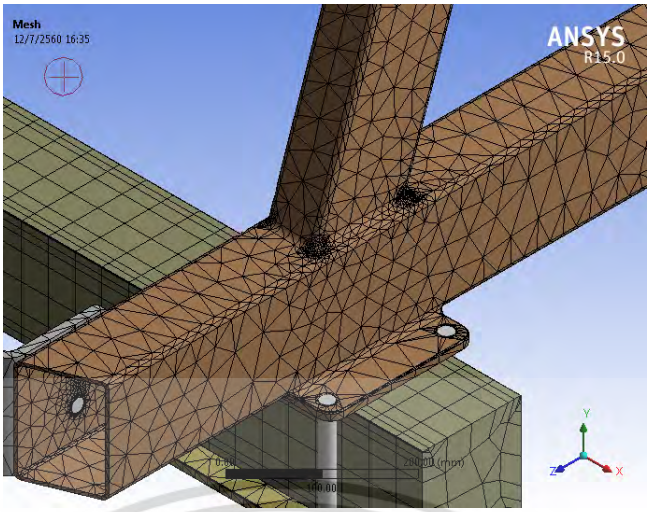

Figure 3.28 Element of loader structure on fillet

3.4.2.3 Contact Conditions

As there are 11 parts of the loader structure and each part can be detach, therefore, the contact condition is applied by Frictional-contacts feature in ANSYS software which two faces of each component are free to separate in their normal direction as well as sliding in their tangential direction and friction coefficient between each parts, μ is 0.74, which is friction coefficient of steel to steel (http://www.engineershandbook.com/Tables/frictioncoefficients.htm), as shown in Figure 3.29. Moreover, as each component of loader structure is designed to assemble by bolts and nuts, therefore, Beam-contacts feature in ANSYS software is applied to simulate as fasteners with realistic bolt diameter (*Introduction to ANSYS Mechanical Part 2*, 2013), as shown in Figure 3.30 and Figure 3.31. The summary of contact condition of loader structure is shown in Table 3.3 and Figure 3.32.

Table 3.3 Contact conditions between each component of loader structure

Part No. 1	Part No. 2	Contact Condition 1	Contact Condition 2
Frame	Front cross member	Frictional ($\mu = 0.74$)	Beam connection (body to body)
	Rear cross member	Frictional ($\mu = 0.74$)	Beam connection (body to body)
	Left Plate	-	Beam connection (body to body)
	Right Plate	-	Beam connection (body to body)
	Rigid Beam	Frictional ($\mu = 0.74$)	-
	Right transmission-frame support	Frictional ($\mu = 0.74$)	Beam connection (body to body)
	Left transmission - frame support	Frictional ($\mu = 0.74$)	Beam connection (body to body)
	Right engine-frame support	Frictional ($\mu = 0.74$)	Beam connection (body to body)
	Left engine-frame support	Frictional ($\mu = 0.74$)	Beam connection (body to body)
Rigid Beam	Left Plate	Frictional ($\mu = 0.74$)	-
	Right Plate	Frictional ($\mu = 0.74$)	-
Right transmission-frame support	-	-	Beam connection (body to ground)
Left transmission-frame support	-	-	Beam connection (body to ground)
Right engine -frame support	-	-	Beam connection (body to ground)
Left engine-frame support	-	-	Beam connection (body to ground)
Counter weight support	Right engine-frame support	Frictional ($\mu = 0.74$)	Beam connection (body to body)
	Left engine-frame support	Frictional ($\mu = 0.74$)	Beam connection (body to body)
	-	-	Beam connection (body to ground)

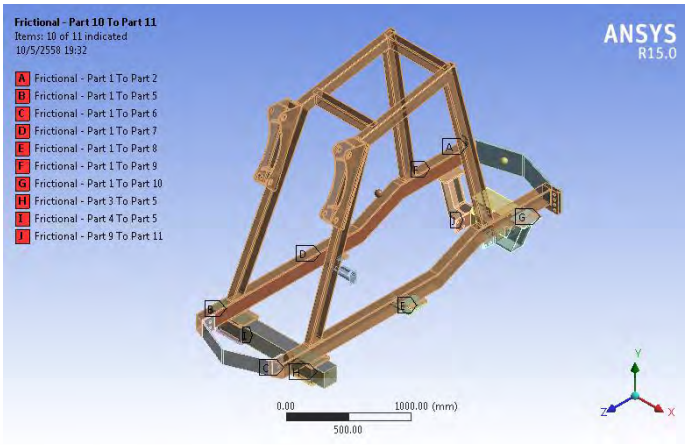

Figure 3.29 Applied Friction coefficient by Frictional-contact feature

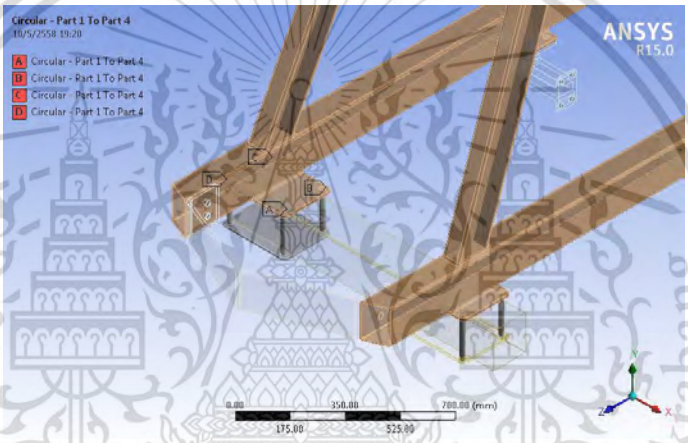

Figure 3.30 Virtual fasteners by Beam-contacts feature (body to body)

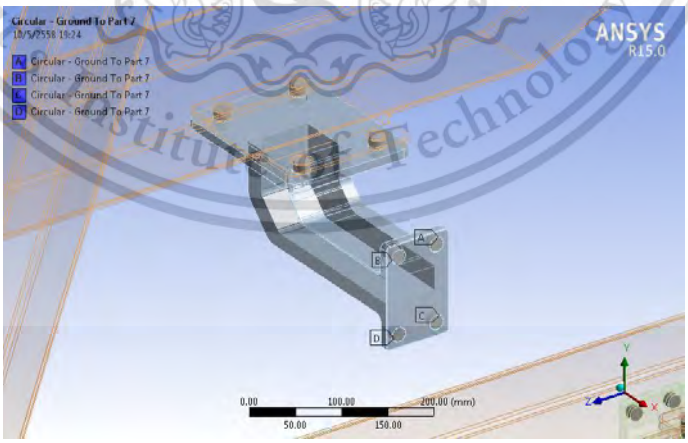

Figure 3.31 Virtual fasteners by Beam-contacts feature (body to ground)

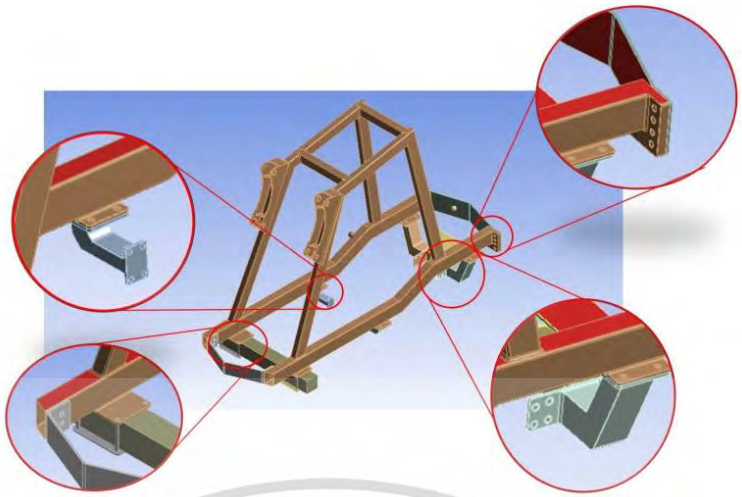

Figure 3.32 Contact condition of each component of loader structure

3.4.2.4 Boundary Conditions

There are 4 main loads and 1 constraint acting to the loader structure model:

1) Longitudinal load from weight of body parts, 100kg is applied on the frame by Point mass feature in ANSYS.

2) Load from weight of the counter weight, 1,100 kg is applied at the attached point of the counter weight to the frame by Point mass feature in ANSYS.

3) Force at point A is 55,373 N, and point B is 65,829 N (from the chapter 3.3.2; static force analysis of loader structure). The forces are applied by Force feature in ANSYS.

4) Gravitational acceleration is 9.81 m/s^2 which acting to the whole loader structure.

5) The loader structure model is attached by fixed supports around the side area of the rigid beam. In other words, there is no movement and no rotation in 3 axles (X, Y, and Z) which is assumed as the sugarcane loader structure is placed on the rigid beam virtually and the boundary conditions are shown in Figure 3.33

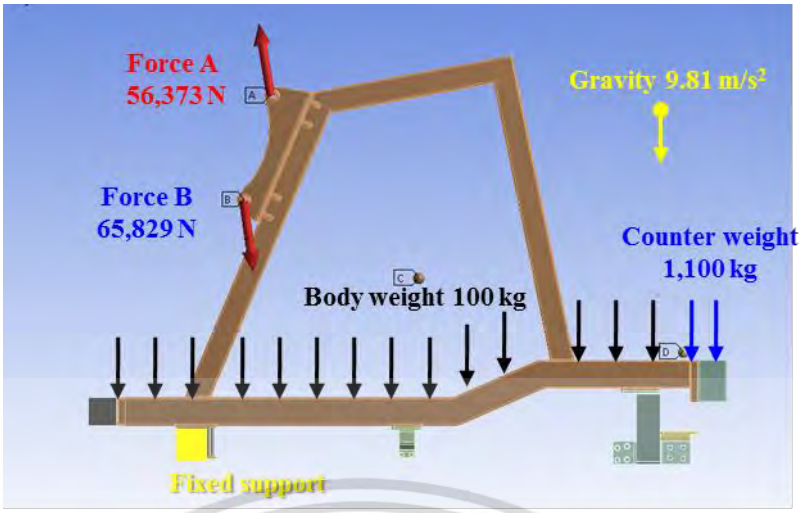

Figure 3.33 Boundary conditions of loader structure

3.4.2.5 Material Properties

The material specification of the sugarcane loader structure model is ss400 carbon steel tubs as same as loader arm. It is easy to find in the market and worldwide popular use in construction work, and its behavior is linear elastic. The mechanical properties of ss400 are shown in Table 3.4.

Table 3.4 Material properties of ss400 Carbon steel tube

Density (kg/m^3)	Young modulus (GPa)	Poisson's ratio	Yield strength (MPa)
7,850	205	0.29	250

In this chapter, after the Finite Element of loader arm and loader structure are applied mesh and element, boundary conditions, contact conditions and material properties, the result of strength analysis are shown in chapter 4.1; strength analysis result of sugarcane loader structure by Finite Element Method.

3.5 Creating 2D Drawings and Bill of Materials

After analyzed the strength of the Sugarcane loader structure by Finite Element Method, improved the strength of the design model and finalize 3D mode (The finalize 3D of Sugarcane loader structure is shown in chapter 4), next step is create the 2D drawings and Bill of Materials (BOM) as to prepare the fabrication of the Sugarcane loader structure prototype. The 2D drawings and Bill of Materials (BOM) are document that use to communicate between designer and manufacturing plant for the sugarcane loader structure prototype fabrication. The 2D drawings show the dimension of sub-component and the assembly procedure. The Bill of Materials show list of the raw materials, sub-assemblies, intermediate assemblies, sub-components, parts and the quantities of each needed for manufacturing. For more details of 2D drawings and Bill of Materials of Sugarcane loader structure are explained in chapter 5.1; 2D drawings and Bill of Materials of Sugarcane loader structure. Moreover, the sample of 2D drawing is shown in Figure 3.34.

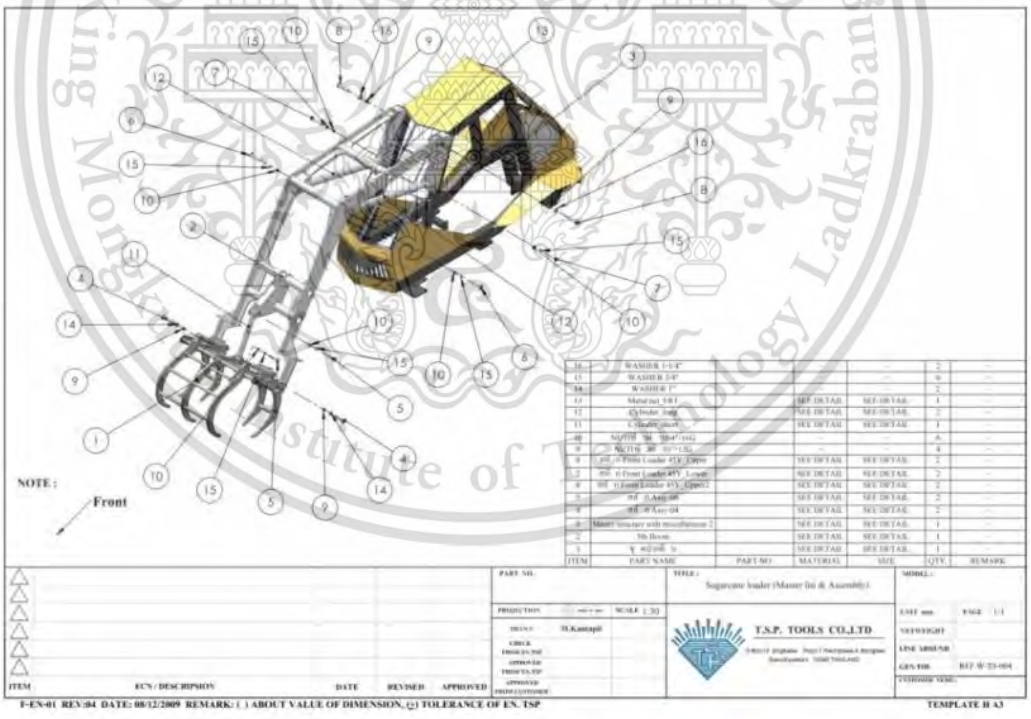

Figure 3.34 2D drawing of sugarcane loader

3.6 Fabrication of Sugarcane Loader Structure Prototype

After created 2D drawings and Bill of Materials, Next step is to fabricate the sugarcane loader structure prototype which is full scale model and for more details of manufacturing process are explained in chapter 5.2; fabrication process of sugarcane loader structure. Moreover, the samples of completed sugarcane loader structure prototype are shown in Figure 3.35 and Figure 3.36.

Figure 3.35 Completed sugarcane loader structure

Figure 3.36 Completed sugarcane loader structure (side view)

CHAPTER 4

RESULTS AND DISCUSSIONS

4.1 Strength Analysis Result of Sugarcane Loader Structure by Finite Element Method

4.1.1 Strength Analysis Result of Loader Arm

From Figure 4.1 and Figure 4.2, the maximum Von Mises stress of the loader arm around the pin hole of hydraulic cylinder that use to lift the loader arm is 69.68 MPa and the minimum Von Mises stress at around the pin hole of hydraulic cylinder that use to life the grabber is 0.015 MPa.

Considering to Von Mises stress theory, the specific chosen designed safety factor is equal or more than 3 (S.F. $\geq$ 3), the maximum Von Mises stress is 69.68 MPa (σ_{von} = 69.68 MPa) which is smaller than the yield strength of steel ss400 (S_y = 250 MPa). Therefore, the calculated value of safety factor is 3.59 (S.F. = 3.59), which is more than the original specified safety factor, which mean that the designed parts are safety to use (Patel & Prajapati, 2012).

In addition, the maximum displacement is 7.55 mm which occurred at the near end of the loader arm closed to the pin-hole that assembled the grabber as shown in Figure 4.3, and it is less displacement value when compared to the minimum thickness of the steel plate that used for the loader arm (Thickness is 19 mm). Therefore, the design of the loader arm is safe to apply loading condition (Patel & Prajapati, 2012).

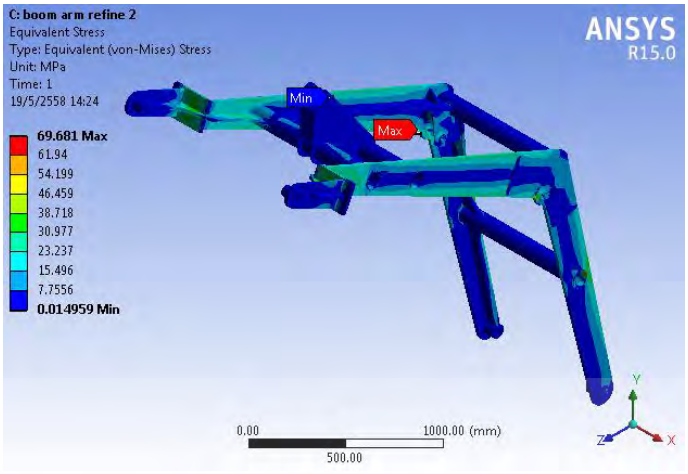

Figure 4.1 Von Mises stress of loader arm

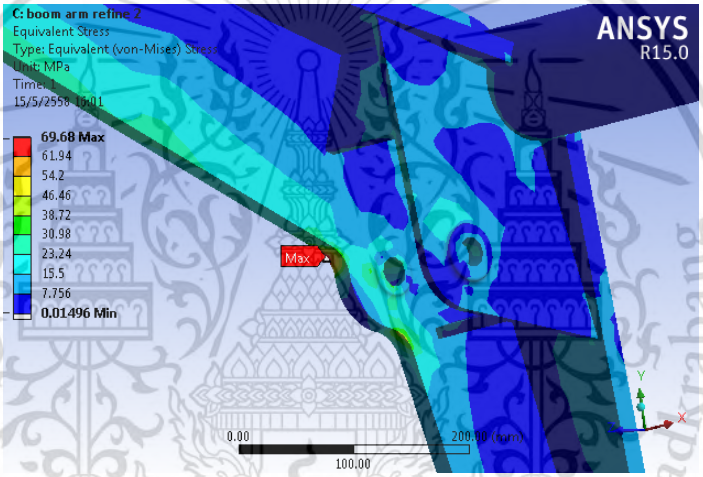

Figure 4.2 Von Mises stress of loader arm (Enlarge view)

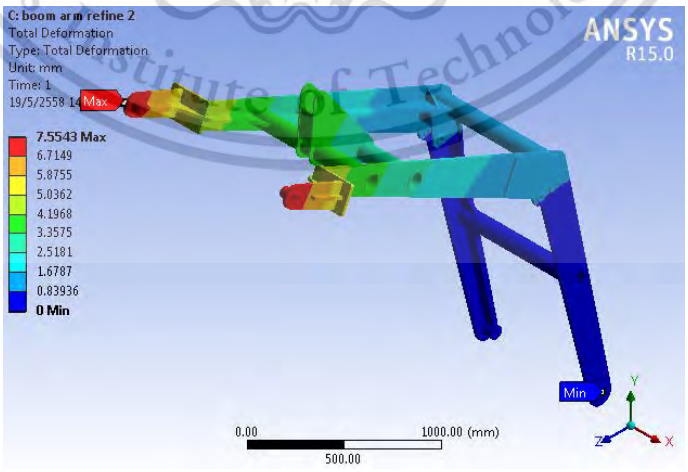

Figure 4.3 Displacement of loader arm

4.1.2 Strength Analysis Result of Loader Structure

4.1.2.1 Strength Analysis Result of Left Transmission-Frame Support

From Figure 4.4 and 4.5, the maximum Von Mises stress of the left transmission-frame support is 16.66 MPa at around the wielding line near the bottom right hole where is for the assemble by bolt and nut to fasten the support with the transmission. The minimum Von Mises stress is 0.011 at around the area of contact surface between the left transmission-frame support with the frame.

When considering the failure criterion theory, as respecting to the specified designed safety factor is equal or more than 3 (S.F. ≥3), the maximum Von Mises stress is 16.66 MPa, (σ_{von} = 16.66 MPa) which is much lesser than the yield strength of steel ss400 (S_y = 250 MPa), it represented the safety factor at 15.01 (S.F. = 15.01), which is much more than the original specified safety factor. Therefore, the designed part is safety to use.

In addition, the maximum displacement of left transmission-frame support is 0.028 mm which occurred between the contact surface of left transmission-frame support and the frame as shown in Figure 4.6, which it is much lesser displacement value when compared to the minimum thickness of the steel plate that used for the left transmission-frame support (Thickness is 10mm). Therefore, the design of left transmission-frame support is safe to apply loading condition.

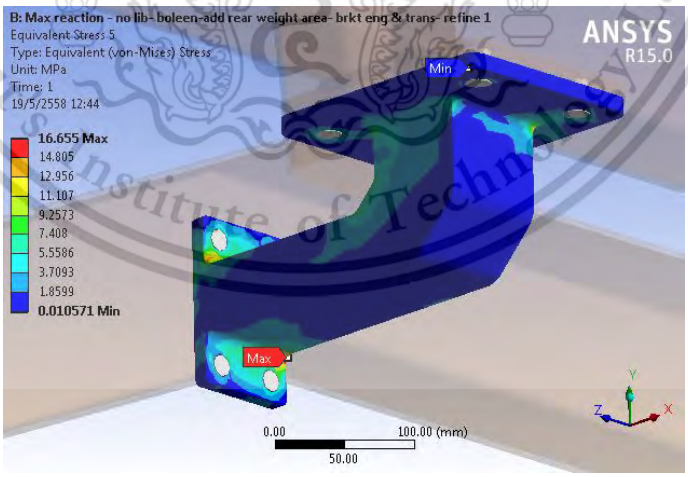

Figure 4.4 Von Mises stress of left transmission-frame support

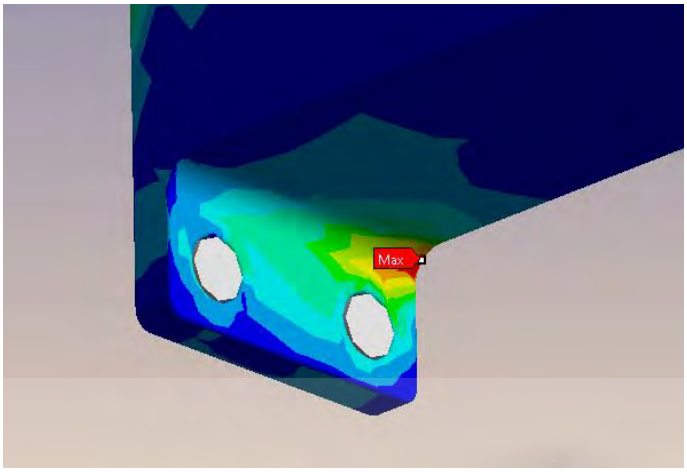

Figure 4.5 Von Mises stress of left transmission-frame support (Enlarge view)

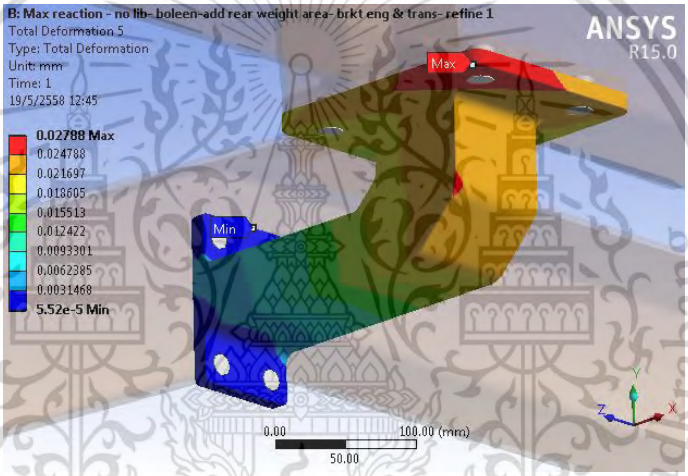

Figure 4.6 Displacement of left transmission-frame support

4.1.2.2 Strength Analysis Result of Right Transmission-Frame Support

From Figure 4.7 and Figure 4.8, the maximum Von Mises stress of the right transmission-frame support is 17.91 MPa at around the wielding line near the bottom left hole where is for the assemble by bolt and nut to fasten the support with the transmission. The minimum Von Mises stress is 0.006 MPa at around the area of contact surface between the right transmission-frame support with the frame.

When considering the failure criterion theory, as respecting to the specified designed safety factor is equal or more than 3 (S.F. $\geq$ 3), the maximum Von Mises stress is 17.91 MPa (σ_{von} = 17.91 MPa), which is much lesser than the yield strength of steel ss400 (S_y = 250 MPa), it represented the safety factor at 13.96 (S.F. = 13.96),

which is much more than the original specified safety factor. Therefore, the designed part is safety to use.

In addition, the maximum displacement of right transmission-frame support is 0.026 mm which occurred between the contact surface of right transmission-frame support and the frame as shown in Figure 4.9, which it is much lesser displacement value when compared to the minimum thickness of the steel plate that used for the right transmission-frame support (Thickness is 10mm). Therefore, the design of right transmission-frame support is safe to apply loading condition.

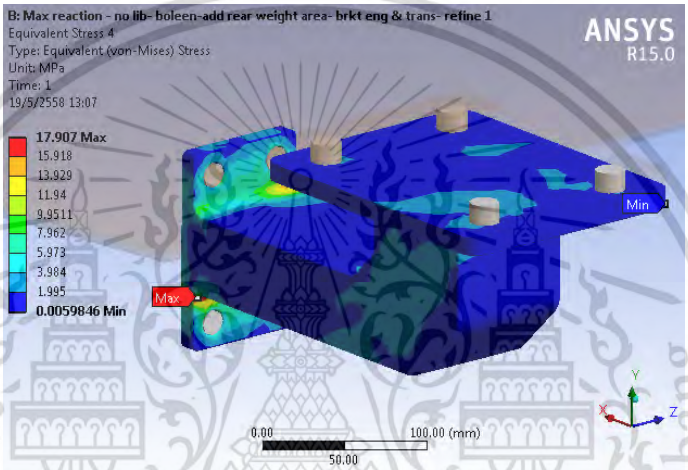

Figure 4.7 Von Mises stress of right transmission-frame support

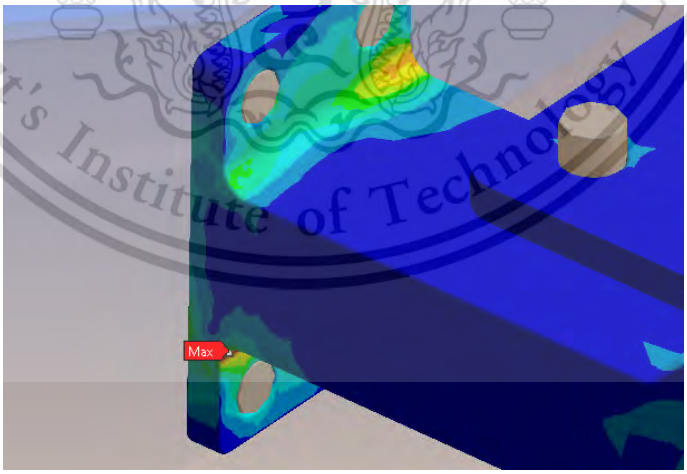

Figure 4.8 Von Mises stress of right transmission-frame support (Enlarge view)

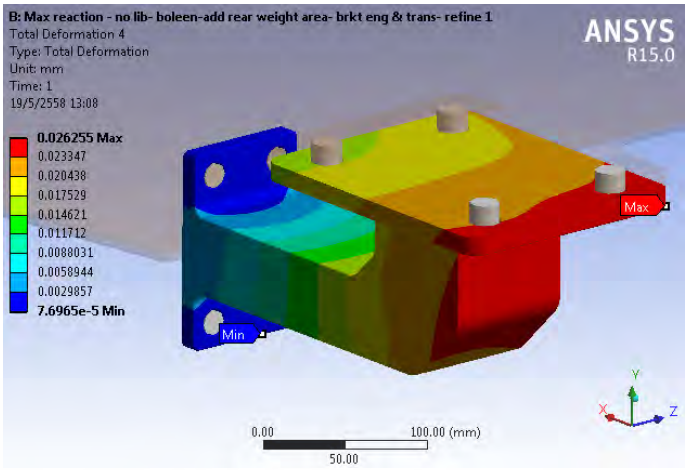

Figure 4.9 Displacement of right transmission-frame support

4.1.2.3 Strength Analysis Result of Left Engine-Frame Support

From Figure 4.10 and Figure 4.11, the maximum Von Mises stress of the left engine-frame support is 69.89 MPa at around the wielding line near the bottom right hole where is for the assemble by bolt and nut to fasten the support with the engine. The minimum Von Mises stress is 0.009 MPa at around the area of contact surface between the left engine-frame support with the frame.

When considering the failure criterion theory, as respecting to the specified designed safety factor is equal or more than 3 (S.F. $\geq$ 3), the maximum Von Mises stress is 69.89 MPa (σ_{von} = 69.89 MPa), which is less than the yield strength of steel ss400 (S_y = 250 MPa), it represented the safety factor at 3.58 (S.F. = 3.58), which is more than the original specified safety factor (S.F. = 3). Therefore, the designed part is safety to use.

In addition, the maximum displacement of left engine-frame support is 0.266 mm which occurred between the contact surface of left engine-frame support and the frame as shown in Figure 4.12, which it is much lesser displacement value when compared to the minimum thickness of the steel plate that used for the left engine-frame support (Thickness is 10mm). Therefore, the design of left engine-frame support is safe to apply loading condition.

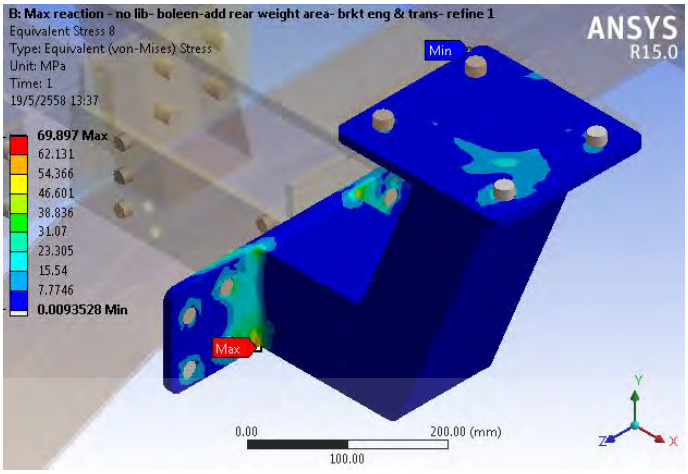

Figure 4.10 Von Mises stress of left engine-frame support

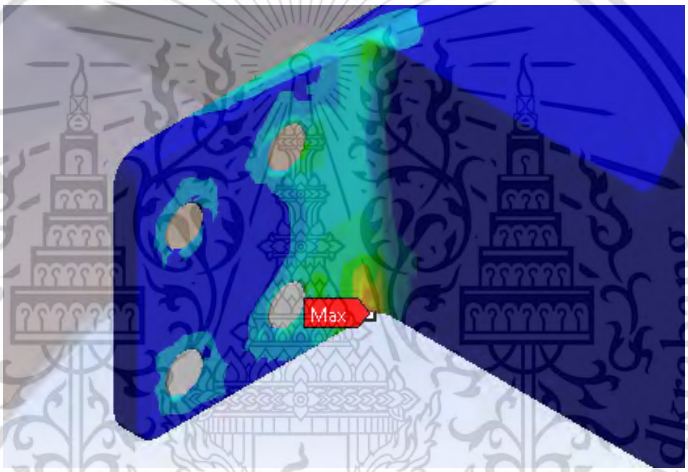

Figure 4.11 Von Mises stress of left engine-frame support (Enlarge view)

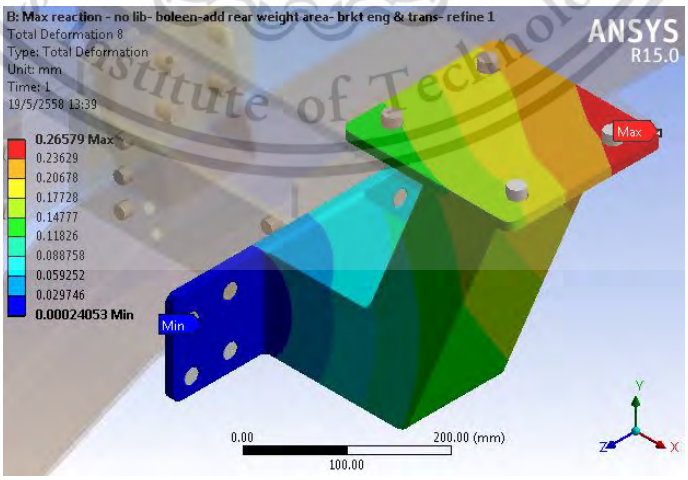

Figure 4.12 Displacement of left engine-frame support

4.1.2.4 Strength Analysis Result of Right Engine-Frame Support

From Figure 4.13 and Figure 4.14, the maximum Von Mises stress of the right engine-frame support is 82.86 MPa at around the wielding line near the bottom left hole where is for the assemble by bolt and nut to fasten the support with the engine. The minimum Von Mises stress is 0.008 MPa at around the bottom of L-shape of right engine-frame support.

When considering the failure criterion theory, as respecting to the specified designed safety factor is equal or more than 3 (S.F. $\geq$ 3), the maximum Von Mises stress is 82.86 MPa (σ_{von} = 82.86 MPa), which is less than the yield strength of steel 3.02 (S_y = 250 MPa), it represented the safety factor at 3.02 (S.F. = 3.02), which is more than original specified safety factor (S.F. = 3). Therefore, the designed part is safety to use.

In addition, the maximum displacement of right engine-frame support is 0.196 mm which occurred between the contact surface of right engine-frame support and the frame as shown in Figure 4.15, which it is much lesser displacement value when compared to the minimum thickness of the steel plate that used for the right engine-frame support (Thickness is 10mm). Therefore, the design of right engine-frame support is safe to apply loading condition.

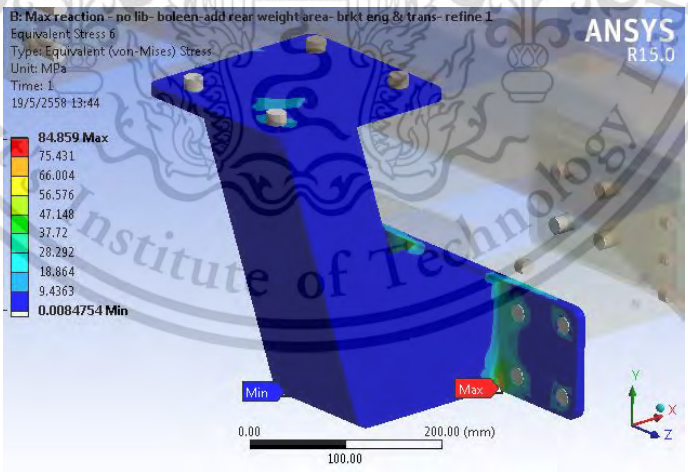

Figure 4.13 Von Mises stress of right engine-frame support

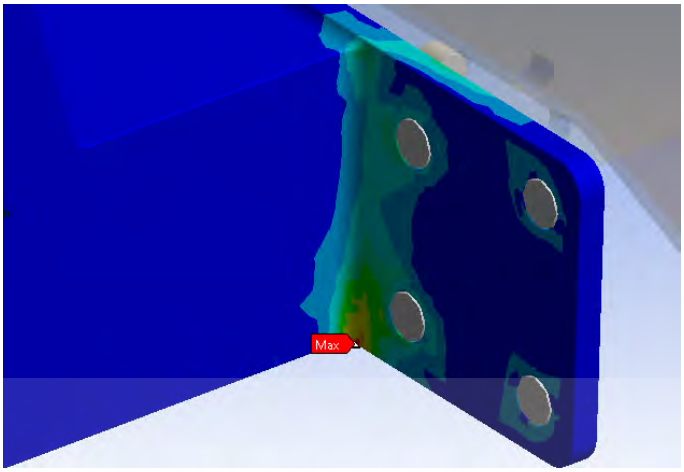

Figure 4.14 Von Mises stress of right engine-frame support (Enlarge view)

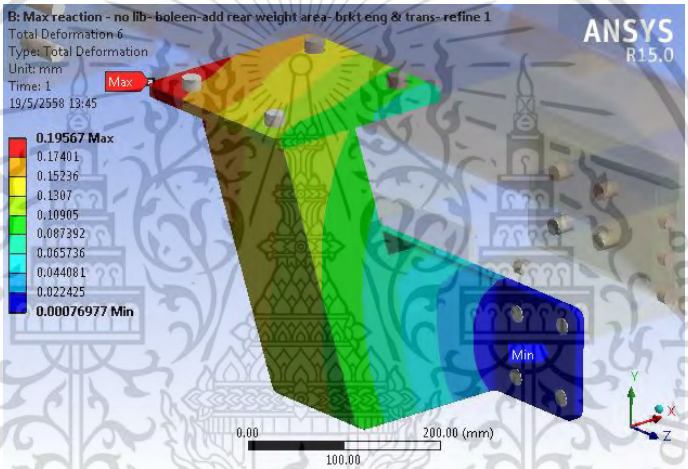

Figure 4.15 Displacement of right engine-frame support

4.1.2.5 Strength Analysis Result of Counter Weight Support

From Figure 4.16 and Figure 4.17, the maximum Von Mises stress of the counter weight support is 68.86 MPa at around the wielding line near the upper right hole where is assembled with bolt and nut to fasten the counter weight support with the engine. The minimum Von Mises stress is 0.003 at around the wielding line near the upper left hole where is for assemble by bolt and nut to fasten the counter weight support with engine.

When considering the failure criterion theory, as respecting to the specified designed safety factor is equal or more than 3 (S.F. $\geq$ 3), the maximum Von Mises stress is 68.86 MPa (σ_{von} = 68.86 MPa), which is less than the yield strength of steel ss400 (S_y = 250 MPa), it represented the safety factor at 3.63 (S.F. = 3.63), which is

more than the original specified safety factor (S.F. = 3). Therefore, the designed part is safety to use.

In addition, the maximum displacement of counter weight support is 0.172 mm which occurred between the contact surfaces of counter weight that taking the load of 1,100 kg as shown in Figure 4.18, which it is much lesser displacement value when compared to the minimum thickness of the steel plate that used for the counter weight support (Thickness is 10mm). Therefore, the design of counter weight support is safe to apply loading condition.

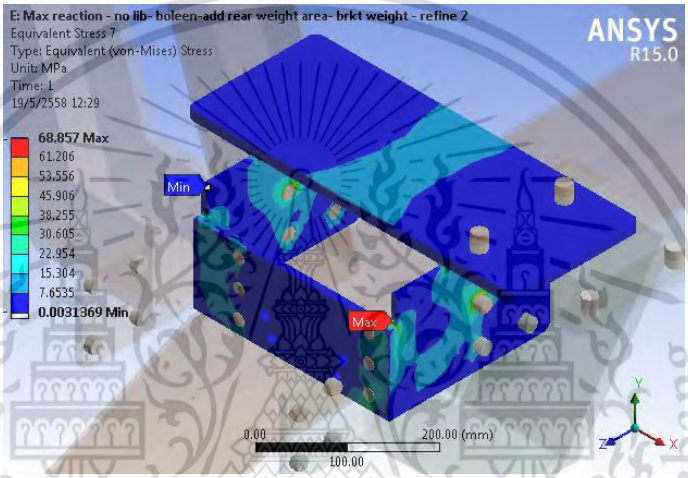

Figure 4.16 Von Mises stress of counter weight support

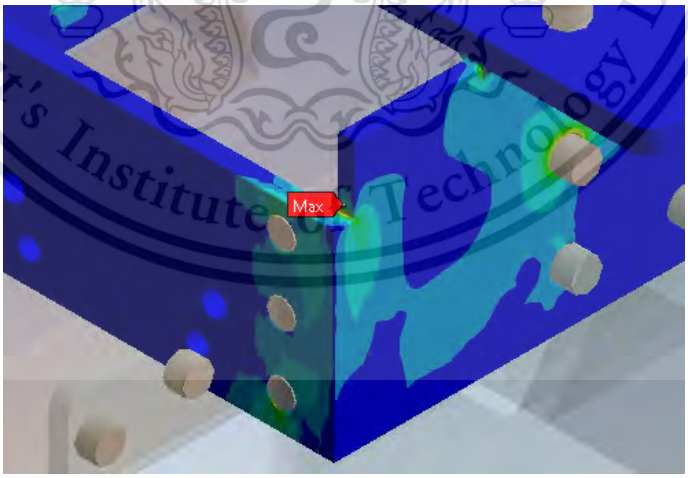

Figure 4.17 Von Mises stress of counter weight support (Enlarge view)

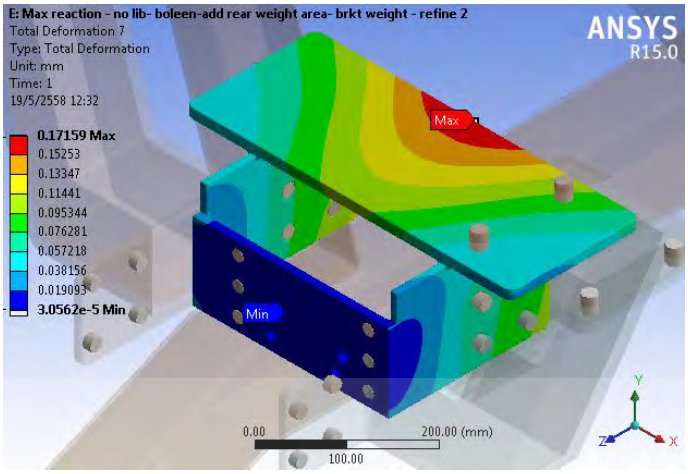

Figure 4.18 Displacement of counter weight support

4.1.2.6 Strength Analysis Result of Front Cross Member

From Figure 4.19 and Figure 4.20, front cross member contains 3.27 MPa of maximum Von Mises stress at the inner area of the hole for bolt and nut attachment, which connects with the frame, and contains 0.015 MPa of minimum Von Mises stress at the outer area of the hole which connects with front cross member.

Considering to Von Mises stress theory, the specific chosen designed safety factor is equal or more than 3 (S.F. $\geq$ 3), the maximum Von Mises stress is 3.27 MPa (σ_{von} = 3.27MPa) which is much lesser than the yield strength of steel SS400 (S_y = 250 MPa). Therefore, the calculated value of safety factor is 76.45 (S.F = 76.45), which is much more than the original specified safety factor (S.F. =3), which mean that the designed part is safety to use.

In addition, the maximum displacement of front cross member is 0.057 mm which occurred around the crease near the hole that will be attached with bolt and nut as shown in Figure 4.21, and it is much lesser displacement value when compared to the minimum thickness of the steel plate that used for the front cross member (Thickness is 12 mm). Therefore, the design of the front cross member is safe to apply loading condition.

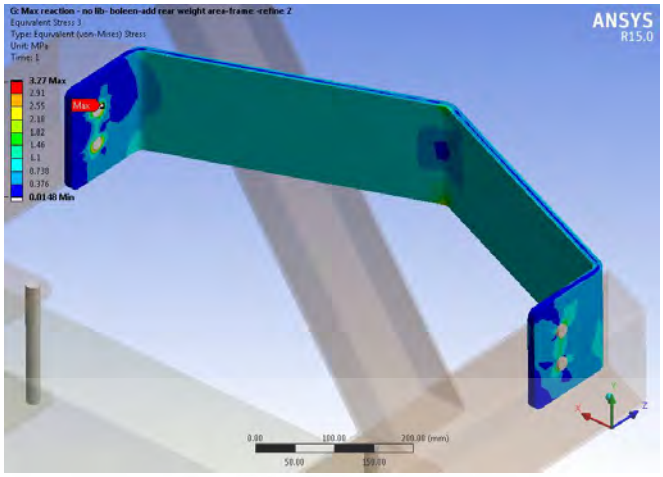

Figure 4.19 Von Mises stress of front cross member

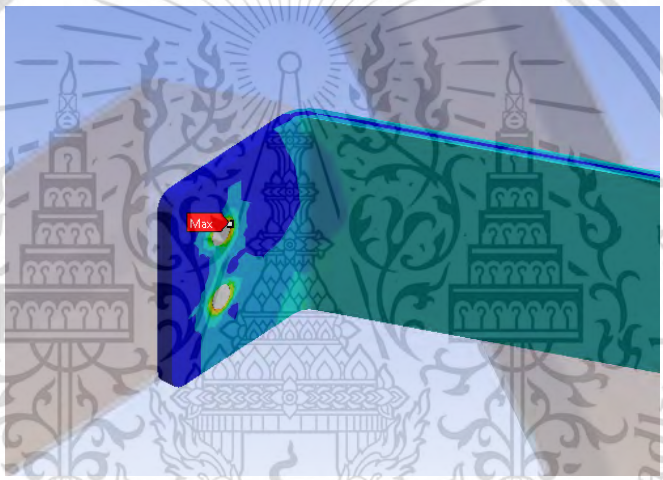

Figure 4.20 Von Mises stress of front cross member (Enlarge view)

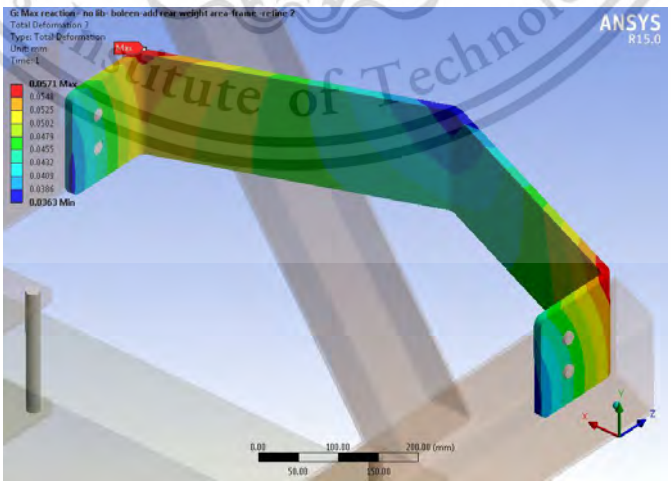

Figure 4.21 Displacement of front cross member

4.1.2.7 Strength Analysis Result of Counter Weight Belt

From Figure 4.22 and Figure 4.23, the maximum Von Mises stress of the counter weight belt is 41.35 MPa at around the hole that will be assembled to the frame by a bolt and nut and the minimum Von Mises stress around the hole that will be assembled to the frame with a bolt and nut is 0.008 MPa.

When considering the failure criterion theory, as respecting to the specified designed safety factor is equal or more than 3 (S.F. $\geq$ 3), the maximum Von Mises stress is 41.35 MPa (σ_{von} = 41.35 MPa), which is smaller than the yield strength of steel ss400 (S_y = 250 MPa), it represented the safety factor at 6.05 (S.F. = 6.05) which is more than the specified designed safety factor (S.F. =3), which mean that the designed part is safety to use.

Future more, the maximum displacement is 1.079 mm which occurred in the middle of the designed part around the crease area as shown in Figure 4.24, which it is much lesser displacement value when compared to the minimum thickness of the steel plate that used for the counter weight belt (Thickness is 12 mm). Therefore, the design of the counter weight belt is safe to apply loading condition.

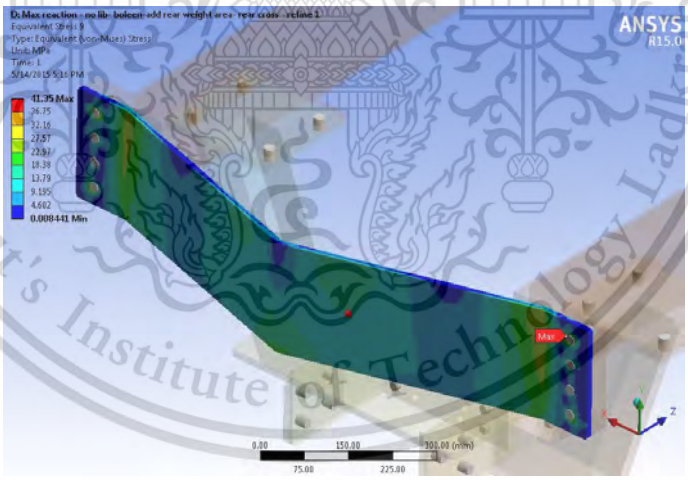

Figure 4.22 Von Mises stress of counter weight belt

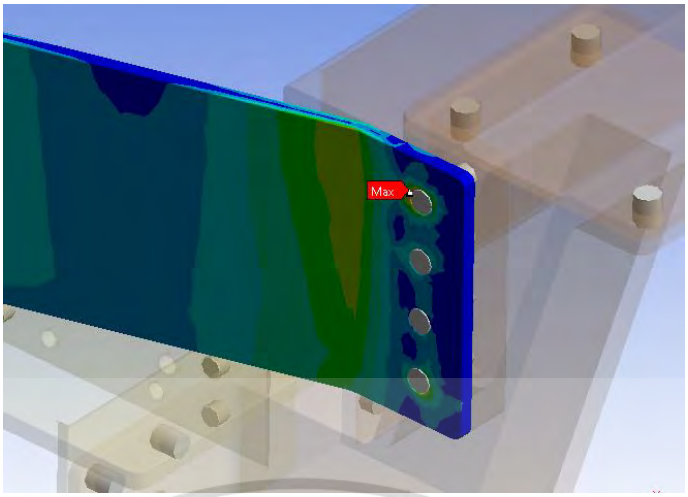

Figure 4.23 Von Mises stress of counter weight belt (Enlarge view)

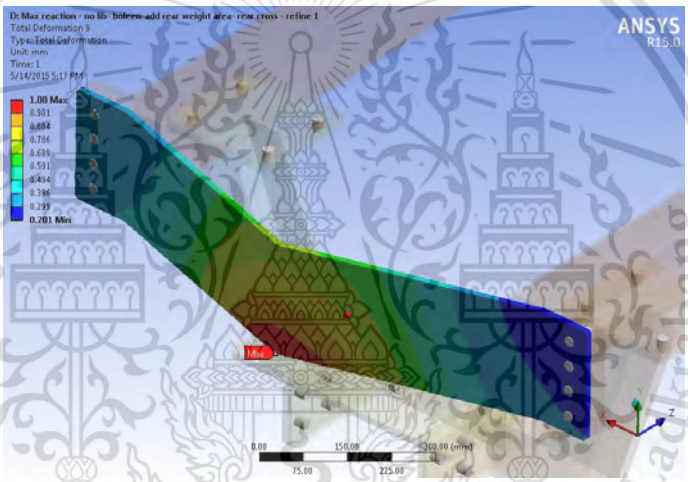

Figure 4.24 Displacement of counter weight belt

4.1.2.8 Strength Analysis Result of Frame

From Figure 4.25, the maximum Von Mises stress of the frame is 249.92 MPa acting at hydraulic cylinder mounting lug, and the minimum Von Mises stress is 0.027 at around the area that taking the force from the hydraulic cylinder.

When considering the failure criterion theory, as respecting to the specified designed safety factor is equal or more than 3 (S.F. $\geq$ 3), the maximum Von Mises stress is 249.92 MPa (σ_{von} = 249.92 MPa), which is very closed to the yield strength of steel ss400 (S_y = 250 MPa), it represented the safety factor at 1.00 (S.F. = 1.00) which is less than the specified designed safety factor (S.F. = 3). Therefore, the designed frame is not safe enough to use and it needs to be improved strength.

Future more, the maximum displacement of frame has is 0.661 mm which occurred around the area that taking the force from the hydraulic cylinder as well as the maximum stress and the minimum displacement that occurred around the contact between the frame and rigid beam is 0.00086 mm as shown in Figure 4.26.

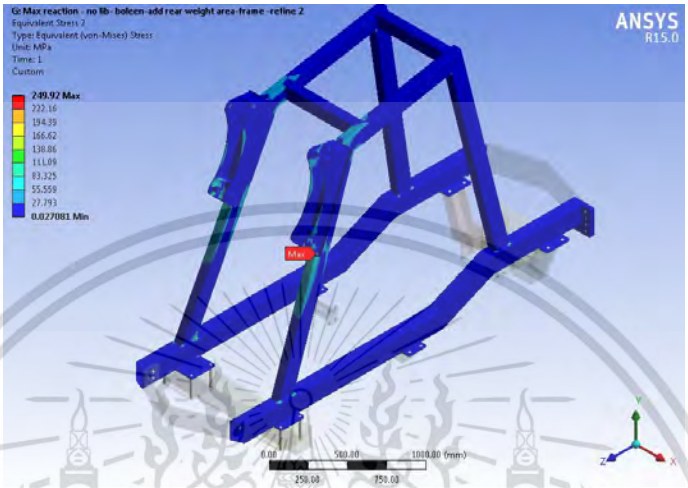

Figure 4.25 Von Mises stress of frame

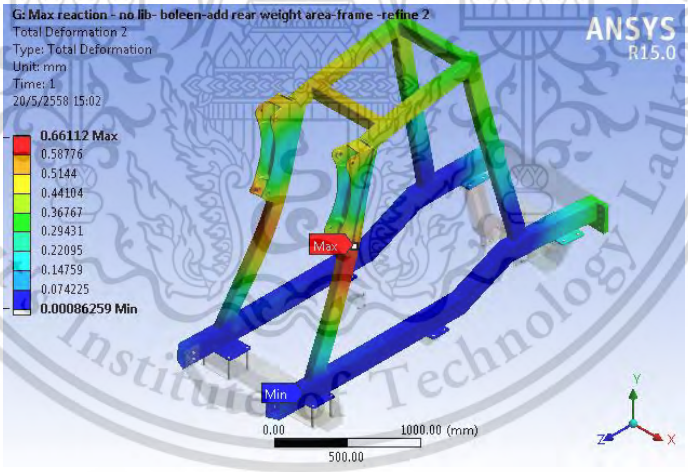

Figure 4.26 Displacement of frame

Moreover, when considering the other areas of frame, there are many of them that contain the safety factor less than the specific designed value (S.F. = 3). In other words, they contain the Von Mises stress more than 83.33 MPa at position number 1-13 which around at the hydraulic cylinder mounting lug and around welding joint of the frame From Figure 4.27, the Von Mises stress of frame on critical points number 1-13 are 105.10 MPa, 249.92 MPa, 118.12 MPa, 110.32 MPa, 151.09 MPa, 157.04

MPa, 140.21 MPa, 89.42 MPa, 116.11 MPa, 163.05 MPa, 171.22 MPa, 146.78 MPa and 185.01 MPa respectively. In other words, the safety factor of frame at critical points number 1-13 are 2.38, 1.00, 2.12, 2.27, 1.65, 1.59, 1.78, 2.80, 2.15, 1.53, 1.46, 1.70 and 1.35 respectively. Therefore, the frame needs to be modified at critical point, number 1-13 to reduce Von Mises stress.

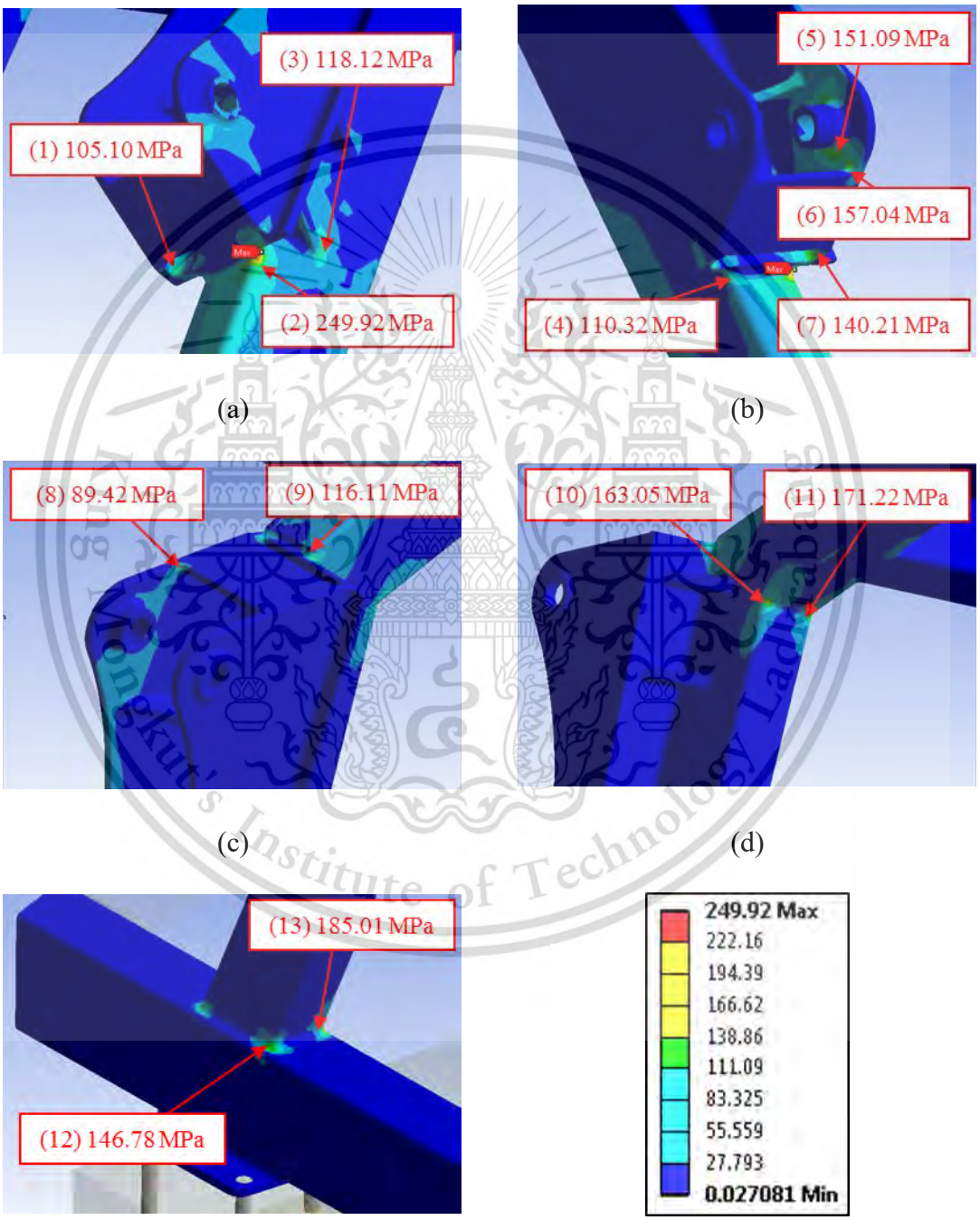

Figure 4.27 Von Mises stress of frame at critical points number 1-13

4.1.3 Summary of Strength Analysis Result of Sugarcane Loader Structure

From Table 4.1, the safety factor of Loader arm, Left transmission-frame support, Right transmission-frame support, Left engine-frame support, Right engine - frame support, Counter weight support, Front cross member and Counter weight belt are 3.59, 15.01, 13.96, 3.58, 3.02, 3.63, 76.54 and 6.05 respectively, which are more than specified safety designed factor (S.F. = 3), It means those designed component are safe with safety factor more than 3.

Despite the designed frame, the safety factor is only 1 (S.F. = 1), which is less than the specified safety designed factor (S.F. = 3) Therefore, it is not safe and needs to be modified to reduce stress. Moreover, there are 13 critical points on the frame, which safety factor is less than 3, as shown in Figure 4.28 and Table 4.2. Therefore, the frame needs to be modified in all critical points to suit the design criterion, which is will be explained in chapter 4.3; strength improvement of frame.

Table 4.1 Summary of strength analysis of sugarcane loader structure

Component	Yield strength (MPa)	Max stress (MPa)	Safety factor (S.F.)	Status
1. Loader arm	250	69.68	3.59	Safe
2. Loader structure				
2.1 Left transmission-frame support	250	16.66	15.01	Safe
2.2 Right transmission-frame support	250	17.91	13.96	Safe
2.3 Left engine-frame support	250	69.89	3.58	Safe
2.4 Right engine-frame support	250	82.86	3.02	Safe
2.5 Counterbalance weight support	250	68.86	3.63	Safe

Table 4.1 Summary of strength analysis result of sugarcane loader structure (cont.)

Component	Yield strength (MPa)	Max stress (MPa)	Safety factor (S.F.)	Status
2.6 Front cross member	250	3.27	76.45	Safe
2.7 Counterbalance weight belt	250	41.35	6.05	Safe
2.8 Frame	250	249.92	1.00	Not safe

Table 4.2 Summary of strength analysis result of frame on critical point 1-13

Critical point	Von Mises stress (MPa)	Safety factor (S.F.)
1	105.10	2.38
2	249.92	1.00
3	118.12	2.12
4	110.32	2.27
5	151.09	1.65
6	157.04	1.59
7	140.21	1.78
8	89.42	2.80
9	116.11	2.15
10	163.05	1.53
11	171.22	1.46
12	146.78	1.70
13	185.01	1.35

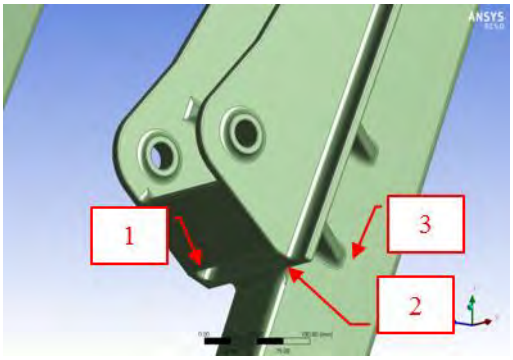

(a)

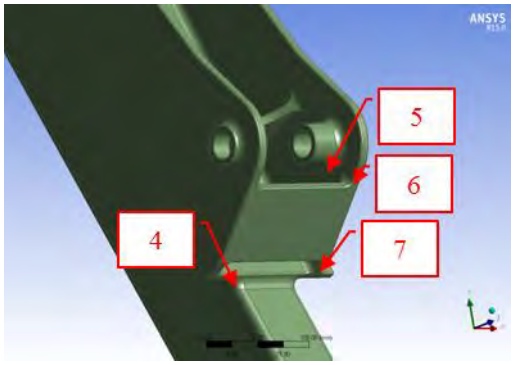

(b)

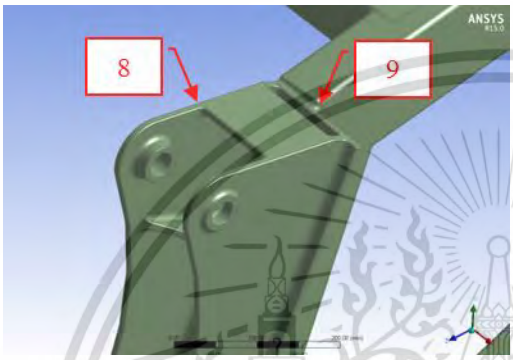

(c)

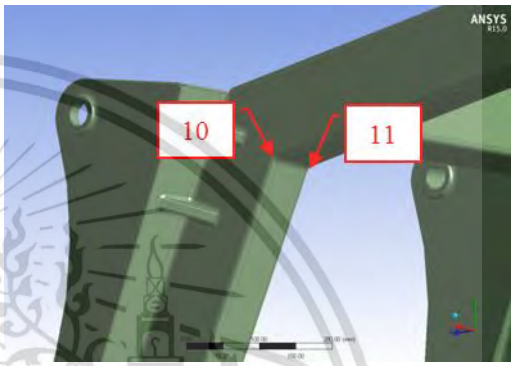

(d)

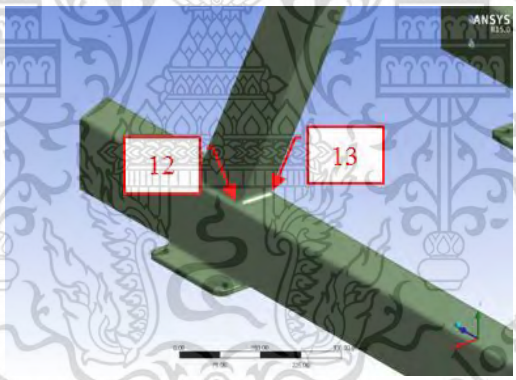

(e)

Figure 4.28 Critical points of frame

4.2 Simple Finite Element Model of Loader Structure

From chapter 4.1.2; strength analysis of the loader structure by Finite Element Method, the frame which is one of the parts in the loader structure is not safe to use. In other words, there are 13 critical points which the safety factor is less than 3 (S.F. < 3)**.** Therefore, it will be improve the safety factor of the frame to be more than 3 (S.F. ≥ 3) in chapter 4.3, strength improvement of frame.

As more computational time of Finite Element model of loader structure and the frame is only one of the parts in the loader structure which needs to be modified. Therefore, to decrease the evaluation time of the huge 3D computer model, and the complexity of boundary conditions specification in ANAYS software, the boundary conditions must be changed. As to assume that the virtual frame is places on the rigid object, and has no frame supports, the change of the boundary conditions may affect the precision of the results. Therefore, there must be comparability of strength analysis results between the completed Finite Element model of loader structure with the simple Finite Element model of loader structure first, if it can be replaceable.

4.2.1 Strength Analysis of Simple Finite Element Model of Loader Structure

4.2.1.1 Computer Modeling

Computer modeling of strength analysis of the simple Finite Element model loader structure is only focusing on the frame. For the other parts: Front cross member, Counter weight belt, Right engine-frame support, Right engine-frame support, Right transmission-frame support, Right transmission-frame support, Counter weight support, Right Plate, Left Plate, and Rigid beam are suppressed as shown in Figure 4.29.

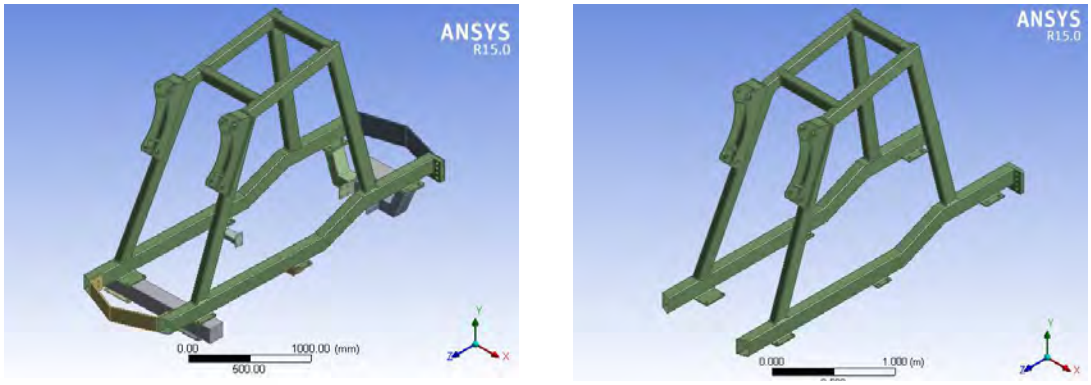

(a) (b)

Figure 4.29 Geometry of loader structure, (a) completed FE model, (b) simple FE model

4.2.1.2 Meshing and Element

Assign the element to be tetrahedral element with minimum element size 2.5 mm as same as the completed Finite Element model of loader structure in chapter 3.4.2. But the amount of nodes is drop from 730,704 nodes to 521,020 nodes, and the amount of elements is drop from 463,374 elements to 307,759 elements.

4.2.1.3 Boundary Conditions

Assign 4 main loads to the boundary condition as same as the completed Finite Element model of loader structure in chapter 3.4.2:

1) Longitudinal load from weight of body parts, 100kg is applied on the frame by Point mass feature in ANSYS.

2) Load from weight of the counter weight, 1,100 kg is applied at the attached point of the counter weight to the frame by Point mass feature in ANSYS.

3) Force at point A is 55,373 N, and point B is 65,829 N which are applied by Force feature in ANSYS.

4) Gravitational acceleration is 9.81 m/s^2 which acting to the whole parts

And summary of the loadings are shown in Figure 4.30. In addition, the simple Finite Element model of loader structure is assigned to be attached by fixed supports at the surface contact area between the Frame and Supports. In other words, there are no movement and no rotation in X, Y, and Z axis as the whole Frame, is placed on a rigid object. And as the simple Finite Element model of loader structure is only the

Frame, therefore, there are no contact condition and no virtual fastener (by beam-contact feature) between components as shown in Figure 4.31.

(a) (b)

Figure 4.30 Loadings of loader structure, (a) completed FE model, (b) simple FE model

(a) (b)

Figure 4.31 Constraints of loader structure, (a) completed FE model, (b) simple FE model

4.2.1.3 Material Properties

Assigned ss400 carbon steel, which its behavior is acting as linear elastic, and contains mechanical properties as same as the completed Finite Element model of loader structure in chapter 3.4.2. And it is shown in Table 4.3.

Table 4.3 Material Properties of ss400 carbon steel

Density (kg/m^3)	Young modulus (GPa)	Poisson's ratio	Yield strength (MPa)
7,850	205	0.29	250

4.2.2 Comparison of Strength Analysis Result between Completed Finite Element Model and Simple Finite Element Model of Loader Structure

When compare maximum Von Mises stress that occurred on the completed FE model of loader structure model with the simple FE model, the values are 249.92 MPa and 248.26 MPa respectively and the maximum Von Mises stress is occurred at the attached area of the hydraulic cylinder with the loader arm at the same point as shown in Figure 4.32. Which the values are really closed with each other; it is only 0.66% of deviation as shown in Table 4.4.

When compare the maximum deformation that occurred on the completed FE model of loader structure and the simple FE model, the values are 0.66 mm and 0.61 mm respectively and the maximum deformation is occurred at the attached area of the hydraulic cylinder with the loader arm at the similar point as shown in Figure 4.33. Which the values are closed to each other; it is only 7.58% of deviation as shown in Table 4.4.

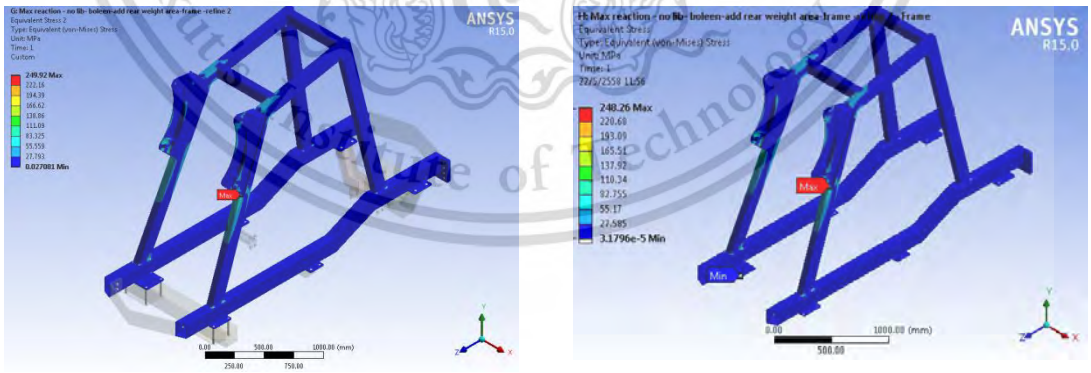

(a) (b)

Figure 4.32 Maximum Von Mises stress of loader structure,
(a) completed FE model, (b) simple FE model

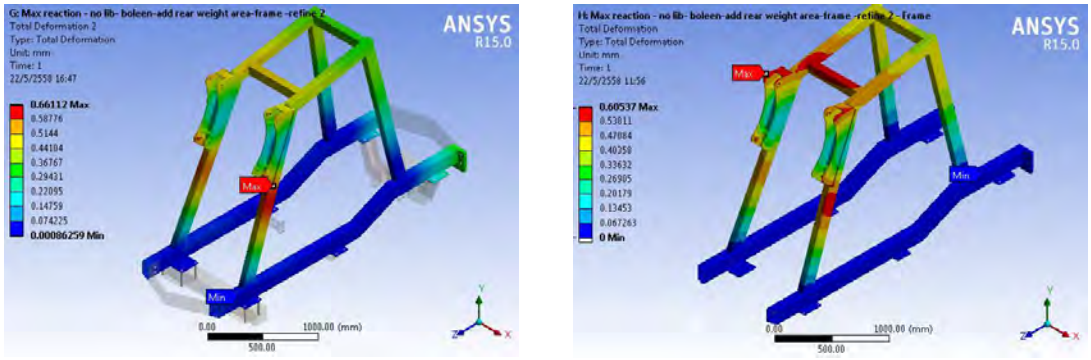

(a) (b)

Figure 4.33 Maximum deformation of loader structure,
(a) completed FE model, (b) simple FE model

Table 4.4 Deviations of maximum stress and maximum deformation

Loader structure	Completed EE Model	Simple FE Model	Deviation (%)
Maximum Von Mises (MPa)	249.92	248.26	0.66
Maximum deformation (mm)	0.66	0.61	7.58

From Figure 4.34, When compare the maximum Von Mises stress that occurred on the completed FE model of loader structure with the simple FE model at critical point number 1-13 of frame (the points are shown in Figure 4.35) where they need to be improved the strength of the frame, because they need extra attention and they are sensitive to the changes, there are a very similar trend of the stress between the completed and the simple FE model. The deviations of the stress on critical points number 1-13 are 4.97%, 0.66%, 4.31%, 0.15%, 7.43%, 0.29%, 0.57%, 10.74%, 1.81%, 2.52%, 2.42%, 5.85% and 6.18% respectively as shown in Table 4.5, which the results are small of deviation or really closed to each other, and there only some differences in some points.

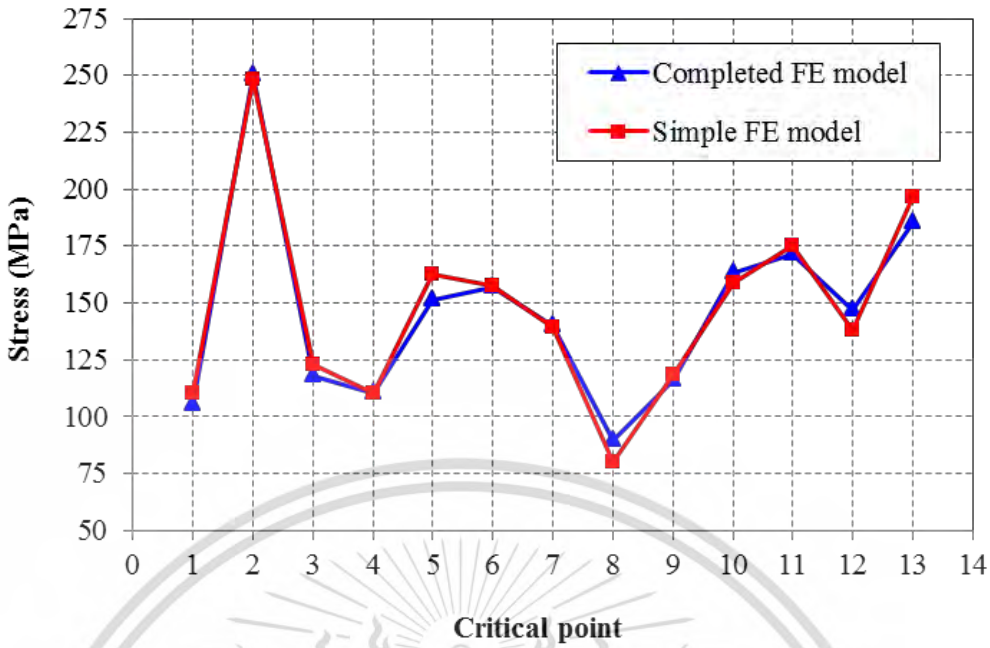

Figure 4.34 Comparison of Von Mises stresses on critical points of frame between completed FE model with simple FE model

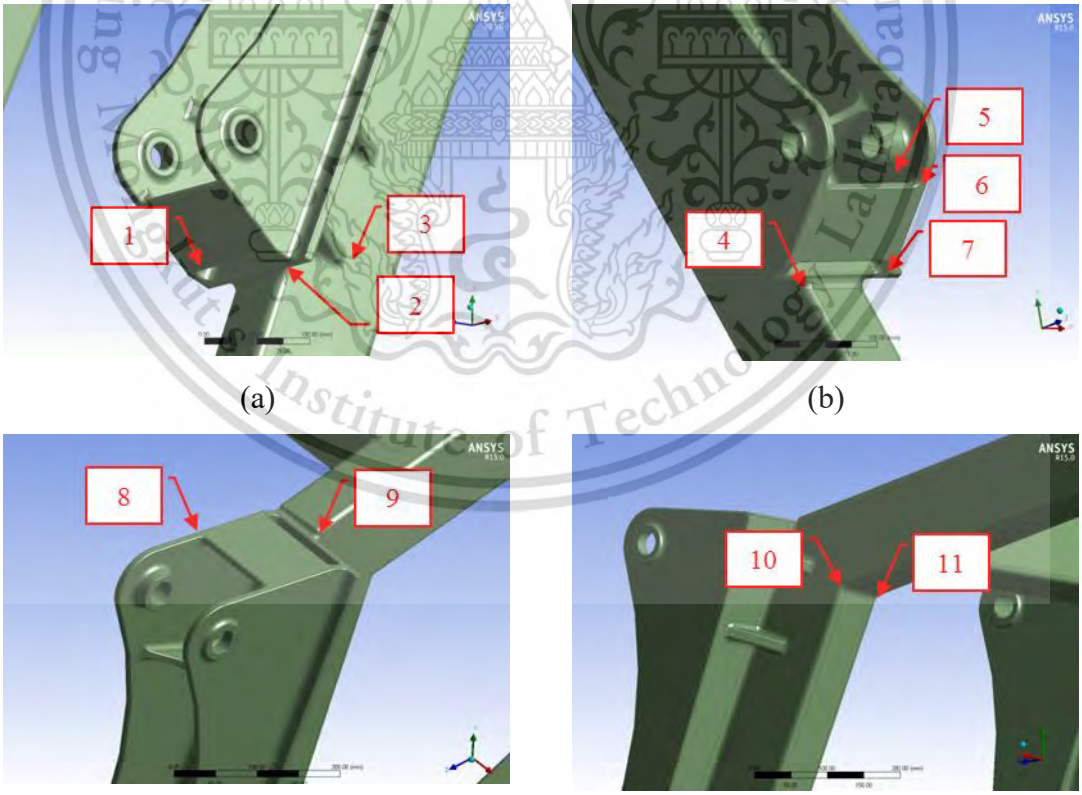

(a) (b)

(c) (d)

Figure 4.35 Critical points of frame

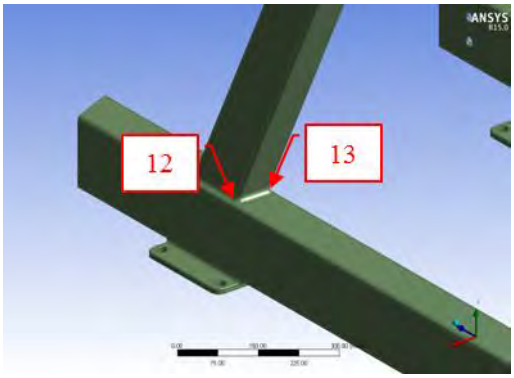

(e)

Figure 4.35 Critical points of frame (cont.)

Table 4.5 Deviations of Von Mises stress on critical points of frame

Critical point	Von Mises stress (MPa)		Deviation (%)
	Completed EE Model	Simple FE Model	
1	105.10	110.32	4.97
2	249.92	248.26	0.66
3	118.12	123.21	4.31
4	110.32	110.48	0.15
5	151.09	162.32	7.43
6	157.04	157.49	0.29
7	140.21	139.41	0.57
8	89.42	79.82	10.74
9	116.11	118.21	1.81
10	163.05	158.94	2.52
11	171.22	175.36	2.42
12	146.78	138.2	5.85
13	185.01	196.44	6.18

From the above comparison values of maximum Von Mises stress, maximum deformation, and Von Mises stress at critical point number 1-13, where it needs to be improved the strength of both completed FE model of loader structure and the simple FE model, the values are really closed to each other and small of deviation. Therefore, the strength analysis of the simple FE model can be considered as it can be substituted instead of the completed FE model of loader structure. Finally, CPU time of FEA is reduced from 6,189.2 seconds (Completed FE model) to 900.4 seconds (Simple FE model), which CPU time is decreased 85.45%. Moreover, the specifications of used workstation computer for FEA simulation are shown in Table 4.6.

Table 4.6 Specifications of used computer for FEA simulation

Item	Specification
Processor model	Intel Xeon (W3550) 3.07GHz
Number of CPU cores	4 Cores
Physical memory (RAM)	24 GB
Graphic card	NVIDIA Quadro 2000 1GB GDDR5
Operating system	Windows 7x64

Regarding to the CPU time of the simple FE model of loader structure was reduced down to 85.45%. There are two possible reasons to explain that why the CPU time is decreased significantly. The first reason is the reduced number of nodes, and the second reason is nonlinear simulation due to contact nonlinearity.

The first reason is the reduced number of nodes. As the simple FE model of loader structure consists of the frame only, which the transmission-frame support, the engine-frame support, the counter weight support, counter weight and front cross-member were suppressed, therefore number of total nodes is reduced from 730,704 to 521,020 nodes and number of total elements is also reduced from 463,374 to 307,759 elements. As the number of nodes is decreased, it means the unknowns of displacement (unknowns of nodal displacement) are also decreased. Therefore, the size of equilibrium equation, equation (4.1) is decreased too. According to the size of

equilibrium equation is decreased, thus the time to complete a simulation is also decreased. That is how simulation time of simple FE model of loader structure is reduced.

Nonlinear equilibrium equation,

$$[K(D)]\{D\} = \{F\} \tag{4.1}$$

Where,

$\{F\}$ is the external force acting on the nodes (Nodal force)

$\{D\}$ is the displacement of the nodes (Nodal displacement)

$[K(D)]$ is the stiffness matrix of structure

As the first reason, the total number of nodes of the simple FE model is reduced 28.70% from the completed FE model but the CPU time is reduced up to 85.45% which the percent decrease of the number of nodes and the decrease percent of CPU time are inconsistent. It clearly means there are other factors related to the reduction of CPU time. The other possible factor is contact nonlinearity.

For the second reason is nonlinear simulation due to contact nonlinearity. The completed FE model of loader structure consists of frame, transmission-frame support, engine-frame support, counter weight support, counter weight and front cross-member where each component is connected by nut and bolt. Two faces of each component are free to separate in their normal direction and also sliding in their tangential direction. To simulate the fasteners, the beam-contact feature in ANSYS software is applied in FE model and to obtain the separation and sliding contact between the components, the frictional-contact feature in ANSYS software is also defined in the FE model which the value of friction coefficient is 0.74. These contact type are called contact nonlinearity, which introduces nonlinear simulation. In linear simulation, the relation between nodal force $\{F\}$ and nodal displacement $\{D\}$ can be plotted as straight line which is shown in Figure 4.36 (a). The stiffness matrix [K] of linear simulation is constant and the linear equilibrium equation is shown in equation (4.2). However, in a nonlinear simulation, the relation between nodal force $\{F\}$ and nodal displacement $\{D\}$ is nonlinear which is shown in Figure 4.36 (b). The stiffness

matrix [K] of nonlinear simulation is no longer a constant, it changes with $\{D\}$, and that is, [K] is a function of {D} and the nonlinear equilibrium equation is shown in equation (4.1). Therefore, nonlinear problem becomes more difficult to solve due to complexity of equilibrium equation. In problem solving process, each time step of linear simulation requires exactly one equilibrium iteration but nonlinear simulation needs several iterations to complete. It clearly means nonlinear problem solving needs more simulation time due to size and complexity of nonlinear equilibrium equation. As the completed FE model of loader structure is simulated as nonlinear simulation due to contact nonlinearity, but the simple FE model is simulated as linear simulation. Thus, that is how CPU time of simple FE model of loader structure is decreased significantly.

Linear equilibrium equation,

$$[K]\{D\} = \{F\} \tag{4.2}$$

Where,

$\{F\}$ is the external force acting on the nodes (Nodal force)

$\{D\}$ is the displacement of the nodes (Nodal displacement)

$[K]$ is the stiffness matrix of structure

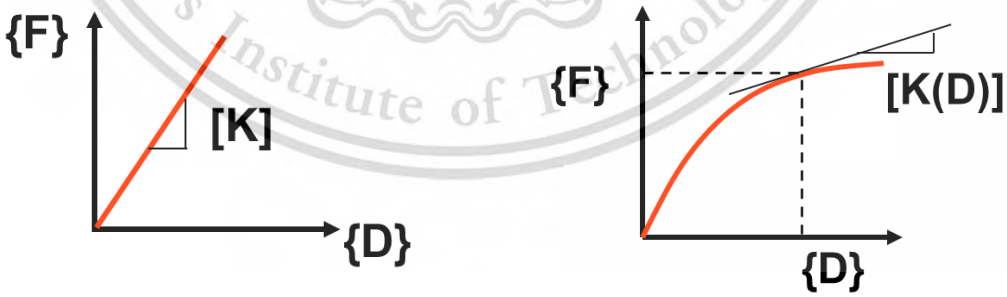

(a) (b)

Figure 4.36 (a) linear behavior, (b) nonlinear behavior

4.3 Strength Improvement of Frame by using Simple Finite Element Model

From chapter 4.2.2; the results of comparison of strength analysis of completed FE model of loader structure with the simple FE model show that the strength analysis of the simple FE model can be substituted instead the completed FE model of loader structure. Therefore, the strength development of loader structure model by Finite Element Analysis will be assigned the boundary conditions as well as the strength analysis of the simple FE model to decrease the CPU time of FEA.

To reduce the stress on critical points number 1-13 of the frame, there are two ideas of strength improvement. The first idea is adding triangle truss members to connect the lower hydraulic cylinder mounting with ladder of the frame, and the second idea is increasing the moment of inertia of section by changing the shape of the frame at critical points.

For the first idea of strength improvement, adding triangle truss members to connect the lower hydraulic cylinder mounting with ladder of the frame, this truss member will support the large deformation of the frame, transfer the hydraulic cylinder force and reduce the stress concentration. There are two sub-ideas of strength improvement. The first sub- idea, 1A, is adding side triangle truss member to connect the lower hydraulic cylinder mounting with ladder of the frame as shown in Table 4.7. The second sub-idea, 1B, is adding side triangle truss members to connect the lower hydraulic cylinder mounting with ladder of the frame as well as adding horizontal member to connect left and right side of the column of the frame at lower hydraulic cylinder mounting as shown in Table 4.7. Moreover, the cross-section of added member in sub-idea 1A and 1B is the same value as the original column of the frame, which the height is 125 mm, the width is 75 mm and thickness is 4.5 mm.

Table 4.7 Comparison of the original shapes of frame, sub-idea 1A and 1B

Name	Geometry	Von Mises stress (MPa)
Original frame (before improvement)		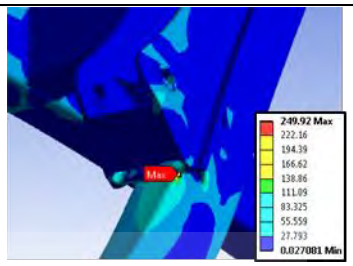
Idea 1A	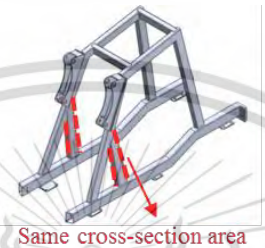 Same cross-section area	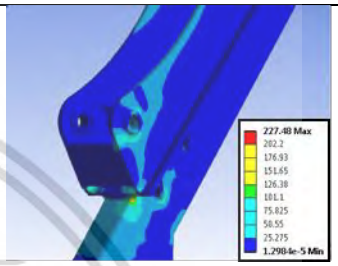
Idea 1B	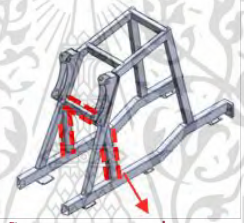 Same cross-section area	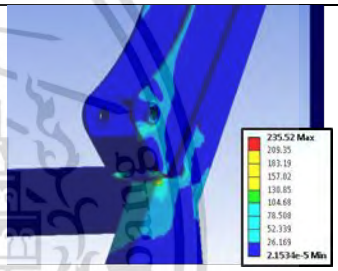

From Figure 4.37, the Von Mises stress comparison of original shapes, sub-idea 1A and sub-idea 1B at critical point number 1, 2, 3, 4 and 7, the Von Mises stresses of the sub-idea 1A are slightly decreased from the original shape. The Von Mises stresses of the sub-idea 1B are slightly also decreased from the original shape which are almost the same value as the sub-idea 1A. Moreover, the safety factors of the sub-idea 1A and the idea 1B are still lower than specific safety factor (the specific safety factor is 3, S.F. = 3), which the highest of safety factor is 2.8 as shown in Figure 4.38. These results showed that the sub-idea 1A and the idea 1B could not help to reduce stress at critical points. Therefore, shape modification of the frame by adding triangle truss member was not acceptable to use in the strength improvement of the frame.

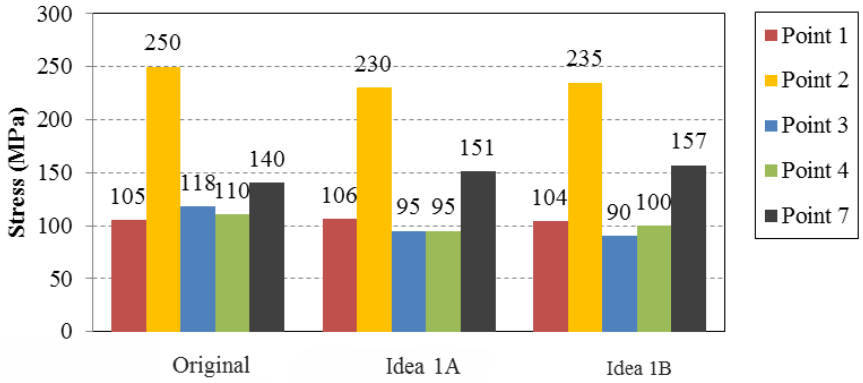

Figure 4.37 Comparison of stresses of different idea of strength improvement

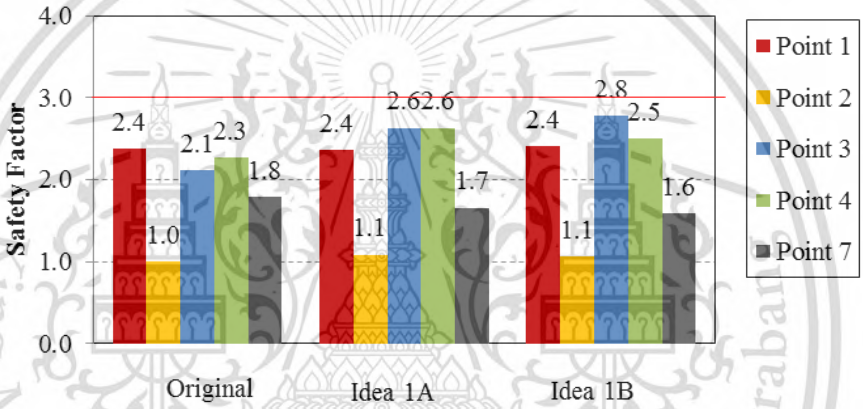

Figure 4.38 Comparison of safety factors of different idea of strength improvement

For the second idea of strength improvement, increasing the moment of inertia of section by changing the shape of frame at critical points. Regarding to the produced stresses at critical points number 1, 2, 3, 4 and 7 of the frame are bending stress which are effect from bending moment. As bending stress in equation (4.3), if moment of inertia of section is increased, bending stress will be decreased.

$$\sigma_{bending} = \frac{My}{I} \tag{4.3}$$

Where,

$\sigma_{bending}$ is Bending stress (MPa)

M is Bending moment (N.mm)

y is Height of section

I is Moment of inertia (mm^4)

As the second idea of strength improvement by increasing moment of inertia of section, there are three sub-ideas of increasing moment of inertia of section: sub-idea 2A, 2B and 2C which are shown in Table 4.8. From Figure 4.39, the Von Mises stress comparison of original shapes, sub-idea 2A, 2B and 2C at critical point number 1, 2, 3, 4 and 7, the Von Mises stresses of the sub-idea 2A are decreased from the original shape plentifully, however the safety factor of the sub-idea 2A at critical point number 2 is still lower than specific safety factor (the specific safety factor is 3, S.F. = 3), which the magnitude of the safety factor is 2.2 as shown in Figure 4.40. The Von Mises stresses of the sub-idea 2B are also decreased from the original shape plentifully, which are almost the same value as the sub-idea 2A. However, the safety factor of the idea 2B at critical point no. 2 is still lower than the specific safety factor (the specific safety factor is 3, S.F. = 3), which the magnitude of the safety factor is 2.5. Considering of the sub-idea 2C, the Von Mises stresses of the sub-idea 2C are decreased from the sub-idea 2B and the safety factor of all critical points are more than the specific safety factor (the specific safety factor is 3, S.F. = 3), which the smallest the safety factor is 4.0. These results showed that the sub-idea 2C could help to reduce stress at critical points. Therefore, shape modification of the frame by increasing moment of inertia of section was acceptable to use in the strength improvement of the frame.

Table 4.8 Comparison of the original shapes of frame, sub-idea 2A, 2B and 2C

Name	Geometry
Original frame (before improvement)	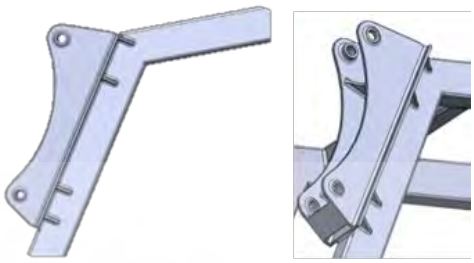
Idea 2A	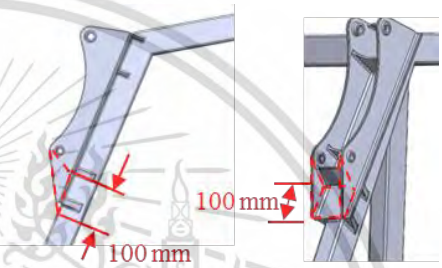
Idea 2B	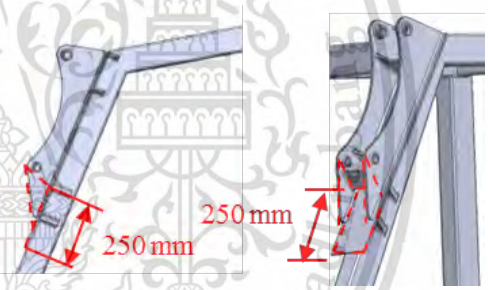
Idea 2C	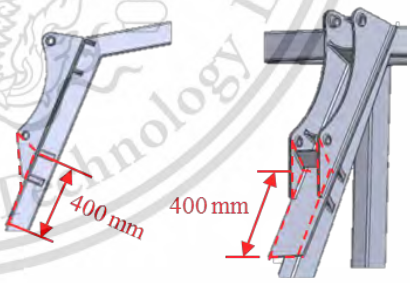

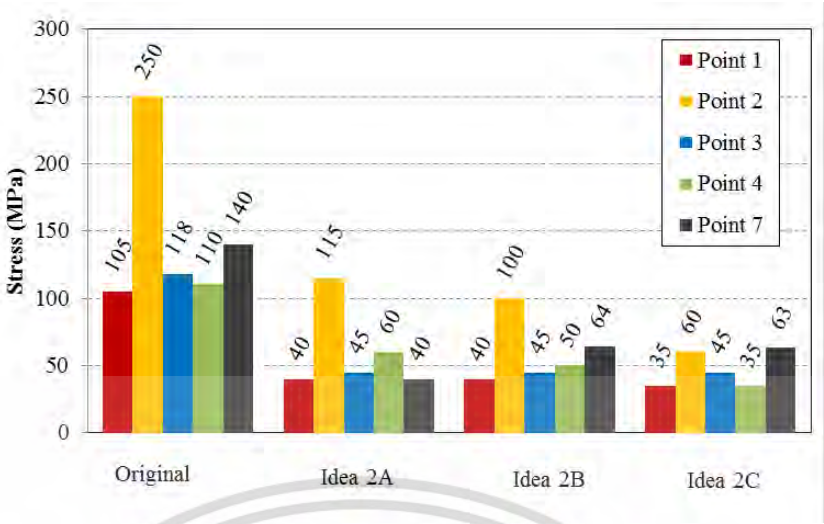

Figure 4.39 Comparison of stresses of different idea of strength improvement

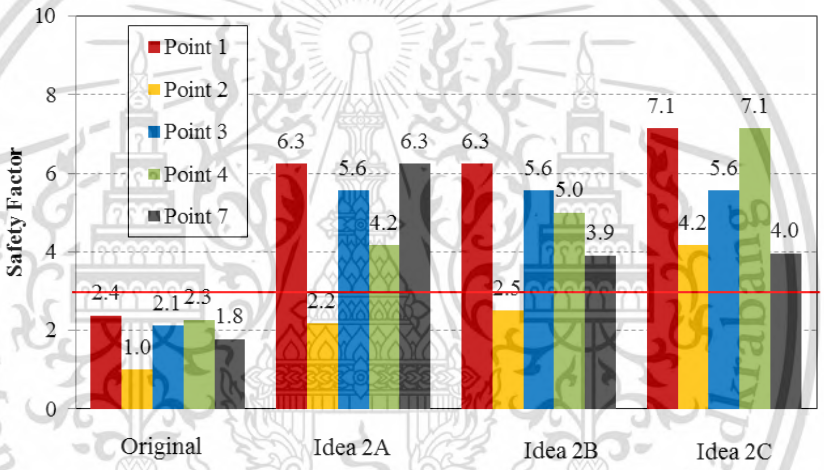

Figure 4.40 Comparison of safety factors of different idea of strength improvement

As shape modification of the frame at critical points number 1, 2, 3, 4 and 7 by increasing moment of inertia of section was acceptable to use in the strength improvement of the frame, therefore the modification of frame at other critical points are the same idea as the critical point number 1, 2, 3, 4 and 7.

To reduce stress on critical point number 1, 2, 3, 4 and 7, the loader arm supporting of the frame is modified by adding reinforcement - 1, as shown in Figure 4.41 and Figure 4.42. The Von Mises stresses on critical point number 1, 2, 3, 4 and 7 are decreased from 105.10 MPa to 40.48 MPa, 249.92 MPa to 80.26 MPa, 118.12 MPa to 42.21 MPa,, 110.32 MPa to 50.12 MPa and 140.21 MPa to 60.28 MPa respectively.

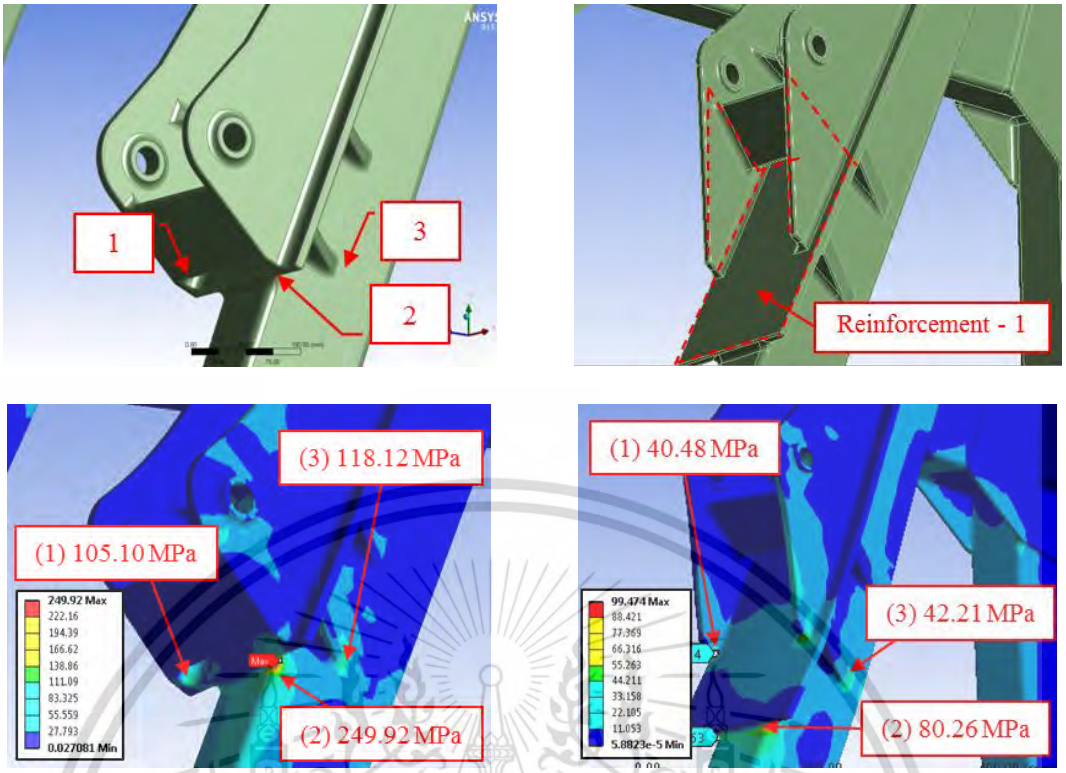

(a) (b)

Figure 4.41 Comparison of stresses of frame at critical point number 1-3, (a) before improvement, (b) after improvement

To reduce stress on critical point number 5 and 6, the lower mounting of hydraulic cylinder of the frame is modified by adding reinforcement plate - 2 (thickness of the reinforcement plate - 2 is 10 mm), as shown in Figure 4.42. The Von Mises stresses on critical point number 5 and 6 are decreased from 151.09 MPa to 59.53 MPa and 157.04 MPa to 64.61 MPa respectively.

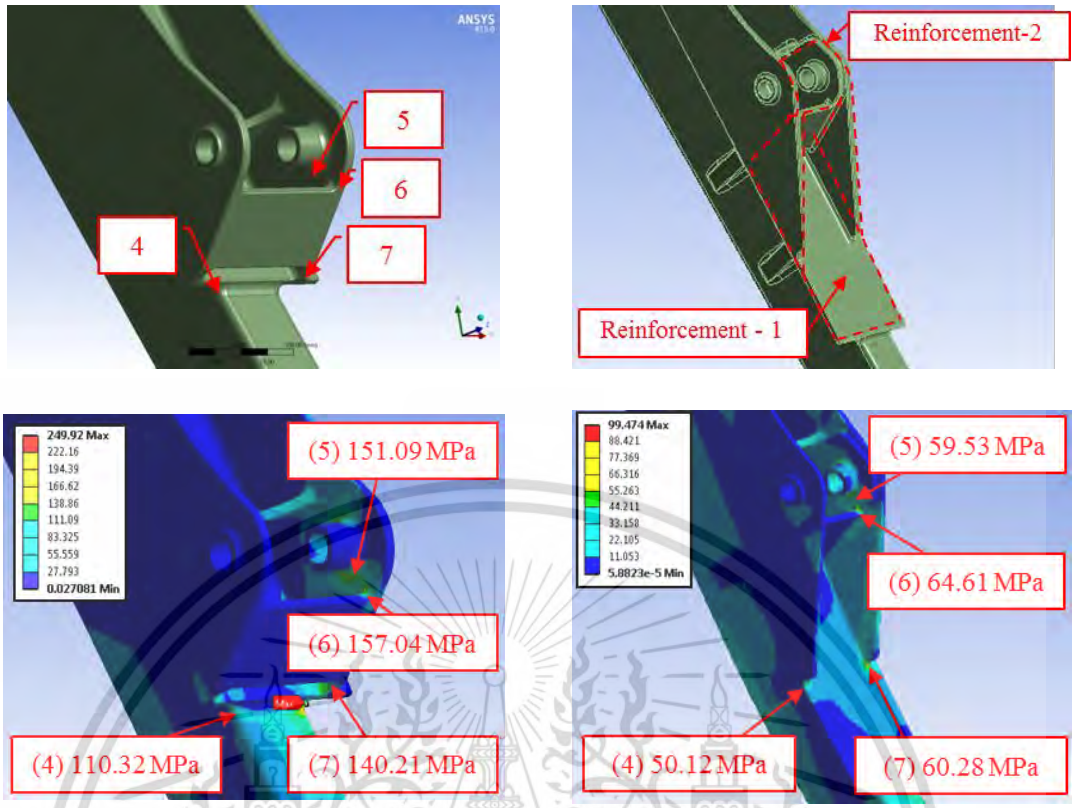

(a) (b)

Figure 4.42 Comparison of stresses of frame at critical point number 4-7, (a) before improvement, (b) after improvement

To reduce stress on critical point number 8, the upper mounting of hydraulic cylinder of the frame is modified by adding reinforcement plate - 3 (thickness of the reinforcement plate - 3 is 10 mm), as shown in Figure 4.43. The Von Mises stress on critical point number 8 is decreased from 89.42 MPa to 5.47 MPa. Moreover, to reduce stress on critical point number 9, the upper joint between the frame with the loader arm support is modified by adding reinforcement plate - 4 (thickness of reinforcement plate - 4 is 15 mm), as shown in Figure 4.43. The Von Mises stress on critical point number 9 is decreased from 116.11 MPa to 30.33 MPa.

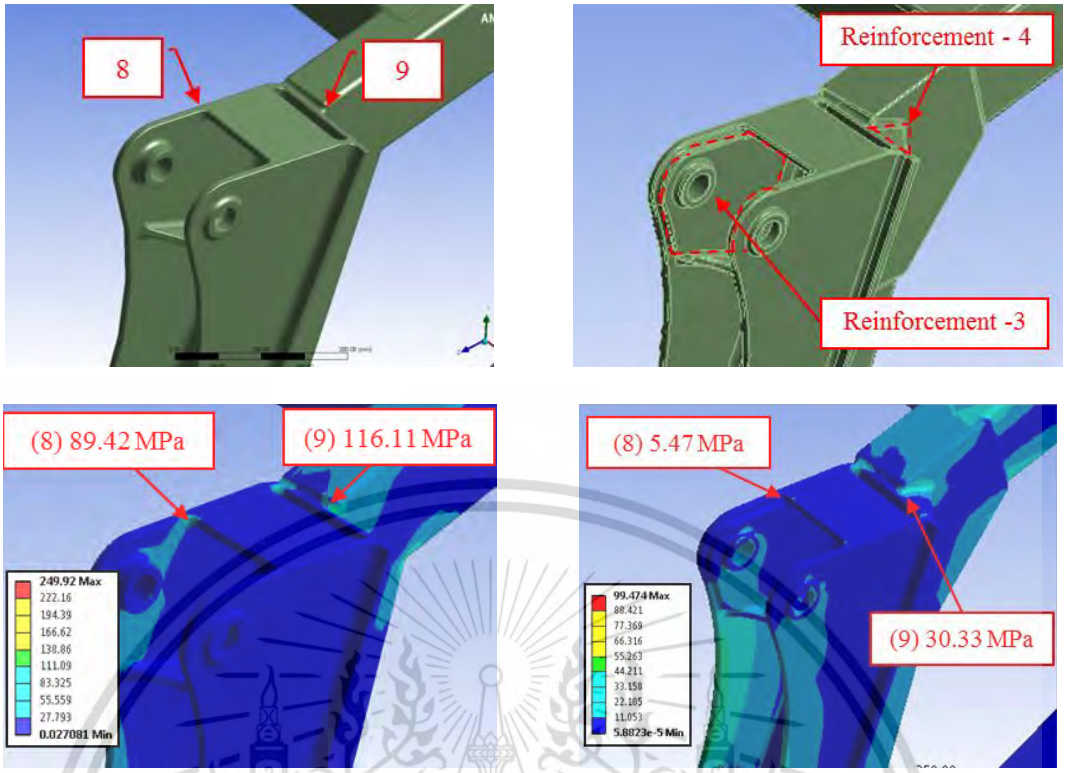

(a) (b)

Figure 4.43 Comparison of stresses of frame at critical point number 8-9, (a) before improvement, (b) after improvement

To reduce stress on critical point number 10 and 11, the upper joint of the frame is modified by adding reinforcement plates - 5 (thickness of the reinforcement plate - 5 is 6 mm), as shown in Figure 4.44. The Von Mises stresses on critical point number 10 and 11 are decreased from 163.05 MPa to 51.85 MPa and 171.22 MPa to 48.12 MPa respectively.

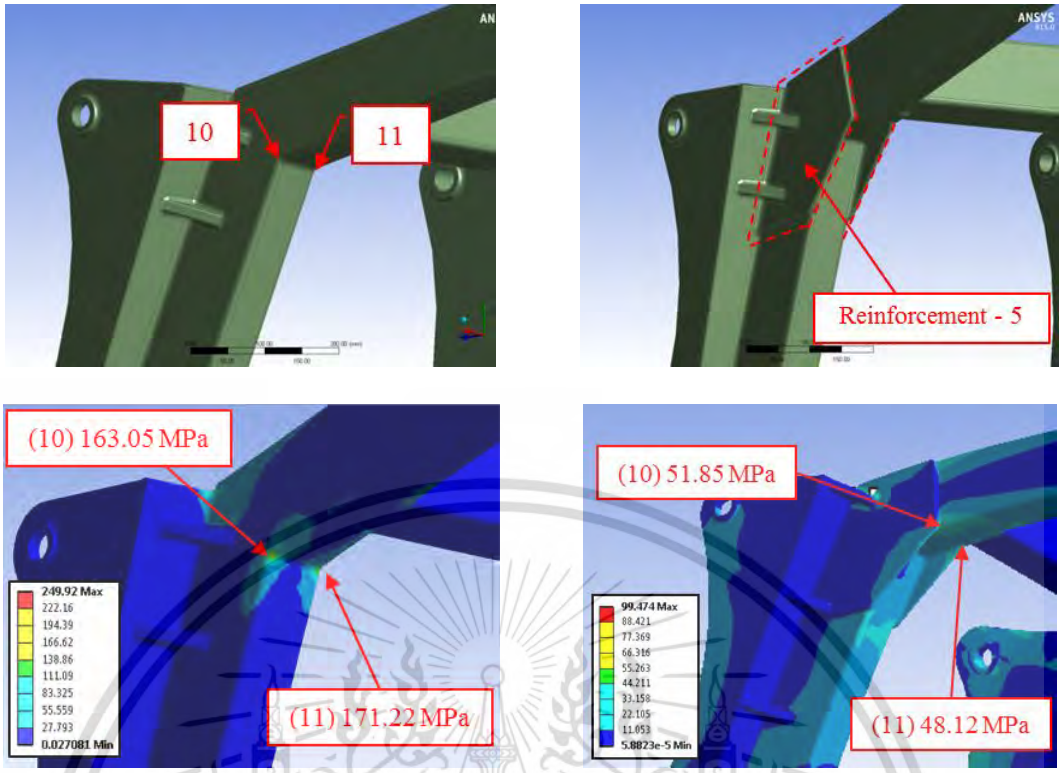

(a) (b)

Figure 4.44 Comparison of stresses of frame at critical point number 10-11, (a) before improvement, (b) after improvement

To reduce stress on critical point number 12 and 13, the lower joint between the column with the ladder of the frame is modified by adding reinforcement plates - 6 (thickness of the reinforcement plate - 6 is 6 mm), as shown in Figure 4.45. The Von Mises stresses on critical point number 12 and 13 are decreased from 146.78 MPa to 35.03 MPa and 185.01 MPa to 36.49 respectively.

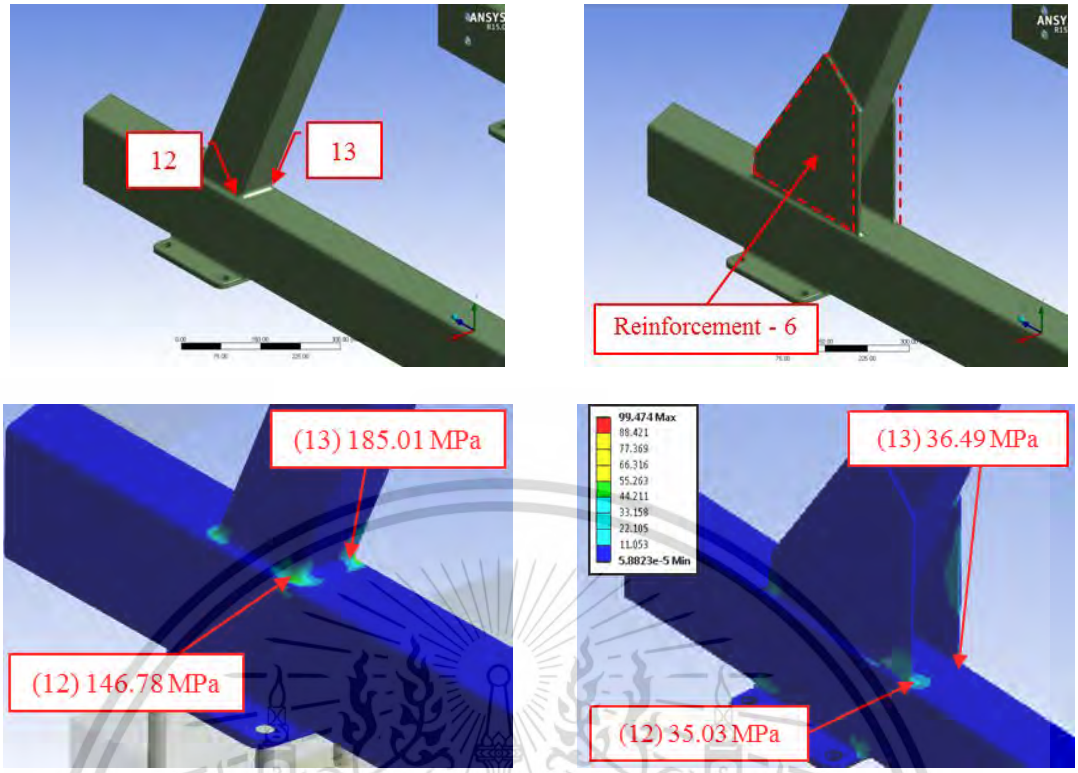

(a) (b)

Figure 4.45 Comparison of stresses of frame at critical point number 12-13, (a) before improvement, (b) after improvement

After the modification of frame, the strength of frame on critical point number 1-13 are increased by 61.48%, 67.89%, 64.27%, 54.57%, 60.60 %, 58.86%, 57.01%, 93.88%, 73.88%, 68.20%, 71.90%, 76.13% and 80.28% respectively, as shown in Table 4.9. Moreover, the safety factors of the frame on critical point number 1-13 are also increased more than 3, which the magnitudes are 6.18, 3.11, 5.92, 4.99, 4.20, 3.87, 4.15, 45.70, 8.24, 4.82, 5.20, 7.14 and 6.85 respectively. It means the frame is safe, therefore this design of frame could be used for the final design. The 3D geometry of frame for prototype fabrication is shown in Figure 4.46.

Table 4.9 Summary of results of strength improvement of frame

Critical point	Von Mises stress (MPa)		Deviation (%)	Safety factor	
	Before	After		Before	After
1	105.10	40.48	61.48	2.38	6.18
2	249.92	80.26	67.89	1.00	3.11
3	118.12	42.21	64.27	2.12	5.92
4	110.32	50.12	54.57	2.27	4.99
5	151.09	59.53	60.60	1.65	4.20
6	157.04	64.61	58.86	1.59	3.87
7	140.21	60.28	57.01	1.78	4.15
8	89.42	5.47	93.88	2.80	45.70
9	116.11	30.33	73.88	2.15	8.24
10	163.05	51.85	68.20	1.53	4.82
11	171.22	48.12	71.90	1.46	5.20
12	146.78	35.03	76.13	1.70	7.14
13	185.01	36.49	80.28	1.35	6.85

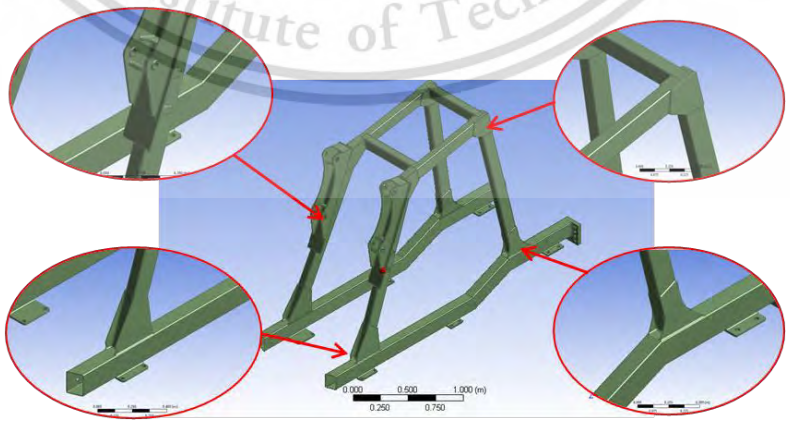

Figure 4.46 The 3D geometry of frame for prototype fabrication

4.4 Verification of Stress Analysis using Classical Theory

As this work does not study the stress measurement on the prototype of sugarcane loader structure by strain gauge due to limitation of time and instrument, therefore, the produced stress on Finite Element Analysis by computational simulation is verified by classical theory; Engineering Mechanic Static, Solid Mechanic, and Machine Design, with the same cross-section in designed part. The verification of stress analysis by classical theory is suggested by Trivedi (2005) and Prajapati & Patel (2013).

The sugarcane loader structure consists of two main components; loader arm and loader structure. As the limitation of classical stress analysis on loader structure; complex shapes and statically indeterminate structure (Static equilibrium equations are insufficient for determining the internal loads and reaction loads on the structure), therefore, in this section is focused on the verification of stress analysis using classical theory on the loader arm only. Regarding to the Von Mises failure theory of ductile material that defined as design criteria in Chapter 3.4; Strength analysis of sugarcane loader structure by Finite Element Method, therefore the produced Von Mises stress at point D on cross-section D-D and at point E on cross-section E-E of the loader arm, which is randomly selected, are used to compare between FEA approach and classical theory. The cross-section D-D is located at the middle of the loader arm which is taken at 1,600 mm from point A and the cross-section E-E is located between point A and point B which is taken at 400 mm from point B as shown in Figure 4.47.

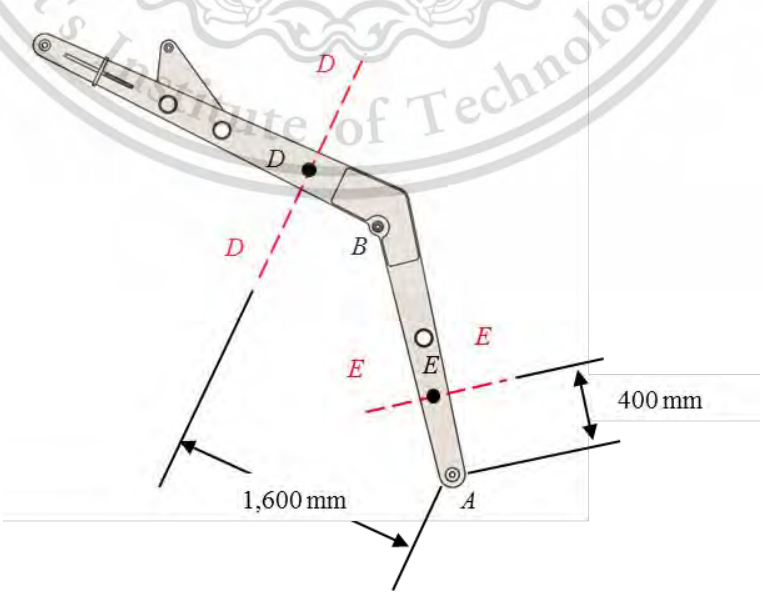

Figure 4.47 Section D-D and E-E in side view of loader arm

As strength analysis of loader arm by Finite Element Method is done in chapter 3.4.1. Figure 4.48, shows the forces acting on the loader arm which are applied in Finite Element Analysis; summation of the grab and sugarcane bundle weight at point C is 483 kg, loader arm weight at C.G is 439 kg, force acting at point A in x direction is -9,184.32 N, force acting at point A in y direction is 55,619.97 N, force acting at point B in x direction is 9,184.32 N and force acting at point B in y direction is 65,184.72N. For stress analysis of loader arm by classical theory, in order to make the stress calculation by classical theory easily, the external force and weight acting on the loader arm are divided by 2 due to the loader arm is symmetry geometry, therefore

Summation of the grab and sugarcane bundle weight at point C is 483/2 = 241.5 kg

Loader arm weight at C.G is 439/2 = 219.5 kg

Force acting at point A in x direction is -9,184.32/2 = -4,592.16 N

Force acting at point A in y direction is 55,619.97/2 = 27,809.99N

Force acting at point B in x direction is 9,184.32/2 = 4,592.16 N

Force acting at point B in y direction is 65,184.72/2 = 32,592.36 N

And forces acting on the loader arm which will be applied for stress verification using classical theory are shown in Figure 4.49.

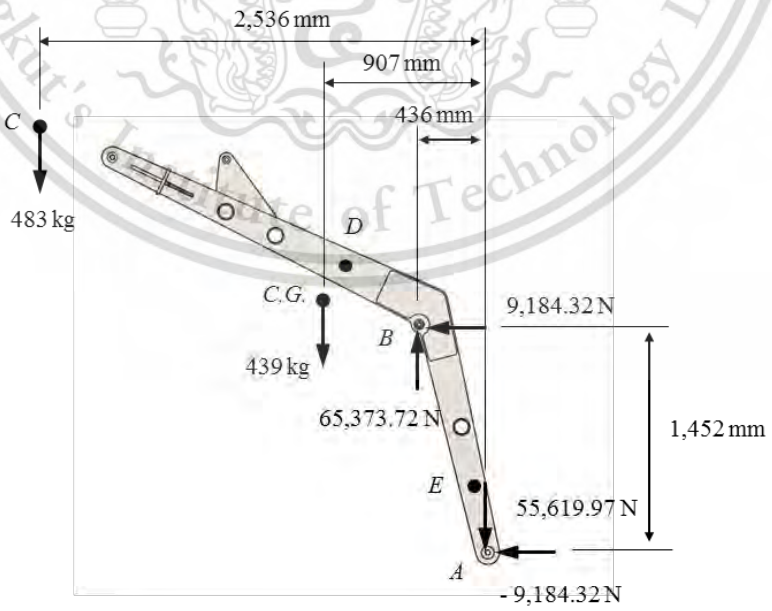

Figure 4.48 Free body diagram of loader arm for stress analysis using FEA

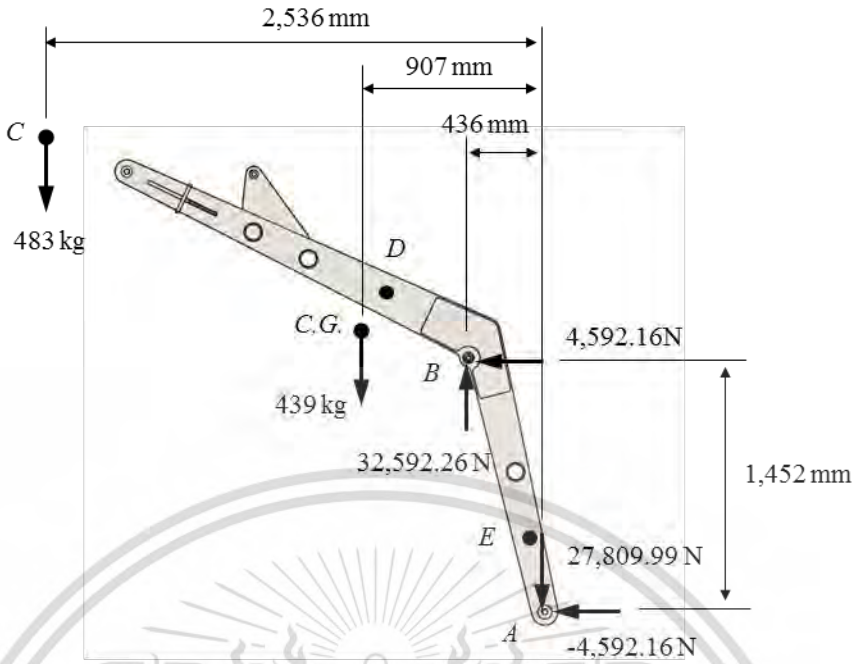

Figure 4.49 Free body diagram of loader arm for stress verification using classical theory

4.4.1 Stress Analysis of Loader Arm on cross-section D-D using Classical Theory

The internal loadings at point D on cross-section D-D are found out by using free body diagram of the section CD of loader arm shows in Figure 4.50. There are three internal loadings: Normal force, N_D, acting normal to loader arm at the cut section, Shear force, V_D, acting tangent to the section and Bending moment, M_D. The magnitudes of those internal loading are determined by Equation of Equilibrium as below,

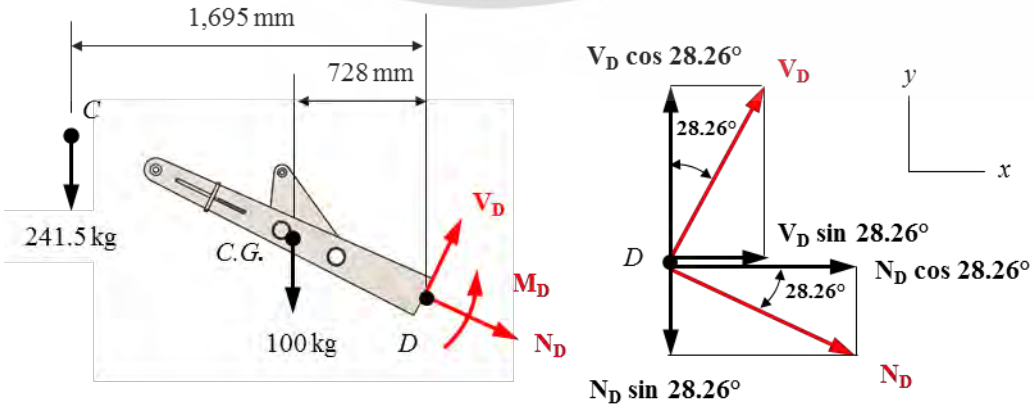

Figure 4.50 Free body diagram of loader arm on cross-section D-D

Equations of Equilibrium,

$$+\downarrow \sum F_y = 0;$$

$$(241.5\text{kg})(9.81\text{m/s}^2) + (100\text{kg})(9.81\text{m/s}^2) + N_D \sin 28.62^\circ - V_D \cos 28.62^\circ = 0$$

$$N_D = 1.83V_D - 6994N \tag{4.4}$$

$$\overset{+}{\rightarrow} \sum F_x = 0;$$

$$N_D \cos 28.62^\circ - V_D \sin 28.62^\circ = 0$$

$$V_D = -1.83N_D \tag{4.5}$$

Substituted equation (4.5) in equation (4.4),

$$N_D = -1608.22\text{N}$$

$$V_D = 2943.04\text{N}$$

$$\sum M_D = 0;$$

$$(241.5\text{kg})(9.81\text{m/s}^2)(1695\text{mm}) + (100\text{kg})(9.81\text{m/s}^2)(780\text{mm}) + M_D = 0 \tag{4.6}$$

$$M_D = -4780829.93\text{N} \cdot \text{mm}$$

Summary of magnitude and direction of internal loadings at point D of cross-section D-D is shown below with Figure 4.51,

$$N_D = -1608.22\text{N}$$

$$V_D = 2943.04\text{N}$$

$$M_D = -4780829.93\text{N} \cdot \text{mm}$$

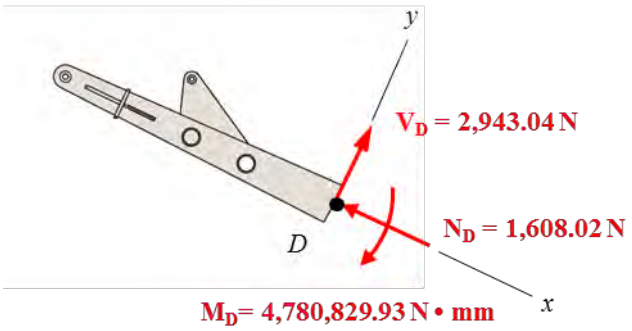

Figure 4.51 Summary of forces acting on cross-section D-D of loader arm

As geometric properties of section D-D in Figure 4.52,

Moment of inertia of the cross-section D-D about z –axis, $I_z = 21239729\ \text{mm}^4$

Area of the cross-section D-D, A = (89mm - 19mm)(19mm) + (112mm + 123mm)(19mm) = 5795 mm^2

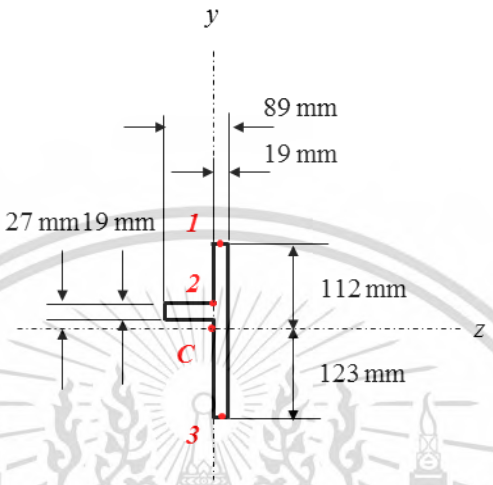

Figure 4.52 Geometric properties of loader arm on section D-D

Stresses at point 1 (on cross-section D-D),

Stress due to axial force and bending moment,

$$\sigma_{x,1} = \sigma_{axial} + \sigma_{bending1} \tag{4.7}$$

$$= -\frac{N}{A} + \frac{M_z y}{I_z}$$

$$= -\frac{1608.22\text{N}}{5795\text{mm}^2} + \frac{(4780829.93\text{N}\cdot\text{mm})(112\text{mm})}{21239729\text{mm}^4}$$

$$= -0.28\text{MPa} + 25.21\text{MPa}$$

$$\sigma_{x,1} = 24.93\text{MPa}$$

Shear stress,

$$\tau_{xy} = \frac{V}{A} \tag{4.8}$$

$$= \frac{2943.04\text{N}}{5795\text{mm}^2}$$

$$\tau_{xy} = 0.51\text{MPa}$$

Von Mises stress,

$$\sigma_{von\ mises1} = \sqrt{\sigma^2{}_x - \sigma_x\sigma_y + \sigma^2{}_y + 3\tau^2{}_{xy}} \tag{4.9}$$

$$= \sqrt{24.93^2 - (24.93)(0) + (0)^2 + 3(0.51)^2}$$

$$\sigma_{von\ mises1} = 24.95\text{MPa}$$

Stresses at point 2 (on cross-section D-D),

Stress due to axial force and bending moment,

$$\sigma_{x,2} = \sigma_{axial} + \sigma_{bending2} \tag{4.10}$$

$$= -\frac{N}{A} + \frac{M_z y}{I_z}$$

$$= -\frac{1608.22\text{N}}{5795\text{mm}^2} + \frac{(4780829.93\text{N}\cdot\text{mm})(27\text{mm})}{21239729\text{mm}^4}$$

$$= -0.28\text{MPa} + 6.08\text{MPa}$$

$$\sigma_{x,2} = 5.80\text{MPa}$$

Shear stress,

$$\tau_{xy} = \frac{V}{A} \tag{4.11}$$

$$= \frac{2943.04\text{N}}{5795\text{mm}^2}$$

$$\tau_{xy} = 0.51\text{MPa}$$

Von Mises stress,

$$\sigma_{von\ mises2} = \sqrt{\sigma^2{}_x - \sigma_x\sigma_y + \sigma^2{}_y + 3\tau^2{}_{xy}} \tag{4.12}$$

$$= \sqrt{5.80^2 - (5.80)(0) + (0)^2 + 3(0.51)^2}$$

$$\sigma_{von\ mises2} = 5.87\text{MPa}$$

Stresses at point 3 (on cross-section D-D),

Stress due to axial force and bending moment,

$$\sigma_{x,3} = \sigma_{axial} + \sigma_{bending3} \tag{4.13}$$

$$= -\frac{N}{A} - \frac{M_z y}{I_z}$$

$$= -\frac{1608.22\text{N}}{5795\text{mm}^2} - \frac{(4780829.93\text{N}\cdot\text{mm})(123\text{mm})}{21239729\text{mm}^4}$$

$$= -0.28\text{MPa} - 27.69\text{MPa}$$

$$\sigma_{x,3} = -27.97\text{MPa}$$

Shear stress,

$$\tau_{xy} = \frac{V}{A} \tag{4.14}$$

$$= \frac{2943.04\text{N}}{5795\text{mm}^2}$$

$$\tau_{xy} = 0.51\text{MPa}$$

Von Mises stress,

$$\sigma_{von\ mises3} = \sqrt{\sigma^2{}_x - \sigma_x\sigma_y + \sigma^2{}_y + 3\tau^2{}_{xy}} \tag{4.15}$$

$$= \sqrt{(-27.97)^2 - (-27.97)(0) + (0)^2 + 3(0.51)^2}$$

$$\sigma_{von\ mises3} = 27.98\text{MPa}$$

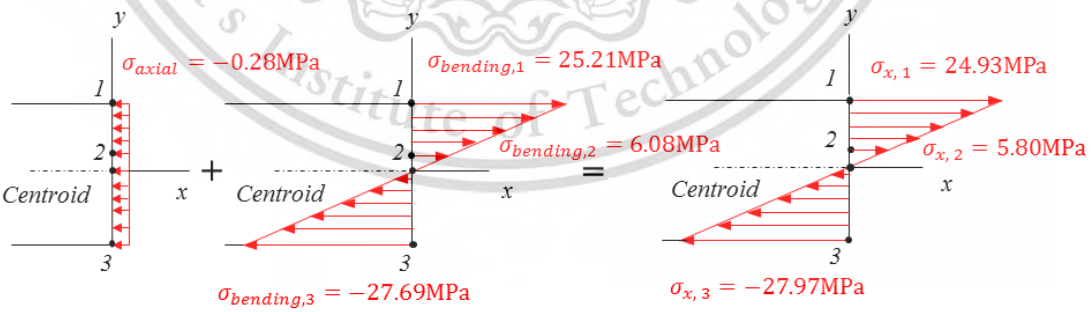

Figure 4.53 Stresses due to axial force and bending moment on section D-D of loader arm

Now, the Von Mises stresses on section D-D are determined by classical theory. The magnitudes of Von Mises stress at point number 1 (at upper surface of cross-section D-D), point number 2 (at middle of cross-section D-D) and point number 3 (at below of cross-section D-D) are 24.95 MPa, 5.87 MPa and 27.98 MPa respectively. Moreover, as the Von Mises stresses of loader arm have been found out by FEA approach in Chapter 4.1.1; strength analysis results of loader arm by Finite Element Method. The result shows that the magnitudes of stress at point number 1, 2, and 3 (on cross-section D-D) are 26.07 MPa, 6.14 MPa and 28.05 MPa respectively, which are shown in Figure 4.54. It clearly indicates that the stresses between FEA and classical theory are very close.

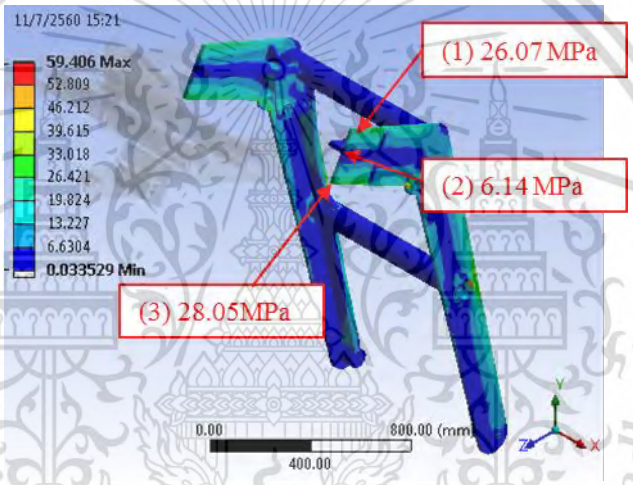

Figure 4.54 Stress results on section D-D by FEA

4.4.2 Stress Analysis of Loader Arm on cross-section E-E using Classical Theory

The internal loadings at point E on cross-section E-E are found by using free body diagram of the section CE of loader arm as shown in Figure 4.55. There are three internal loadings: Normal force, N_E, acting normal to loader arm at the cut section, Shear force, V_E, acting tangent to the section and Bending moment, M_E. The magnitudes of those internal loading are determined by Equation of Equilibrium as below,

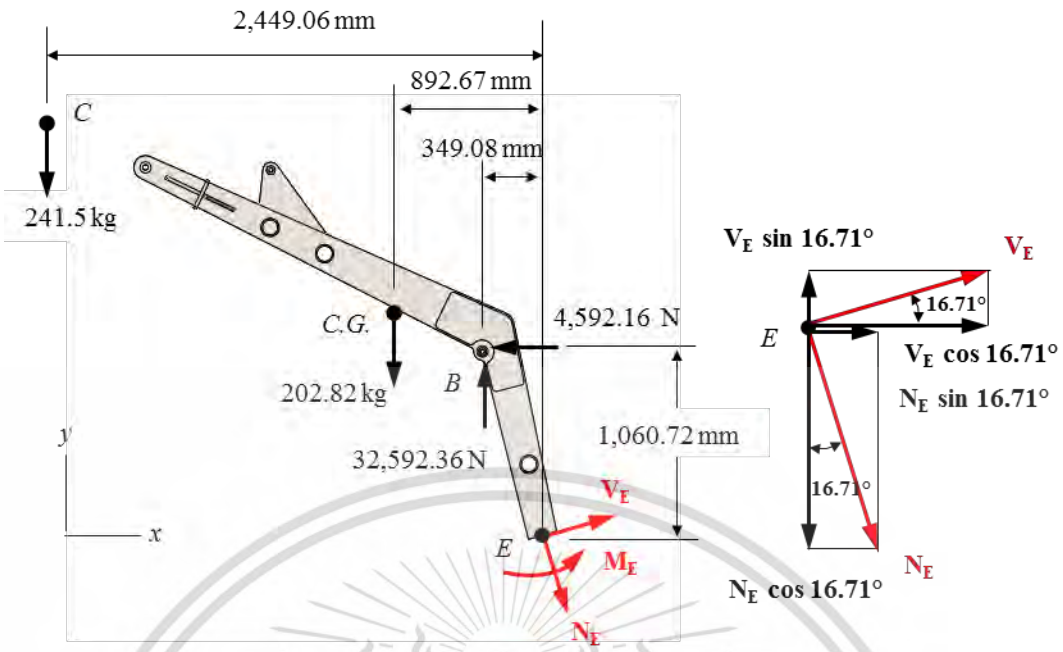

Figure 4.55 Free body diagram of loader arm on cross-section E-E

Equations of Equilibrium,

$$+\downarrow \sum F_y = 0;$$

$$(241.5\text{kg})(9.81\text{m/s}^2) + (202.82\text{kg})(9.81\text{m/s}^2) - 32592.36N - V_E \sin 16.71^\circ - N_E \cos 16.71^\circ = 0$$

$$N_E = 0.3V_E + 28233.58N \tag{4.16}$$

$$\overset{+}{\rightarrow} \sum F_x = 0;$$

$$V_E \cos 16.71^\circ + N_E \sin 16.71^\circ - 4592.16N = 0$$

$$N_E = -3.33V_E + 15971.19N \tag{4.17}$$

Equation (4.16) equal (4.17),

$$V_E = -3378.07\text{N}$$

$$N_E = 29247\text{N}$$

$$\sum M_E = 0;$$

$$M_E + (4592.16\text{N})(1060.72\text{mm}) - (32592.36\text{N})(349.08\text{mm}) + (202.82\text{kg})(9.81\text{m/s}^2)$$

$$(892.67\text{mm})+(241.5\text{kg})(9.81\text{m/s}^2)(2449.06\text{mm})=0 \quad (4.18)$$

$$M_E = -1071873.25\text{N}\cdot\text{mm}$$

Summary of magnitude and direction of internal loadings at point E of cross-section E-E as shown below with Figure 4.56,

$$V_E = -3378.07\text{N}$$

$$N_E = 29247\text{N}$$

$$M_E = -1071873.25\text{N}\cdot\text{mm}$$

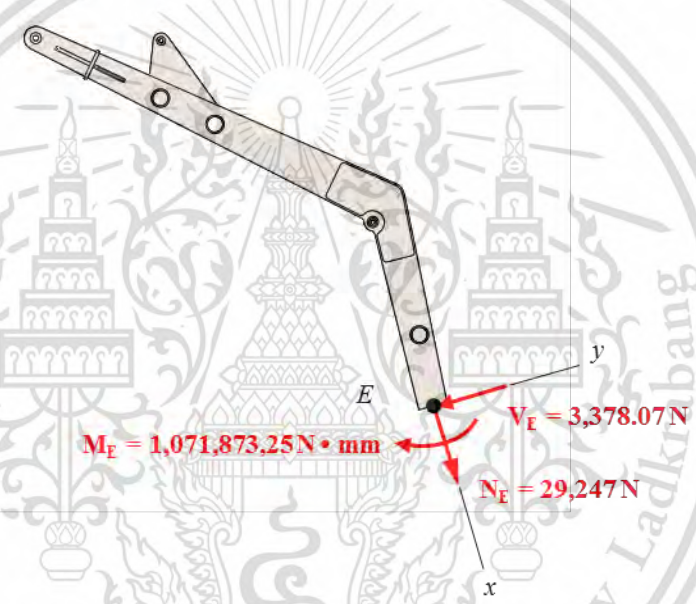

Figure 4.56 Summary of forces acting on cross-section E-E of loader arm

As geometric properties of section E-E in Figure 4.57,

Moment of inertia of the cross-section E-E about z –axis, I_z = 7565551 mm^4

Area of the cross-section E-E, A = (84 mm - 19 mm)(19 mm) + (81.49 mm + 86.19 mm)(19 mm) = 4420.92 mm^2

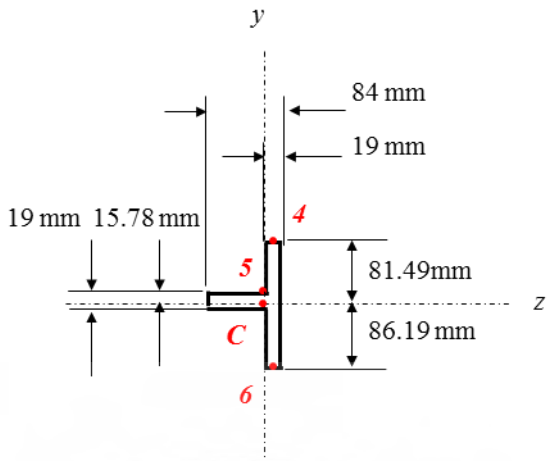

Figure 4.57 Geometric properties of loader arm on section E-E

Stresses at point 4 (on cross-section E-E)

Stress due to axial force and bending moment,

$$\sigma_{x,4} = \sigma_{axial} + \sigma_{bending4} \tag{4.19}$$

$$= \frac{N}{A} + \frac{M_z y}{I_z}$$

$$= \frac{29247\text{N}}{4420.92\text{mm}^2} + \frac{(1071873.25\text{N}\cdot\text{mm})(81.49\text{mm})}{7565551\text{mm}^4}$$

$$= 6.62\text{MPa} + 11.55\text{MPa}$$

$$\sigma_{x,4} = 18.17\text{MPa}$$

Shear stress,

$$\tau_{xy} = \frac{V}{A} \tag{4.20}$$

$$= \frac{3378.07\text{N}}{4420.92\text{mm}^2}$$

$$\tau_{xy} = 0.76\text{MPa}$$

Von Mises stress,

$$\sigma_{von\ mises4} = \sqrt{\sigma^2{}_x - \sigma_x\sigma_y + \sigma^2{}_y + 3\tau^2{}_{xy}} \tag{4.21}$$

$$= \sqrt{18.17^2 - (18.17)(0) + (0)^2 + 3(0.76)^2}$$

$$\sigma_{von\ mises4} = 18.22\text{MPa}$$

Stresses at point 5 on cross-section E-E,

Stress due to axial force and bending moment,

$$\sigma_{x,5} = \sigma_{axial} + \sigma_{bending5} \tag{4.22}$$

$$= \frac{N}{A} + \frac{M_z y}{I_z}$$

$$= \frac{29247\text{N}}{4420.92\text{mm}^2} + \frac{(1071873.25\text{N}\cdot\text{mm})(15.78\text{mm})}{7565551\text{mm}^4}$$

$$= 6.62\text{MPa} + 2.24\text{MPa}$$

$$\sigma_{x,5} = 8.86\text{MPa}$$

Shear stress,

$$\tau_{xy} = \frac{V}{A} \tag{4.23}$$

$$= \frac{3378.07\text{N}}{4420.92\text{mm}^2}$$

$$\tau_{xy} = 0.76\text{MPa}$$

Von Mises stress,

$$\sigma_{von\ mises5} = \sqrt{\sigma^2{}_x - \sigma_x\sigma_y + \sigma^2{}_y + 3\tau^2{}_{xy}} \tag{4.24}$$

$$= \sqrt{8.86^2 - (8.86)(0) + (0)^2 + 3(0.76)^2}$$

$$\sigma_{von\ mises5} = 8.96\text{MPa}$$

Stresses at point 6 (on cross-section E-E),

Stress due to axial force and bending moment,

$$\sigma_{x,6} = \sigma_{axial} + \sigma_{bending6} \tag{4.25}$$

$$= \frac{N}{A} - \frac{M_z y}{I_z}$$

$$= \frac{29247\text{N}}{4420.92\text{mm}^2} - \frac{(1071873.25\text{N}\cdot\text{mm})(86.19\text{mm})}{7565551\text{mm}^4}$$

$$= 6.62\text{MPa} - 12.21\text{MPa}$$

$$\sigma_{x,6} = -5.59\text{MPa}$$

Shear stress,

$$\tau_{xy} = \frac{V}{A} \tag{4.26}$$

$$= \frac{3378.07\text{N}}{4420.92\text{mm}^2}$$

$$\tau_{xy} = 0.76\text{MPa}$$

Von Mises stress,

$$\sigma_{von\ mises6} = \sqrt{\sigma^2{}_x - \sigma_x\sigma_y + \sigma^2{}_y + 3\tau^2{}_{xy}} \tag{4.27}$$

$$= \sqrt{(-5.59)^2 - (-5.59)(0) + (0)^2 + 3(0.76)^2}$$

$$\sigma_{von\ mises6} = 5.74\text{MPa}$$

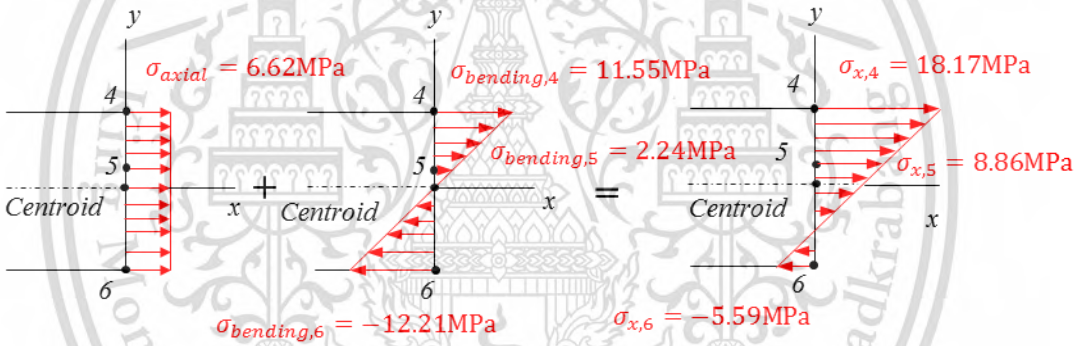

Figure 4.58 Stresses due to axial force and bending moment on section E-E of loader arm

Now, the Von Mises stresses on section E-E are determined by classical theory. The magnitudes of Von Mises stress at point number 4 (at upper surface of cross-section E-E), point number 5 (at middle of cross-section E-E), and point number 6 (at below of cross-section E-E) are 18.22 MPa, 8.96 MPa, and 5.74 MPa respectively. Moreover, as the Von Mises stresses of loader arm have found out by FEA approach in Chapter 4.1.1, strength analysis results of loader arm by Finite Element Method. The results show that the magnitudes of stress at point number 4, 5 and 6 (on cross-section E-E) are 18.54 MPa, 8.75 MPa, and 5.68 MPa respectively, which are shown in Figure 4.59. It clearly indicates that the stresses between FEA and classical theory are very close.

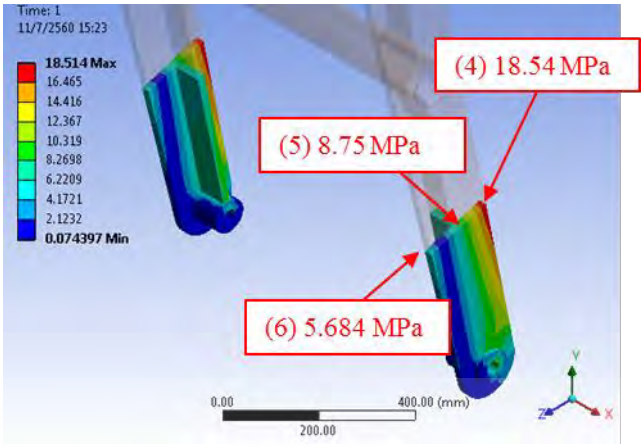

Figure 4.59 Stress results on section E-E by FEA

From Figure 4.60, the comparison of the Von mises stresses at point number 1, 2, 3, 4, 5, and 6 (on cross-section D-D and cross-section E-E) of the loader arm between classical theory and FEA, there are very similar trend of the stresses between the classical theory and FEA. From Table 4.10, the Von Mises stresses of the loader arm from classical theory at point number 1, 2, 3, 4, 5, and 6 (on cross-section D-D and cross-section E-E) are 24.95 MPa, 5.87 MPa, 27.98 MPa, 18.22 MPa, 8.96 MPa, and 5.74 MPa respectively. The Von Mises stresses of the loader arm from FEA at point number 1, 2, 3, 4, 5, and 6 are 26.07 MPa, 6.14 MPa, 28.05 MPa, 18.54 MPa, 8.75 MPa, and 5.68 MPa respectively, which they have found out in Chapter 4.1.1, strength analysis results of loader arm by Finite Element Method, which it clearly indicates that the stresses from classical theory and FEA are very close. Moreover, the percentage of deviations of the stress on classical theory and FEA at point number 1, 2, 3, 4, 5, and 6 are 4.53, 4.60, 0.25, 1.76, 2.34, and 1.05 respectively, which the comparisons show the deviations of stress result of classical theory and FEA are really less. Therefore, the produced stress by FEA approach can be verified by classical theory.

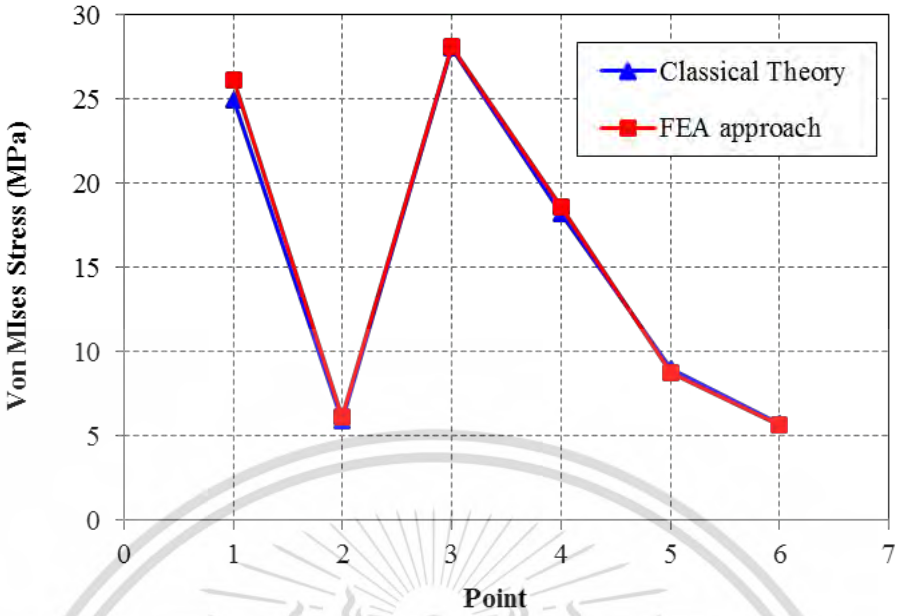

Figure 4.60 Comparison of Von mises stresses on section D-D and E-E of loader arm between classical theory and FEA

Table 4.10 Deviations of Von Mises stress on section D-D and E-E of loader arm

Point		Von Mises stress (MPa)		Deviation (%)
		Classical theory	FEA approach	
Section D-D	1	24.95	26.07	4.53
	2	5.87	6.14	4.60
	3	27.89	28.05	0.25
Section E-E	4	18.22	18.54	1.76
	5	8.96	8.75	2.34
	6	5.74	5.68	1.05

CHAPTER 5

MANUFACTURING PROCESS OF PROTOTYPE

5.1 2D Drawings and Bill of Materials

After analyzed the strength of the sugarcane loader structure by Finite Element Method, improved the strength of the design model and finalize 3D mode (The finalize 3D of Sugarcane loader structure is shown in chapter 4), next step is create the 2D drawings and Bill of Materials (BOM) as to prepare the fabrication of the sugarcane loader structure prototype. The 2D drawings and Bill of Materials (BOM) are document that is used to communicate between designer and manufacturing plant for the sugarcane loader structure prototype fabrication. The 2D drawings show the dimension of sub-component and the assembly procedure. The Bill of Materials show list of the raw materials, sub-assemblies, intermediate assemblies, sub-components, and the quantities of each needed for manufacturing. The sugarcane loader structure consists of 432 sub-parts with 5 main groups of assembly list. The first group is a group of sugarcane loader structure: grabber, loader arm, hydraulic cylinder of grabber (short length), hydraulic cylinder of loader arm (long length), pin, loader arm support, front metal net and loader structure with body parts as shown in Figure 5.1 – Figure 5.7. The second group is a group of loader structure with body parts: front body, side body, rear body, wheel cover, front, metal net, roof and loader structure as shown in Figure 5.8. The third is a group of loader structure: front cross member, transmission-frame support, engine-frame support, counter weight support, counter weight, plate on transaxle and frame with body mounting, as shown in Figure 5.9 - Figure 5.15. The fourth group is a group of frame with body mountings: roof mounting, body mounting, metal net mounting and frame as shown in Figure 5.16. And the fifth group is a group of frame: column and ladder as shown in Figure 5.17 – Figure 5.19.

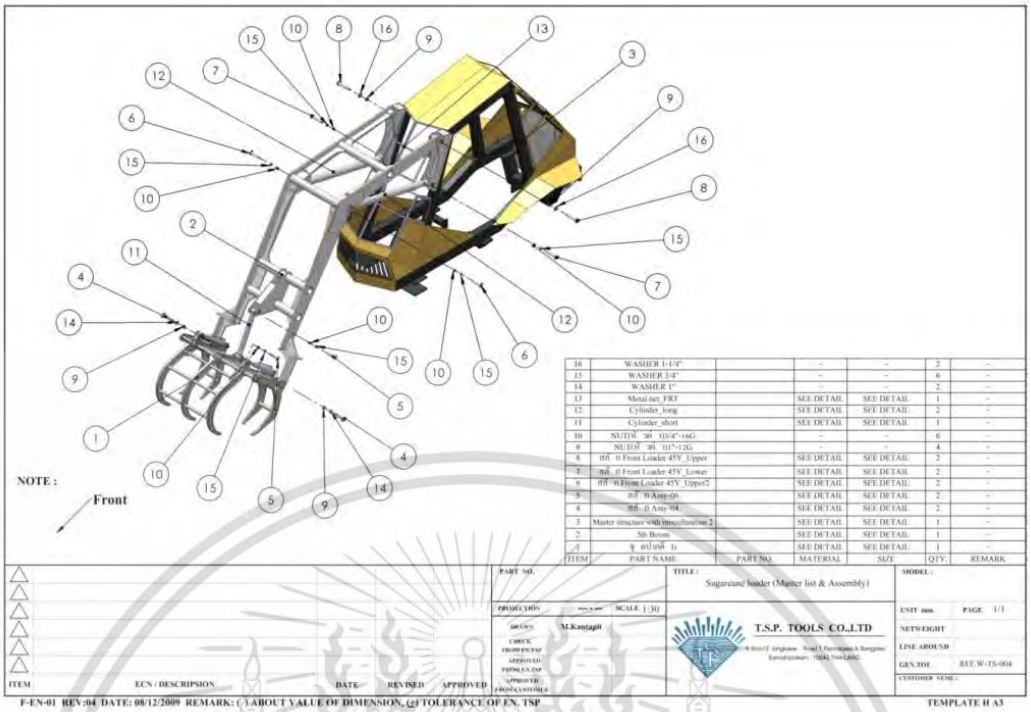

Figure 5.1 Assembly list of Sugarcane loader structure

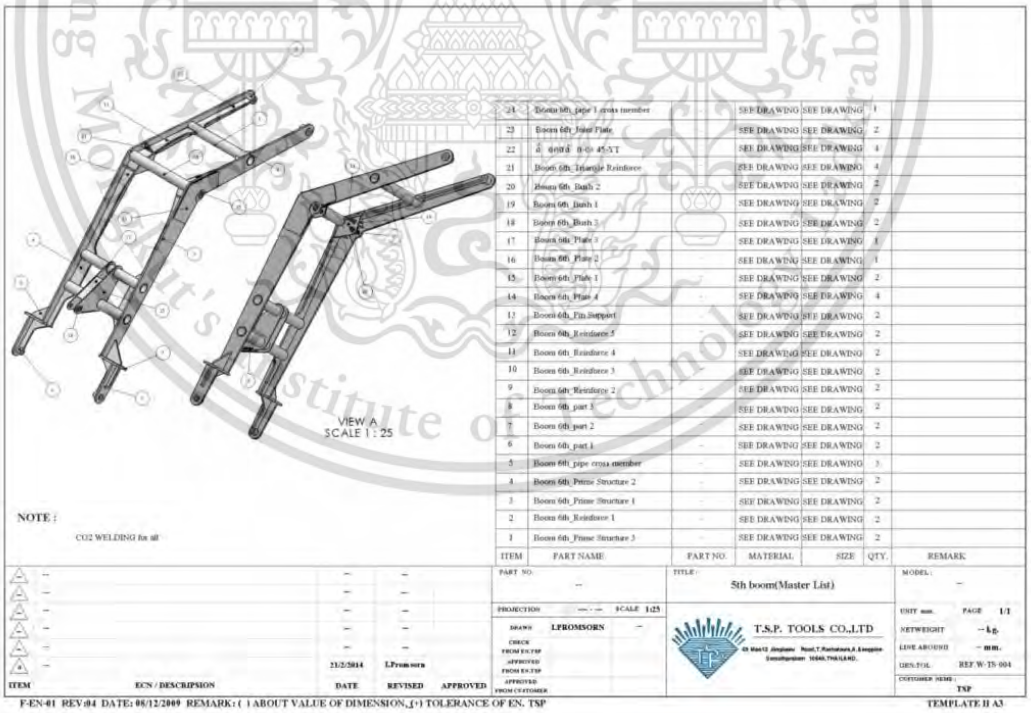

Figure 5.2 Assembly list of loader arm

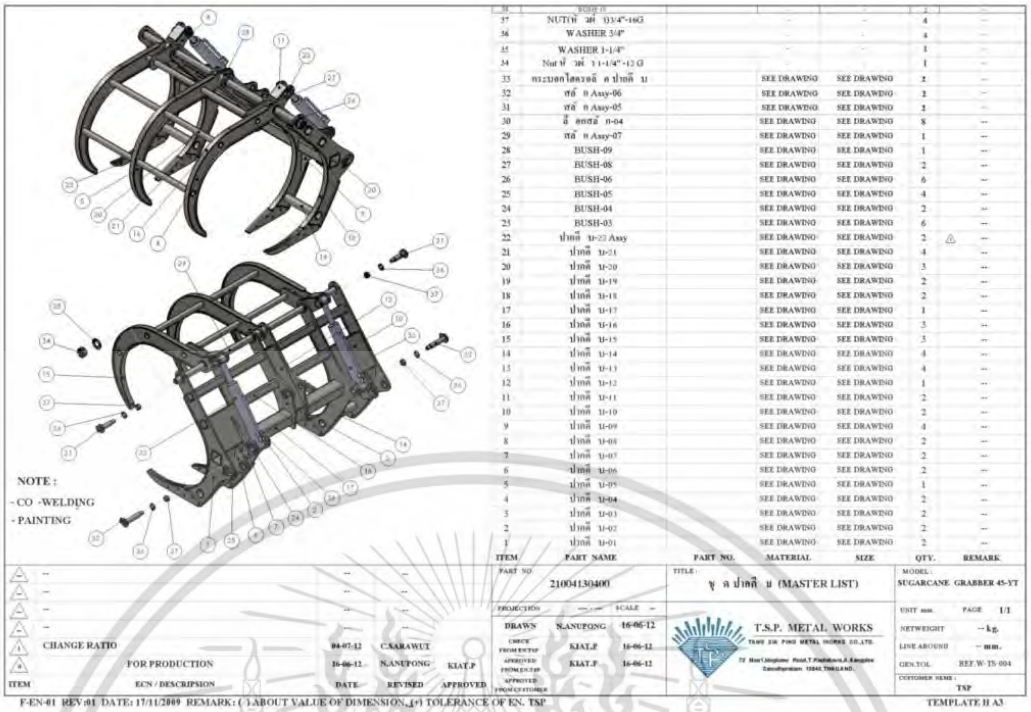

Figure 5.3 Assembly list of grabber

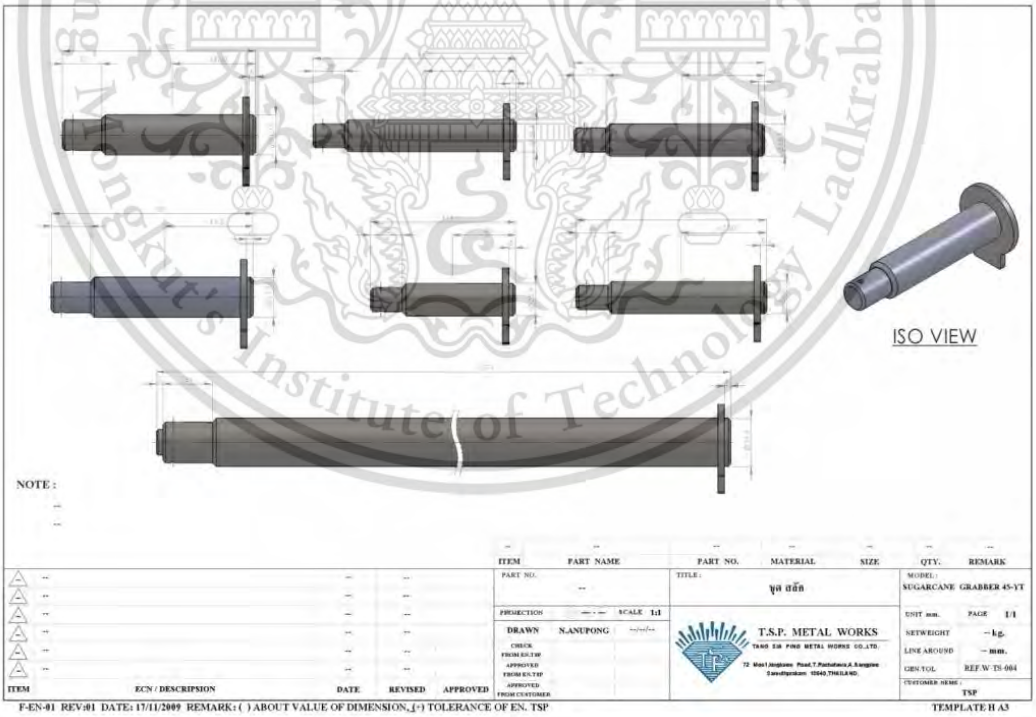

Figure 5.4 Drawing of pin

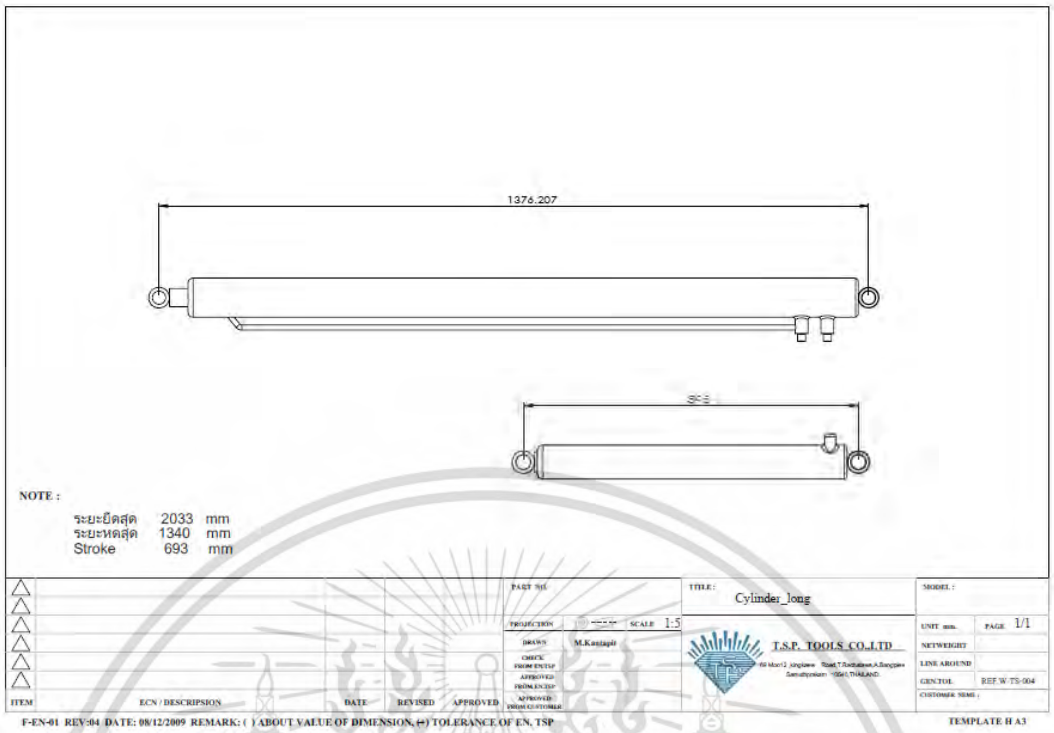

Figure 5.5 Drawing of hydraulic cylinder

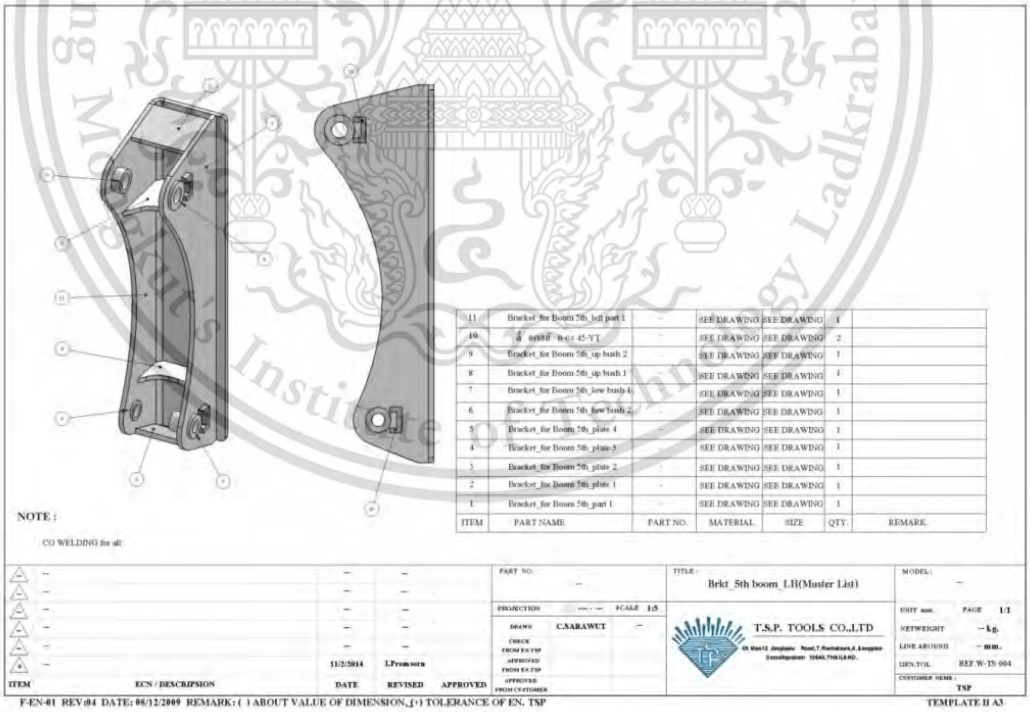

Figure 5.6 Assembly list of loader arm support-LH

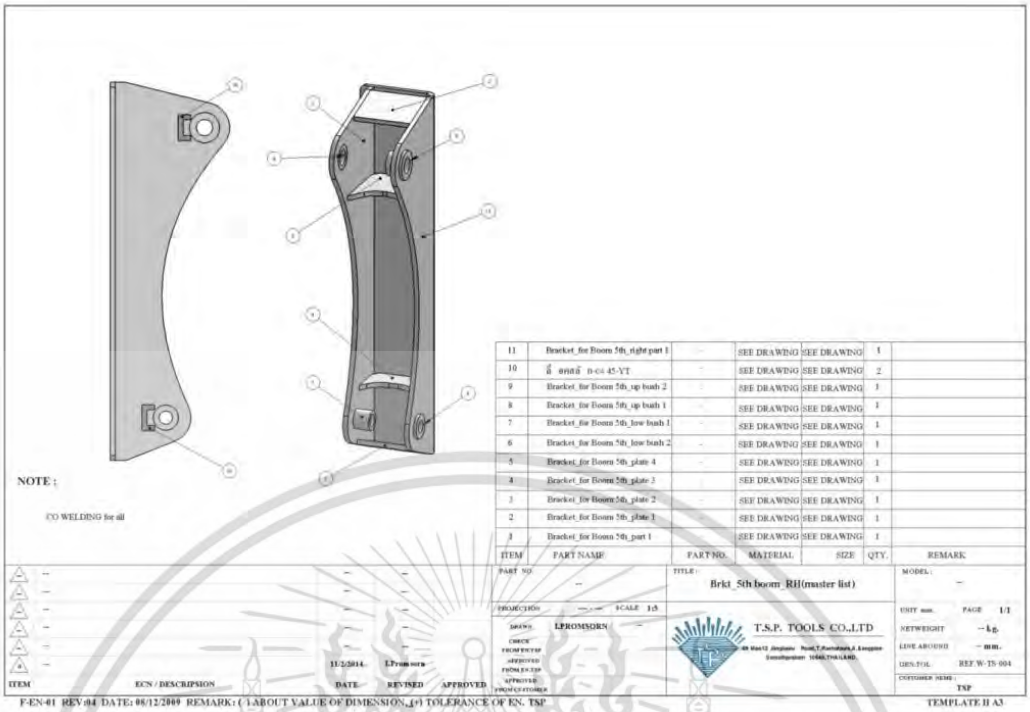

Figure 5.7 Assembly list of loader arm support-RH

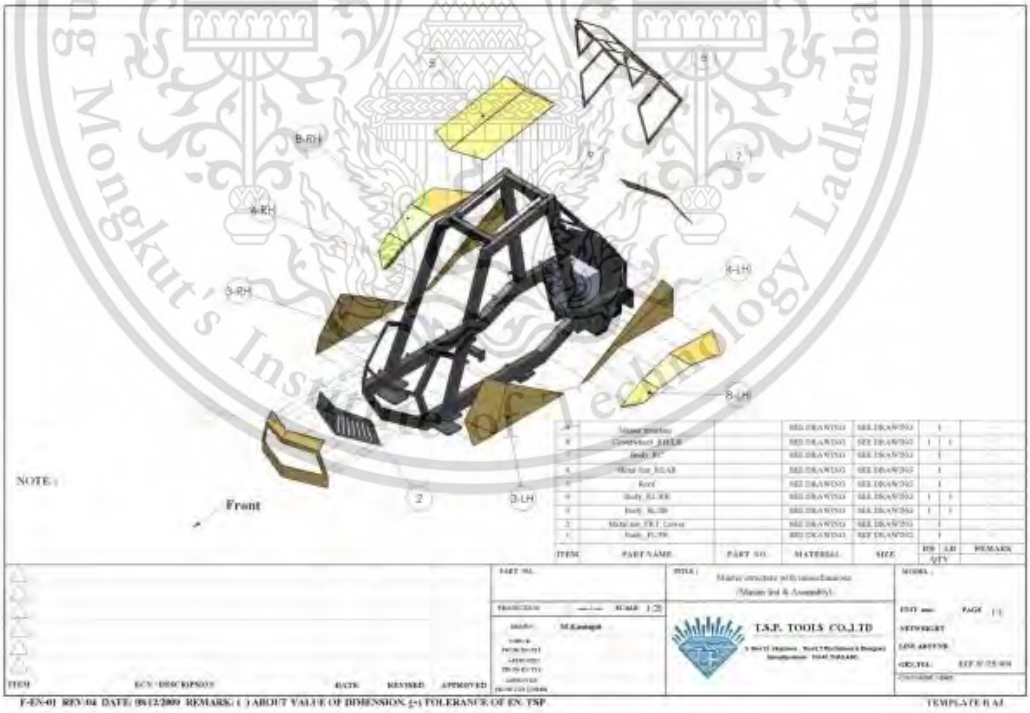

Figure 5.8 Assembly list of loader structure with body parts

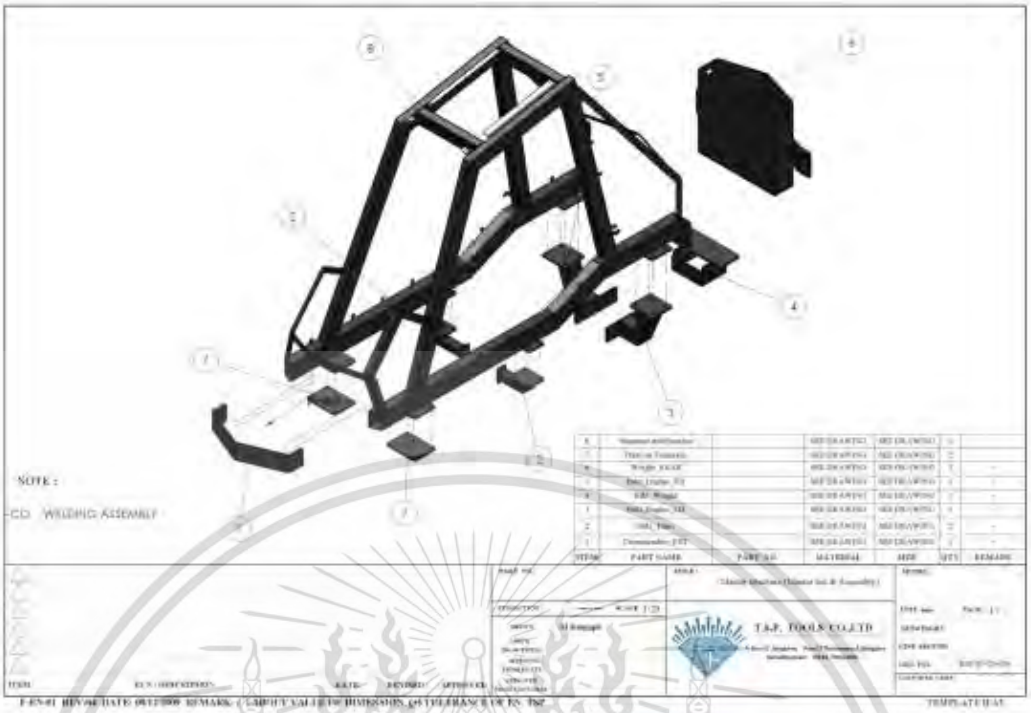

Figure 5.9 Assembly list of loader structure

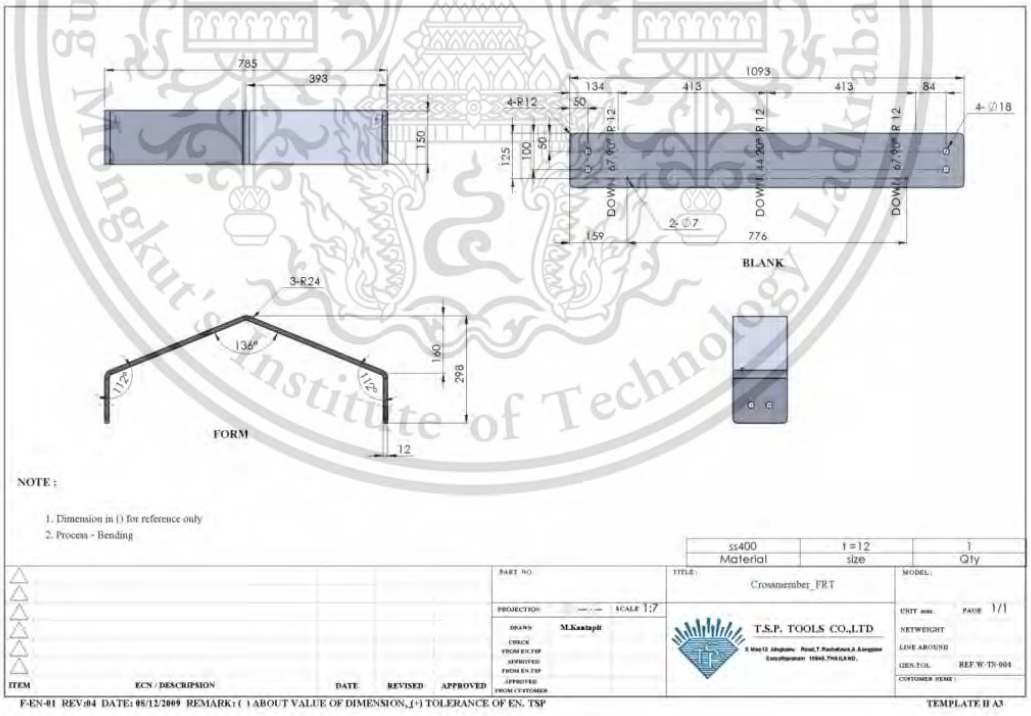

Figure 5.10 Drawing of front cross member

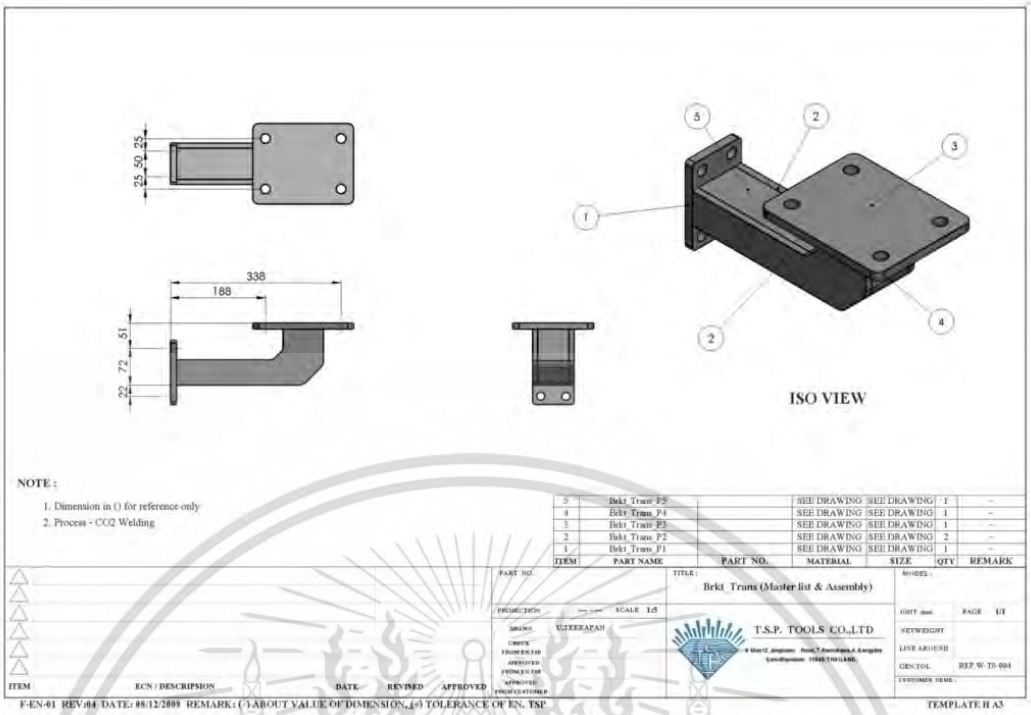

Figure 5.11 Assembly list of left and right transmission-frame support

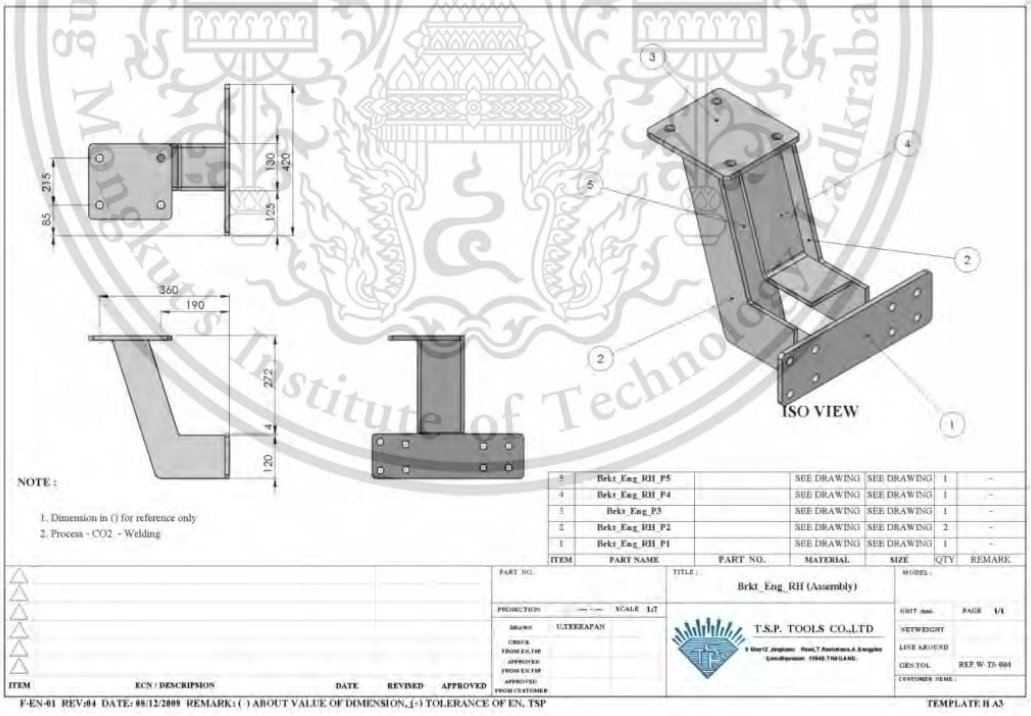

Figure 5.12 Assembly of right engine-frame support

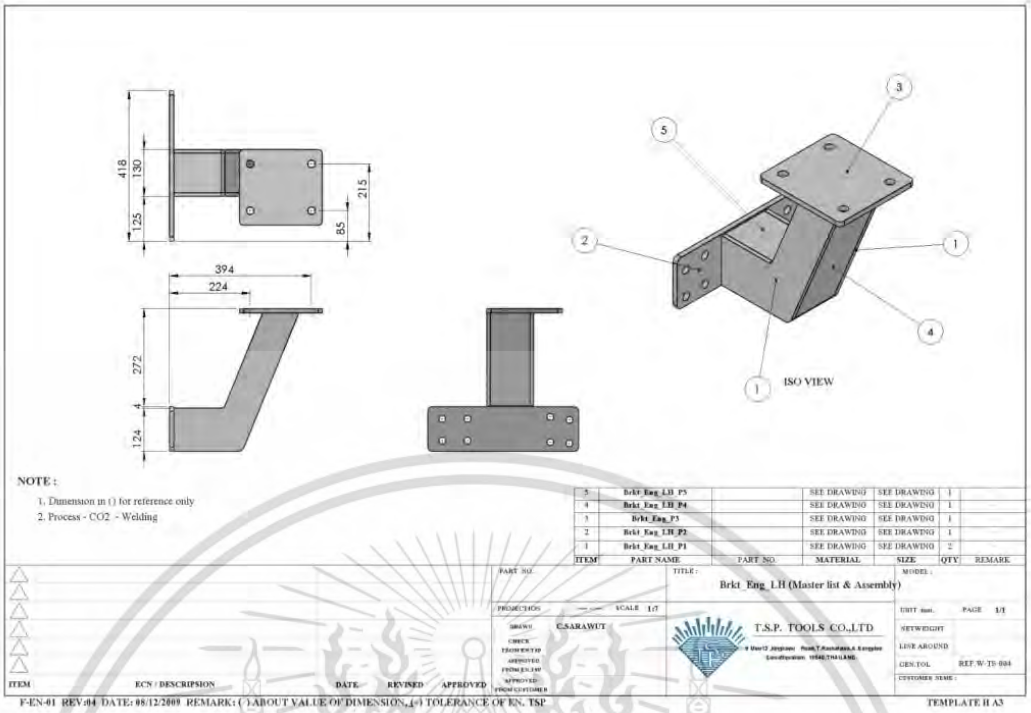

Figure 5.13 Assembly list of left engine-frame support

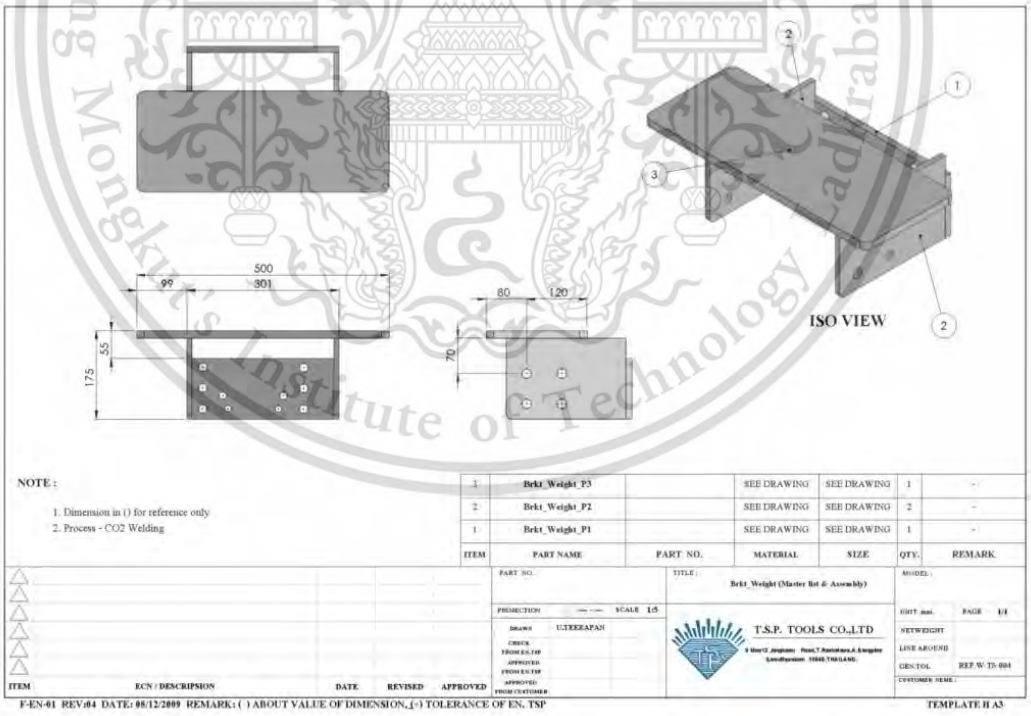

Figure 5.14 Assembly list of counter weight support

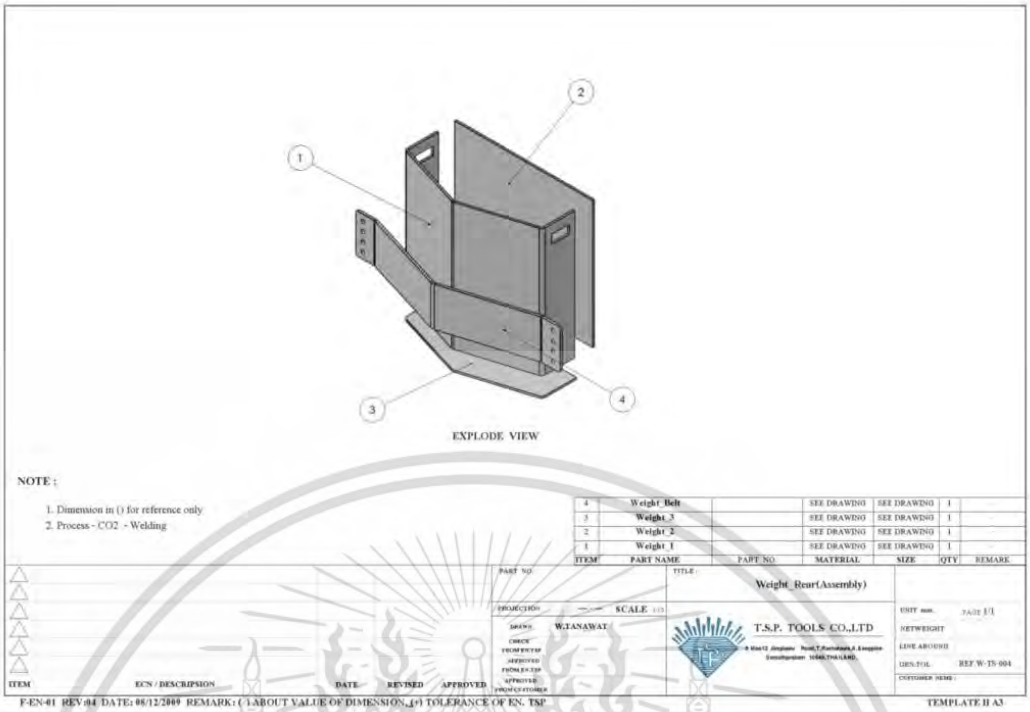

Figure 5.15 Assembly list of counter weight

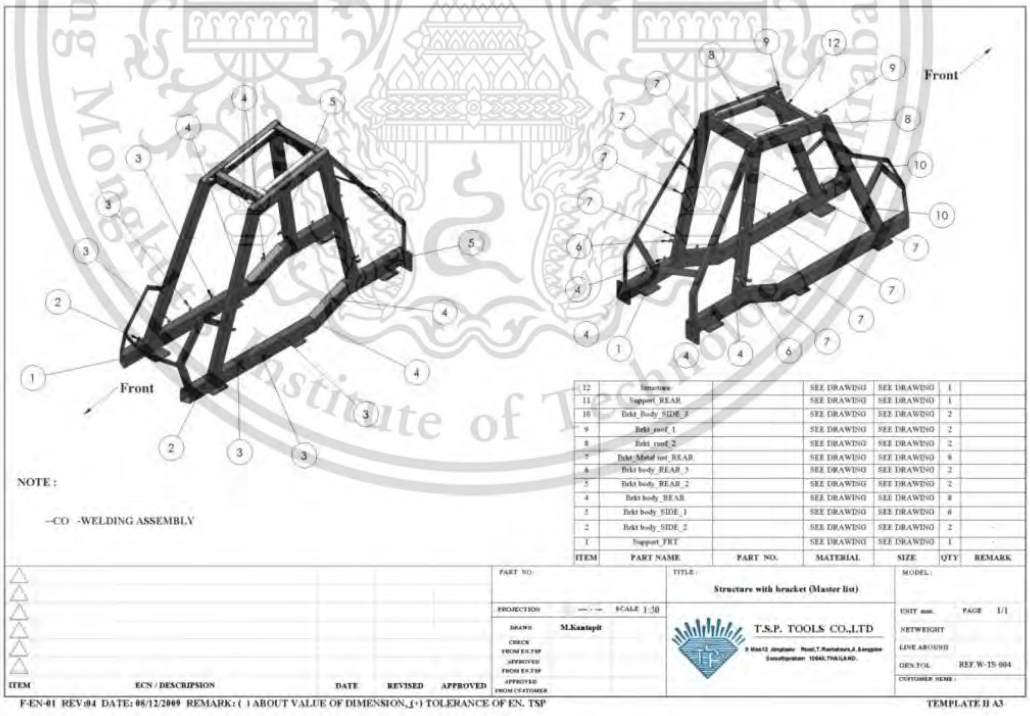

Figure 5.16 Assembly list of frame with body mounting

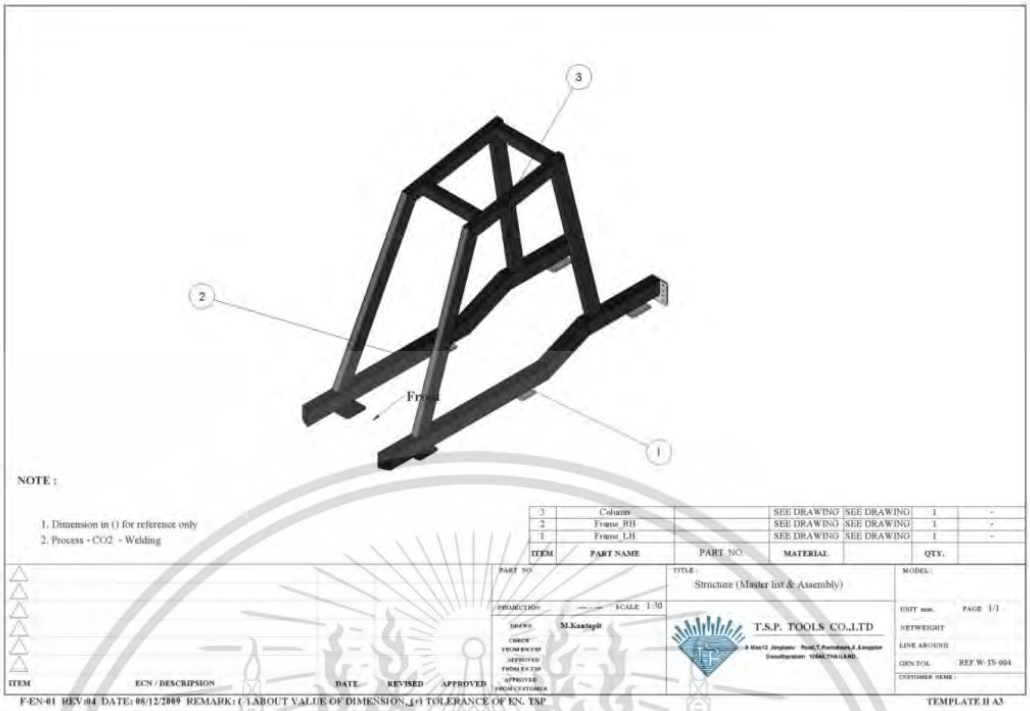

Figure 5.17 Assembly list of frame

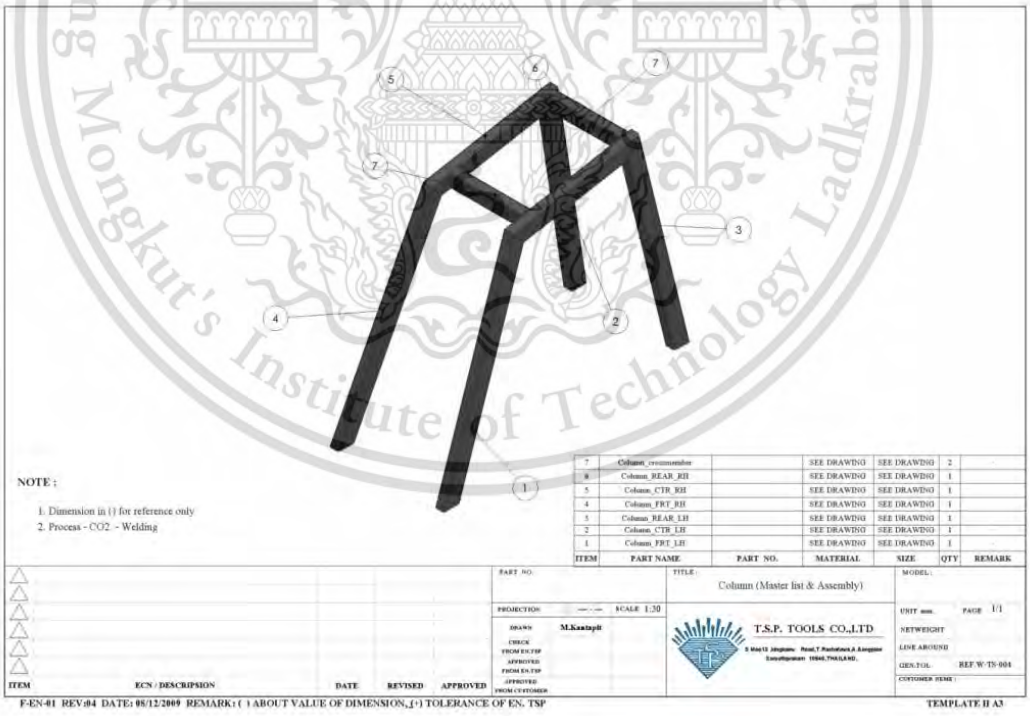

Figure 5.18 Assembly list of column

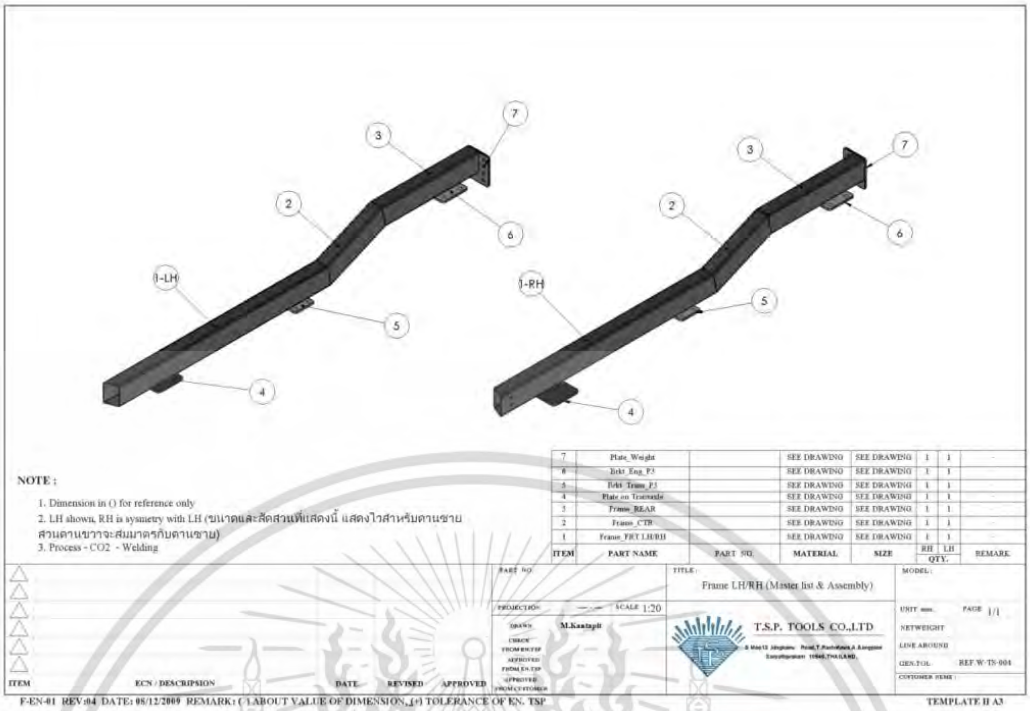

Figure 5.19 Assembly list of ladder

5.2 Fabrication Process of Sugarcane Loader Structure

After created 2D drawings and Bill of Materials, Next step is to fabricate the full scale of sugarcane loader structure prototype and the fabrication process is shown below,

5.2.1 Prepare components of hydraulic system: hydraulic cylinder, hydraulic hose, hydraulic tube and control valve, which are shown in Figure 5.20 - Figure 5.23.

Figure 5.20 Hydraulic cylinder (short length)

Figure 5.21 Hydraulic hose

Figure 5.22 Hydraulic tube

Figure 5.23 Control valve

5.2.2 Create the sub components by cutting sizes, bending, drilling holes and welding. The completed sub components are shown in Figure 5.24 - Figure 5.31.

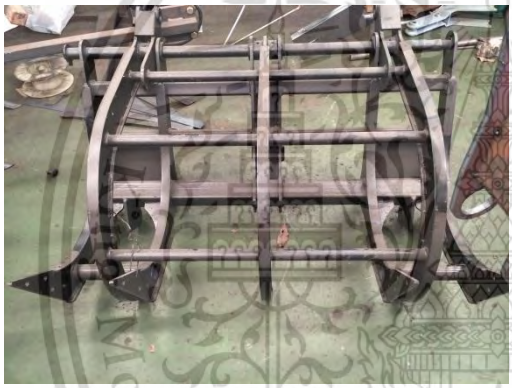

Figure 5.24 Grabber

Figure 5.25 Loader arm

Figure 5.26 Transmission-frame support

Figure 5.27 Engine-frame support

Figure 5.28 Counter weight support

Figure 5.29 Counter weight

Figure 5.30 Wheel cover

Figure 5.31 Front body

5.2.3 Create the frame with body mountings by cutting size, bending, drilling holes and welding, which are shown in Figure 5.32 - Figure 5.38.

Figure 5.32 Cut rectangular tube

Figure 5.33 Weld frame

Figure 5.34 Weld body mounting to frame

Figure 5.35 Weld loader arm support to frame

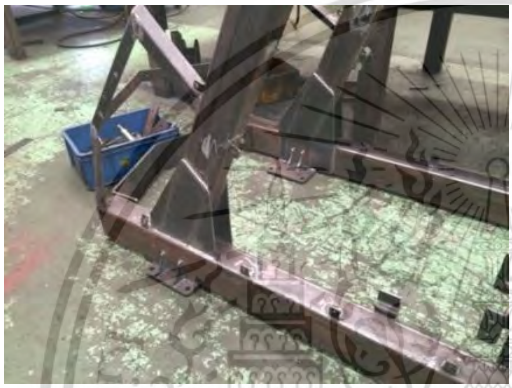

Figure 5.36 Weld lower reinforcement to frame

Figure 5.37 Weld upper reinforcement to frame

Figure 5.38 Completed frame with body mountings

5.2.4 Assemble the body parts to the frame by wrenching fasteners, which are shown in Figure 5.39 - Figure 5.42.

Figure 5.39 Assemble front body to frame

Figure 5.40 Assemble rear body to frame

Figure 5.41 Assemble side body to frame

Figure 5.42 Completed frame with body parts

5.2.5 Assemble the loader structure to KUBOTA ZL-1-455 tractor by wrenching fasteners, which are shown in Figure 5.43 - Figure 5.47.

Figure 5.43 Assemble frame support to tractor

Figure 5.44 Assemble counter weigh support to tractor

Figure 5.45 Assemble frame with body parts to tractor

Figure 5.46 Assemble counter weight to loader structure

Figure 5.47 Completed loader structure with body parts

5.2.6 Assemble the loader arm, the grabber and hydraulic system to the loader structure by wrenching fasteners, which are shown in Figure 5.48 - Figure 5.52.

Figure 5.48 Assemble loader arm to loader structure

Figure 5.49 Assemble hydraulic cylinder (long length) to loader structure

Figure 5.50 Assemble grabber to loader arm

Figure 5.51 Assemble hydraulic cylinder (short length) to loader arm

Figure 5.52 Assemble hydraulic tube, hydraulic hose and control valve

5.2.7 Finally, paint sugarcane loader structure with red and grey colors and completed sugarcane loader structure (prototype) is shown in Figure 5.53.

(a)

(b)

(c)

Figure 5.53 Completed sugarcane loader structure

CHAPTER 6

CONCLUSIONS

1. Maximum hydraulic cylinder force condition (or Maximum stroke of hydraulic cylinder condition) can be used as the severe boundary condition for static FEA of sugarcane loader structure.

2. The 3D model of sugarcane loader structure is found to be safe under maximum hydraulic cylinder force condition by performing static FEA with safety factor of 3. The final safety factor of sub-part of sugarcane loader structure are 3.59, 15.01, 13.96, 3.58, 3.02, 3.63, 6.05, and 3.11 (Loader arm, Left transmission-frame support, Right transmission-frame support, Left engine-frame support, Right engine-frame support, Counter weight support, Counter weight belt, and Frame respectively).

3. Static analysis of sugarcane loader structure by using FEA approach can use to predict stress developed on parts.

3.1 From the results, the maximum stress occurs around the hydraulic cylinder mounting lug of frame due to bending effect and stress concentration. Therefore designer should concern more on strength of this area.

3.2 From the results, the maximum stress occurs around the hydraulic cylinder mounting lug of frame and the safety factor of the first design is lower than specific safety factor which the value is 3. Therefore, the designed part needs to be modified to reduce stress. The suggested idea of strength improvement is to increase moment of inertia of section. (It is not necessary to add triangle truss member). Therefore, designer can use this point for the idea of strength improvement.

4. In case of studying strength of frame only, the CPU time of Finite Element mode of loader structure can be reduced by suppressing all frame support (Engine-frame support, Transmission-frame support, Counter weight support, Front cross-member and Counter weight belt) as well as suppressing the contact nonlinearity between each component. As suppressing all frame support and contact nonlinearity, the number of total node is reduced and this simulation is become linear simulation. After the simplified FE model, the Von Mises stresses on critical points are very close to the stress result of the completed FE model. Although, the maximum deviation of the stress on critical point is 10.74%, but the CPU time can be reduced down to 85.46% from 6,189.2 seconds to 900.4 seconds.

5. As this work does not study the stress measurement on the prototype of sugarcane loader structure by strain gauge due to limitation of time and instrument, therefore, the produced stress on Finite Element Analysis by computational simulation is verified by classical theory with the same cross-section of designed parts. However, the limitation of stress analysis on loader structure by classical theory; complex shapes and in state of statically indeterminate structure (Static equilibrium equations are insufficient for determining the internal loads and the reaction loads on the structure) therefore, the stress verification by classical theory is analyzed on the loader arm only. From the results, stress development on section D-D and section E-E of loader arm from static FEA and classical theory are very close and the percentage of deviations at point number 1, 2, 3, 4, 5 and 6 of loader arm are 4.53%, 4.60%, 0.25%, 1.76, 2.34% and 1.05% respectively, which the deviations are really less. Therefore the produced stresses by FEA approach can be verified by applying the classical theory.

REFERENCES

Abril, G., & Juan, G. (2013). *Design, analysis and optimization of an orange peel grapple.* AGH University of Science and Technology, Poland.

Andy, (2010, December 14). Stress singularities [Blog post]. Retrieved from https://andreweib.wordpress.com/2010/12/14/stress-singularities/

Burr, A., & Cheatham, J. (1995). *Mechanical Design and Analysis* (2nd ed). Prentice-Hall.

Coefficient of friction. Retrieved March 15, 2015 from Engineering Hand Book website, http://www.engineershandbook.com/Tables/frictioncoefficients.htm

Erklig, A., & Yeter, E. (2013). The improvement of the backhoe-loader arms, *Modeling and Numerical Simulation of Material Science*, *3*, 142-148. doi: http://dx.doi.org/10.4236/mnsms.2013.34020

Joints, Springs and Beams. (2013). Introduction to ANSYS Mechanical Part 2, ANSYS Training Course Material (14.0, 17-18). Canonsburg, Pittsburgh, USA.

Juvinall, R. C., & Marshek, K. M. (2006). *Fundamentals of Machine Component Design* (4th ed). John Wiley & Sons.

Martinez, J. (2013, April 4). What my FEA professor never taught me [Blog post]. Retrieved from https://engineerjau.wordpress.com/2013/04/13/what-my-fea-professor-never-taught-me/

Naren Chaithanee, Anon Phanijjiva, Panyaporn Loetsriphaisan, Ek-u Thammakornbunjut, Sombat Tamna, &Nuttapol Limjeerajarus. (2014). *3D structural analysis of an electric tree-wheeled vehicle integrating with a battery switching system*. Paper presented at the 5th TSME International Conference on Mechanical Engineering, Chiang Mai, Thailand.

Natchaya Murachai (2013). *Design and strength analysis of the seat anchorages for large passenger vehicles using Finite Element Method* (Master's thesis). Suranaree University of Technology, Thailand.

REFERENCES

(Continued)

Patel, S. (2017). SolidWorks 2017 simulation – avoiding singularities [Blog post]. Retrieved from http://www.goengineer.com/2016/12/02/solidworks-2017-simulation-avoiding-singularities/blog/

Patel, B. P., & Prajapati, J. M. (2012). Evaluation of bucket capacity, digging force calculations and static force analysis of mini hydraulic backhoe excavator. *Machine Design-The Journal of Faculty of Technical Sciences, 4*(1), 59-66.

Patel, B. P., & Prajapati, J. M. (2012). Static analysis of mini hydraulic backhoe excavator attachment using FEA approach. *International Journal of Mechanical Engineering and Robotics Research, 1*(3), 163-175.

Patel, B. P., & Prajapati, J. M. (2013). Structural optimization of mini hydraulic backhoe excavator attachment using FEA approach. *Machine Design-The Journal of Faculty of Technical Sciences, 5*(1), 43-56.

Patel, V. A. (2012). Static structural analysis of backhoe loader chassis. *International Journal of Advanced Science, Engineering and Technology, 1,* 17-20.

Rahman, R. A., Tamin, M. N., & Kurdi, O. (2008). Stress analysis of heavy duty truck chassis as a preliminary data using FEM. *Journal Mekanikal,* (26), 76 – 85.

Somsak Siwadamrongpong, Supakit Rooppakhun, Natchaya Murachai, & Pakorn Burakorn. (2013). Strength analysis of the seat anchorages for large passenger vehicle using Finite Element Method. Advance Materials Research, 658, 340-344. doi: 10.4028/www.scientific.net/AMR.658.340

Thorat, A., & Rao, G. S. (2013). Static analysis of loader backhoe chassis 770 model. *International Journal of Engineering Science & Research Technology, 2*(7).

Trivedi, R. R. (2005). *Calculation of static forces and Finite Element Analysis of attachments of an excavator* (Master's thesis). Nirma University, Institute of Science and Technology, Ahmedabad, India.

APPENDIX:

PUBLICATION

The 6th TSME International Conference on Mechanical Engineering
16-18 December 2015
Cha-Am, Phetchaburi, Thailand

CST011

Harmonized Engineering Technologies

Design and Development of Sugarcane Loader Frame Structure

Kantapit Meetam[1]*, Preechar Karin[2], Chi-na Benyajati[3], Masaaki Okuma[4] and Thanapol Luckanawat[5]

[1,2] International College, King Mongkut's Institute of Technology Ladkrabang, Bangkok, Thailand 10520
[3] Automotive Laboratory, National Metal and Material Technology Center, National Science and Technology Development Agency, Pathum thani, Thailand 12120
[4] Department of Mechanical and Aerospace Engineering, Graduate School of Science and Engineering, Tokyo Institute of Technology, Tokyo, Japan 152-8550
[5] Department of Teacher Training in Mechanical Engineering, Faculty of Technical Education, King Mongkut's University of Technology North Bangkok, Bangkok, Thailand 10800
*Corresponding Author: k.meetam@gmail.com

Abstract

The Entrepreneurs in small and medium sized enterprise (SME) have an experience in sugarcane loader construction for a long time but it has not been developed with sufficient and appropriate engineering and technologies. Thus, the purpose of this research is to design and development a sugarcane loader structure base on engineering. The structure of sugarcane loader will be designed by Computer Aided Design (CAD) and Computer Aided Engineering (CAE), for the KUBOTA ZL-1 Reverse tractor with a 45 horsepower, which can install grab equipment to lift the 300 kilogram of Sugarcane mass on 5 meters from ground, that total weight is approximately 3.5 tons. Use finite element method (FEM) to simulate stress contour occur on part with the sufficient structural strength to operate on the farm. The knowledge gained from design and development of sugarcane loader structure base on engineering can be transferred to the companies for sugarcane loader proceeding. The model of sugarcane loader structure are designed and analyzed under bending case

Keywords: Sugarcane loader structure, Finite element method, Computer Aided Design, Computer Aided Engineering

1. Introduction

Sugarcane loader is one kind of harvesting machine that was operated in farm. It was used to pick sugarcane bundle from ground to truck. Normally, sugarcane loader consists of 3 main parts, first is farm tractor, second is loader boom and third is the grab. The advantage point of this machine is to reduce harvesting time, to reduce labor and also to increase product quantity. In Thailand, the Entrepreneurs have an experience in sugarcane loader fabrication for a long time but it has not been developed with sufficient and appropriate engineering technologies. There are many parts often fail when operate in farm, that mean it not safe, quite dangerous for farmer and also lose cost. Thus, the purpose of this research is to design and development a sugarcane loader frame structure prototype base on engineering that can withstand the weights and force on the most critical case, study on static finite element analysis (FEA) of sugarcane loader and provide a sugarcane loader frame structure design proceeding base on engineering for Thai entrepreneurs.

2. Research Methodology

2.1 Conceptual design

At the first, Starting from collect entrepreneurs and farmer requirements that define as the main design concept as follow: First, Using existing tractor for the base of sugarcane loader structure. The exiting tractor was used in this work is KUBOTA SUNSHINE ZL1-455. The Power was generated by 2.4 liter Diesel engine, 5 cylinders with 45.3 horsepower. The transmissions system can be switched in both 2WD and 4WD. The suspension type is rigid suspension. No spring and no shock absorber. Total tractor weight about 1.7 Tons. Wheelbase is 1.98

Fig. 1 Sugarcane loader prototype

m and wheel track is 1.45 m. Second, the sugarcane loader structure must be able to assembled and

disassembled from exiting tractor chassis. Out of sugarcane harvesting season, the sugarcane loader structure can be removed from existing tractor and farmer can use tractor for general work. And finally, the sugarcane loader structure must be able to withstand to lift 300 kg of sugarcane bundle on maximum lift height 5 meters from ground.

2.2 Geometry design

According to conceptual design, the sugarcane loader structure must be able to mounted on KUBOTA SUNSHINE ZL1-455 tractor. Thus, the sugarcane loader structure was designed to be 8 components as follow: front cross member, frame, right engine-frame support, left engine-frame support, right transmission-frame support, left transmission-frame support, counterbalance weight belt and counterbalance weight support, as shown in Fig. 2. Each component was connected by bolt and nut.

2.2.1 Front cross member

Front cross member is a bending steel plate which was jointed ladders each side together.

2.2.2 Frame

The frame are consist of four rectangular steel columns, two rectangular steel ladders and two upper cross member that be fixed on rear axle and lower frame support. Cross section of columns and ladders are 75x100x6 mm and 100x150x 6 mm respectively. Both side of loader arm and corresponding lift cylinders supposed to be mounted on frame.

2.2.3 Right engine-frame support

The right engine-frame support is lower support of frame which mounted to right side of the engine. This parts are fabricated as strong part to support the frame while the loader operation

2.2.4 Left engine-frame support

The left engine-frame support function is similar to right engine-frame support but the shape is not symmetry.

2.2.5 Right transmission-frame support

The right transmission-frame support is lower support of frame which mounted to right side of the transmission and also connected to counterbalance weight support at rear of frame

2.2.6 Left transmission -frame support

The left transmission-frame support function is similar to right transmission-frame support but the shape is not symmetry

2.2.7 Counterbalance weight belt

Cause of vehicle stability, the counterbalance weight was assembled to sugarcane loader. The belt was designed to mount balance weight with frame together and to make sure balance weight will not translate while loader operate in unstable farm ground

2.2.8 Counterbalance weight support

Counterbalance weight support was designed to support balance weight around 1,000 kg that mounted to left/right engine -frame supports and engine.

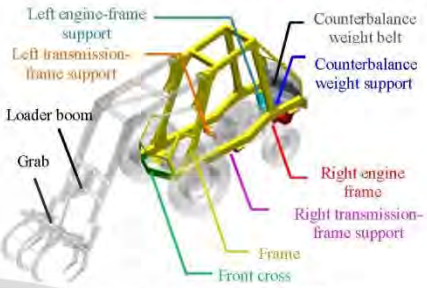

Fig. 2 Sugarcane loader parts

2.3 Static force analysis

2.3.1 Static force analysis of loader boom

Considering the free body diagrams of loader boom in Fig. 3 found that the force acting on the loader boom, occur from the grab weight, loader boom weight, sugarcane bundle weight and force acting though hydraulic cylinder (F_{BC}). The force acting though hydraulic cylinder (F_{BC}) can be calculated as follows:

$$F_{BC} = \frac{W_D d_A W_D + W_E d_A W_E}{d_A F_{BC}} \quad (1)$$

The force acting on boom arm hinge point A (F_A) can be calculated as follows:

$$A_y = F_{BC} sin\theta - W_E - W_D \quad (2)$$

$$A_x = -F_{BC} cos\theta \quad (3)$$

$$F_A = \sqrt{{A_x}^2 + {A_y}^2} \quad (4)$$

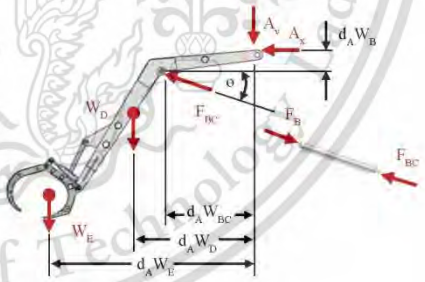

Fig. 3 Free body diagrams of loader boom

When W_E is the gravitational force acting on boom arm at C.G. of sugarcane bundle (300 kg). W_D is the gravitational force acting on the loader boom at C.G. of loader boom and grab (675 kg). d_AW_E is the perpendicular distance with W_E from hinge point A. d_AW_D is the perpendicular distance with W_D from hinge point A. d_AF_{BC} is the perpendicular distance with F_{BC} from hinge point A. A_x is the horizontal force

acting on loader boom hinge point A. A_y is the vertical force acting on boom arm hinge point A.

According to loader boom able to lift 300 kg of sugarcane bundle on maximum lift height 5 meters from ground, the horizontal force acting on loader boom hinge point A (A_x), the vertical force acting on loader boom hinge point A (A_y) and force acting though hydraulic cylinder (F_{BC}) will be depend on the angle between the hydraulics cylinder with the horizontal plane (θ) range 12.54 ° to 81.98 ° (lowest grab position to highest grab position). Therefore, it is necessary to find an angle that causes the maximum reaction force as critical condition [1]. From Fig. 4 showed that the maximum reaction force acting on loader boom hinge point A and force acting though hydraulic cylinder (F_{BC}) occur at angle 81.98 ° and value are shown below.

F_A = 56,373.15 N
A_x = -9,184.32 N
A_y = 55,619.97 N
F_{BC} = 65,828.56 N
$F_{BC,x} = F_{BC} \cos\theta$ = 9,184.32 N
$F_{BC,y} = F_{BC} \sin\theta$ = 65,373.15 N

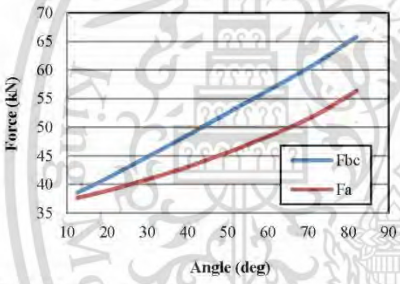

Fig. 4 Maximum reaction force acting on loader boom at various angle

2.3.2 Static force analysis of sugarcane loader structure

Considering the free body diagrams of sugarcane loader structure as shown in Fig. 5 found that the force acting on the sugarcane loader structure hinge point A (F_A) and force acting though hydraulic cylinder (F_{BC}) can be calculated as follows step 2.3.1 but the direction is opposite. Thus, the maximum reaction force acting on sugarcane loader structure are shown below.

A_x = - 9,184.32 N
A_y = 55,619.97 N
$F_{BC,x}$ = 9,184.32 N
$F_{BC,y}$ = 65,373.15 N

2.4 Finite Element Analysis

From static force analysis in step 2.3.2 found that the reaction force acting on structure is maximum when the grab was lift to maximum highest position. Therefore the strength of sugarcane loader structure will analyze follow the critical condition. In this work the material of sugarcane loader structure is ductile material, so the design of all parts should be on the basis of Von misses stress yield criterion as Eq. 1. The Von misses stress acting on parts must be less than the ratio of yield strength of material and safety factors [2]. If the result is not as following, the designed parts were failure and should redesign until those condition were passed. In this case the safety factor is 3. [3]

$$\sigma_{von} \leq \frac{S_y}{S.F.} \quad (5)$$

When σ_{von} is von mises stress, S_y is yield strength of material. S.F. is safety factor.

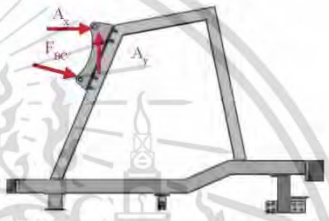

Fig. 5 Free body diagrams of sugarcane loader structure

2.4.1 Computer model

The sugarcane loader structure model are consist of 11 components as follow: front cross member, frame, Solid beam, right plate, left plate, right engine-frame support, left engine-frame support, right transmission-frame support, left transmission-frame support, counterbalance weight belt and counterbalance weight support. In order to provide the most realistic simulation, solid beam was added to serve as rear axle which used to be front support of frame as shown in Fig. 6 Side of solid beam will be fix support face in constraint condition. Furthermore, in order to avoid stress singularities which cause for divergent simulation result, the location of sharp corner and welding joint of structure was represented with fillet feature. [4]

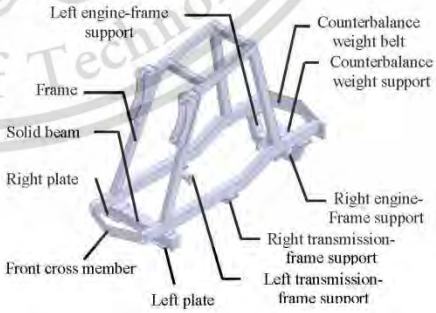

Fig. 6 3D model of sugarcane loader structure

2.4.2 Meshing & element

The sizes of element used in this analysis are varied depending on the positions of elements. For the elements located at the bolt support, hinged support and sharp corner, the smallest size of element is set to be 2 mm. The element type used is tetrahedral 3D solid element. Number of nodes is 998,253 nodes and Number of elements is 542,321, as shown in Fig. 7

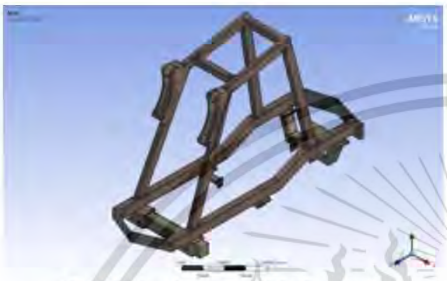

Fig. 7 Finite element model of structure

2.4.3 Contact conditions

In this work, frictional contact type defined as a contact surface which are allowed to slide with friction coefficient 0.78 (steel on steel) [5] and can open-close. This behavior is like two surfaces sliding against each other. In addition to beam connection feature was used to simulate the fasteners [6] and for more detail shown in table

Table. 1 Contact condition of finite element model

Part No. 1	Part No. 2	Contact type no.1	Contact type no.2
Frame	Front cross member	Frictional (μ = 0.74)	Beam connection (body to body)
	Counter balance weight belt	Frictional (μ = 0.74)	Beam connection (body to body)
	Left Plate	-	Beam connection (body to body)
	Right Plate	-	Beam connection (body to body)
	Rigid	Frictional (μ = 0.74)	-
	Right transmission - frame support	Frictional (μ = 0.74)	Beam connection (body to body)
	Left transmission - frame support	Frictional (μ = 0.74)	Beam connection (body to body)
	Right engine - frame support	Frictional (μ = 0.74)	Beam connection (body to body)
	Left engine - frame support	Frictional (μ = 0.74)	Beam connection (body to body)
Solid beam	Left Plate	Frictional (μ = 0.74)	-
	Right Plate	Frictional (μ = 0.74)	-
Right transmission–frame support	-	-	Beam connection (body to ground)
Left transmission - frame support	-	-	Beam connection (body to ground)
Right engine-frame support	-	-	Beam connection (body to ground)
Left engine-frame support	-	-	Beam connection (body to ground)
Counter balance weight support	Right engine - frame support	Frictional (μ = 0.74)	Beam connection (body to body)
	Left engine - frame support	Frictional (μ = 0.74)	Beam connection (body to body)
	-	-	Beam connection (body to ground)

2.4.4 Boundary conditions

The sugarcane loader structure was acted by 4 loads. First is the weight of body and accessories parts which act along the longitudinal of frame. The total weight of body and accessories parts is 100 kg. Second is the counter balance weight 1,100 kg which act on counter balance weight belt. The weight of body, accessories parts and counter balance weight was represented by point mass feature of ANSYS software. Third is the maximum force acting on the hinge point A (F_A) and maximum force acting though hydraulic cylinder (F_{BC}). From static force analysis of sugarcane loader structure in step 2.3.2., the value is 55,373 N and 65,829 N respectively. Finally is Standard Earth Gravity, 9.81 m/s^2 in vertical direction. Moreover, the fixed support was applied on both side face of solid beam that no translation in x, y, z direction and no rotation around x, y, z axis, Fig. 8

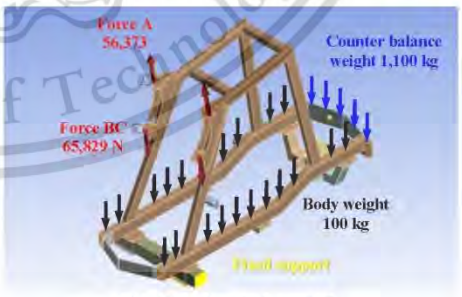

Fig. 8 loading and support

2.4.5 Material properties

The material was refer to SS400 steel with linear elastic behavior. Density is 7,850(kg/m^3). Poisson's ratio is 0.29 and yield strength is 250 MPa.

3. Result & Discussion

3.1 Result of front cross member

Fig. 9 shows the Von Misses stress of the front cross member. The maximum Von Misses stress is 3.27 MPa that is acting at inner of mounting hole and the minimum Von Misses stress is 0.015 MPa that is acting at outer of mounting hole.

Consider the Von misses stress yield criterion, Eq. (5) found that the maximum Von Misses stress (σ_{von}= 3.27 MPa) is lower than the yield strength of ss400 steel by taking safety factor (S_y/S.F. = 250/3 = 83.33 MPa), this clearly indicates, $\sigma_{von} < S_y/S.F$, therefore the design of the front cross member is safe.

Fig. 10 shows the displacement of the front cross member. The maximum displacement occurs at the side fold as 0.057 mm which is lower than the minimum thickness of plate used in the front cross member. Therefore, the design of the front cross member is safe under applied static load. [7]

Fig. 9 Stress of front cross member

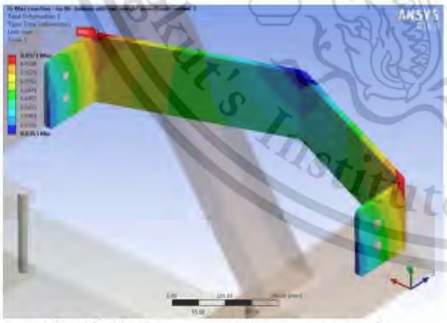

Fig. 10 Displacement of front cross member

3.2 Result of frame

Fig.11 shows the Von Misses stress of the frame. The maximum Von Misses stress is 249.92 MPa that is acting at the hydraulic cylinder mounting lug and the minimum Von Misses stress is 0.027 MPa that is acting at the lower frame.

Consider the Von misses stress yield criterion, Eq. (5) found that the maximum Von Misses stress on frame (σ_{von}= 249.92 MPa) is higher than the yield strength of ss400 steel by taking safety factor (S_y/S.F. = 250/3 = 83.33 MPa), this clearly indicates, $\sigma_{von} > S_y/S.F$, therefore the design of the frame is unsafe. The frame should be redesign to improve strength.

Fig.12 shows the displacement of the frame. The maximum displacement occurs at the hydraulic cylinder mounting lug as 0.661 mm.

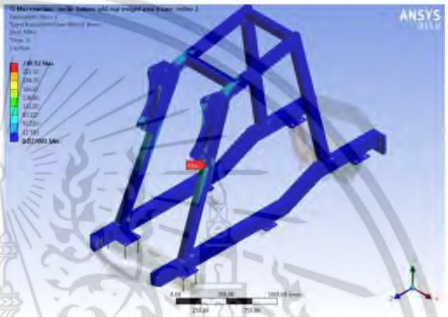

Fig. 11 Stress of frame

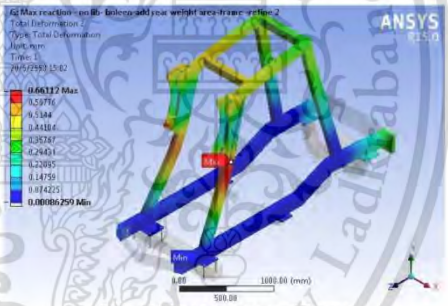

Fig. 12 Displacement of frame

3.3 Result of right transmission-frame support

Fig. 13 shows the Von Misses stress of the right transmission-frame support. The maximum Von Misses stress is 16.66 MPa that is acting at the welding joint of lower flange and the minimum Von Misses stress is 0.011 MPa that is acting at the rim of upper flange.

Consider the Von misses stress yield criterion, Eq. (5) found that the maximum Von Misses stress (σ_{von}= 16.66 MPa) is lower than the yield strength of ss400 steel by taking safety factor (S_y/S.F. = 250/3 = 83.33 MPa), this clearly indicates, $\sigma_{von} < S_y/S.F$, therefore the design of the right transmission-frame support is safe.

Fig. 14 shows the displacement of the right transmission-frame support. The maximum

displacement occurs at the rim of upper flange as 0.028 mm which is lower than the minimum thickness of plate used in the right transmission-frame support. Therefore, the design of the right transmission-frame support is safe under applied static load.

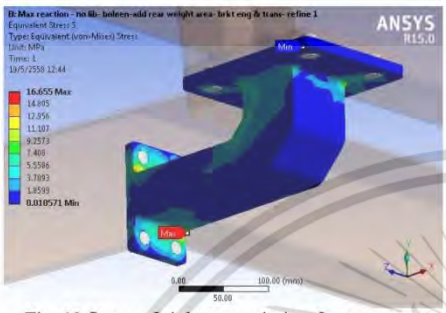

Fig. 13 Stress of right transmission-frame support

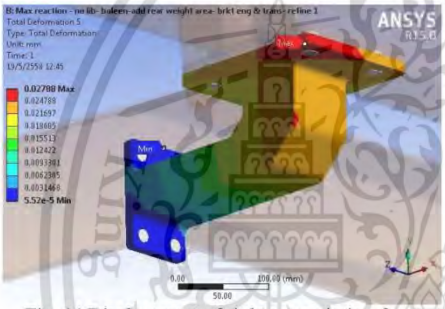

Fig. 14 Displacement of right transmission-frame support

3.4 Result of left transmission-frame support

Fig. 15 shows the Von Misses stress of counterbalance weight belt left transmission-frame support. The maximum Von Misses stress is 17.91 MPa that is acting at the welding joint of lower flange and the minimum Von Misses stress is 0.006 MPa that is acting at the rim of upper flange.

Consider the Von misses stress yield criterion. Eq. (5) found that the maximum Von Misses stress (σ_{von}= 17.91 MPa) is lower than the yield strength of ss400 steel by taking safety factor (S_y/S.F. = 250/3 = 83.33 MPa), this clearly indicates, $\sigma_{von} < S_y/S.F$, therefore the design of the left transmission-frame support is safe.

Fig. 16 shows the displacement of the left transmission-frame support. The maximum displacement occurs at the rim of upper flange as 0.026 mm which is lower than the minimum thickness of plate used in the left transmission-frame support. Therefore, the left transmission-frame support is safe under applied static load.

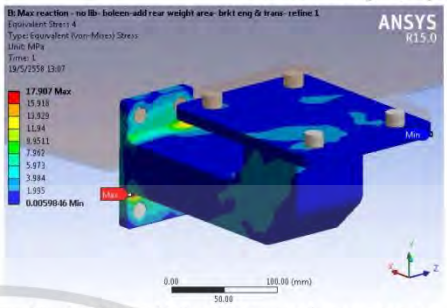

Fig. 15 Stress of left transmission-frame support

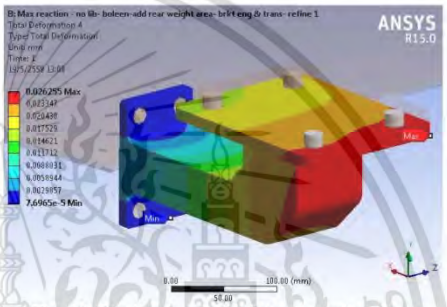

Fig. 16 Displacement of left transmission-frame support

3.5 Result of right engine-frame support

Fig. 17 shows the Von Misses stress of right engine-frame support. The maximum Von Misses stress is 69.90 MPa that is acting at the welding joint of lower flange and the minimum Von Misses stress is 0.009 MPa that is acting at the rim upper flange.

Consider the Von misses stress yield criterion, Eq. (5) found that the maximum Von Misses stress (σ_{von}= 69.90 MPa) is lower than the yield strength of ss400 steel by taking safety factor (S_y/S.F. = 250/3 = 83.33 MPa), this clearly indicates, $\sigma_{von} < S_y/S.F$, therefore the design of the right engine-frame support is safe.

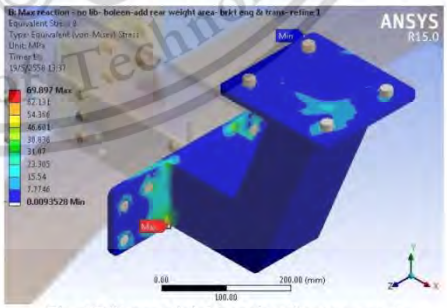

Fig. 17 Stress of right engine-frame support

Fig. 18 shows the displacement of the right engine-frame support. The maximum displacement occurs at the rim of upper flange as 0.266 mm which is lower than the minimum thickness of plate used in the right engine-frame support. Therefore, the design of the right engine-frame support is safe under applied static load.

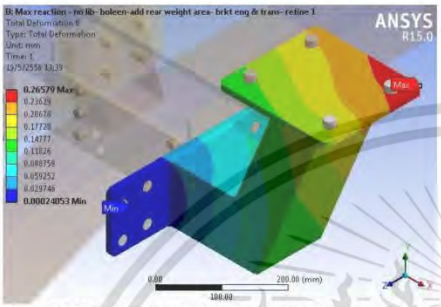

Fig. 18 Displacement of right engine-frame support

3.6 Result of left engine-frame support

Fig. 19 shows the Von Misses stress of the left engine-frame support. The maximum Von Misses stress is 84.86 MPa that is acting at the welding joint of lower flange and the minimum Von Misses stress is 0.008 MPa that is acting at the corner of L-shape.

Consider the Von misses stress yield criterion, Eq. (5) found that the maximum Von Misses stress (σ_{von} = 84.86 MPa) is almost equal to the yield strength of ss400 steel by taking safety factor (S_y/S.F. = 250/3 = 83.33 MPa), this clearly indicates, $\sigma_{von} < S_y/S.F.$, therefore the design of the left engine-frame support is safe.

Fig. 20 shows the displacement of the left engine-frame support. The maximum displacement occurs at the rim of upper flange as 0.196 mm which is lower than the minimum thickness of plate used in the left engine-frame support. Therefore, the design of the left engine-frame support is safe under applied static load.

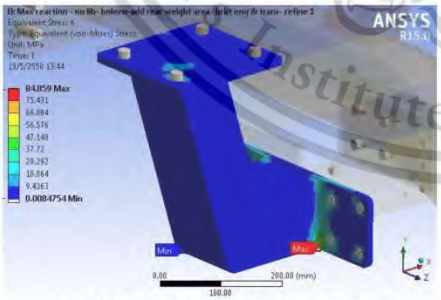

Fig. 19 Stress of left engine-frame support

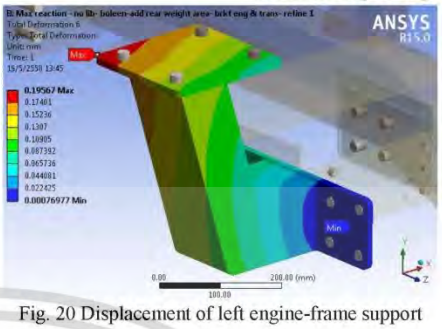

Fig. 20 Displacement of left engine-frame support

3.7 Result of counterbalance weight belt

Fig. 21 shows the Von Misses stress of the counterbalance weight belt. The maximum Von Misses stress is 41.35 MPa that is acting at the inner of mounting hole and the minimum Von Misses stress is 0.008 MPa that is acting at the outer of mounting hole.

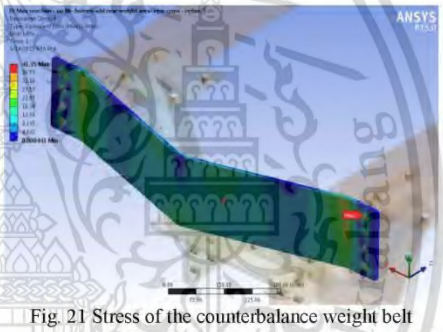

Fig. 21 Stress of the counterbalance weight belt

Consider the Von misses stress yield criterion, Eq. (5) found that the maximum Von Misses stress (σ_{von}= 41.35 MPa) is lower than the yield strength of ss400 steel by taking safety factor (S_y/S.F. = 250/3 = 83.33 MPa), this clearly indicates, $\sigma_{von} < S_y/S.F.$, therefore the design of the counterbalance weight belt is safe.

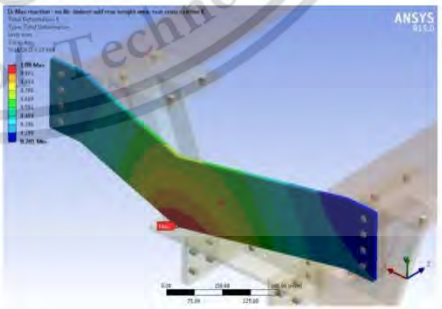

Fig. 22 Displacement of the counterbalance weight belt

Fig. 22 shows the displacement of the counterbalance weight belt. The maximum displacement occurs at the middle fold as 1.079 mm which is lower than the minimum thickness of plate used in the counterbalance weight belt. Therefore, the design of the counterbalance weight belt is safe under applied static load.

3.8 Result of counterbalance weight support

Fig. 23 shows the Von Misses stress of the counterbalance weight support. The maximum Von Misses stress is 68.86 MPa that is acting at welding joint of right plate and the minimum Von Misses stress is 0.008 MPa that is acting nearly the welding joint of left plate.

Consider the Von misses stress yield criterion, Eq. (5) found that the maximum Von Misses (σ_{von}= 41.35 MPa) is lower than the yield strength of ss400 steel by taking safety factor (S_y/S.F. = 250/3 = 83.33 MPa), this clearly indicates, $\sigma_{von} < S_y/S.F$, therefore the design of the counterbalance weight support is safe.

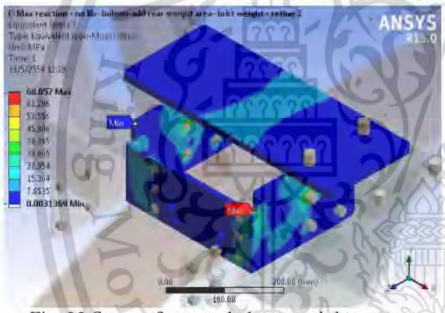

Fig. 23 Stress of counterbalance weight support

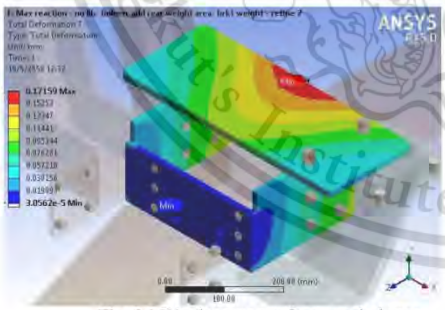

Fig. 24 Displacement of counterbalance weight support

Fig. 24 shows the displacement of the counterbalance weight support. The maximum displacement occurs at the rim of uppermost plate as 0.172 mm which is lower than the minimum thickness of plate used in the counterbalance weight belt. Therefore, the design of the counterbalance weight belt is safe under applied static load.

4. Conclusion

The finite element method was employed to analysis strength of the sugarcane loader structure in the maximum hydraulic force acting on the structure condition which will occur when the grab operate in the maximum highest position, 5meter from ground. The maximum stress of front cross member, frame, right transmission-frame support, left transmission-frame support, right engine-frame support, left engine-frame support, counterbalance weight belt and counterbalance weight support were 3.27 MPa,, 249.92 MPA, 16.66 MPa, 17.91 MPa,69.90 MPa, 84.86 MPa, 41.25 MPa and 68.86 MPa respectively. It clearly show that the parts of sugarcane loader structure are not failure under safety factor is 3, except the frame**.** Therefore, the frame should to redesign and improve the strength by the cross section increasing or shape changing. For the strength improvement of structural will be perform in the future work.

5. Acknowledgement

The author would like to specially thank Tang Sia Ping Metal Works Co., Ltd for financial and facility support and also thank to King Mongkut's Institute of Technology Ladkrabang and National Science and Technology Development, Thailand for scholarship providing.

6. References

[1] Bhaveshkumar P Patel and Prajapati J M (2012). "Evaluation of Bucket Capacity, Digging Force Calculations and Static Force Analysis of Mini Hydraulic Backhoe Excavator", *Machine Design—The Journal of Faculty of Technical Sciences*, Vol. 4, No. 1, pp. 59-66.

[2] Tirupathi R Chandrupatla and Ashok G Belegundu (2005). "Introduction to Finite Elements in Engineering". Pearson Education Publication India Branch, Delhi, India.

[3] Burr, A and Cheatham, J; Mechanical Design and Analysis, 2nd edition, section 5.2. Prentice-Hall, 1995

[4] Andy (2010), Stress singularities, URL: https://andrewcib.wordpress.com/2010/12/14/stress-singularities/ on 14/12/2010

[5] Engineer's handbook, Coefficient of Friction, URL:http://www.engineershandbook.com/Tables/frictioncoefficients.

[6] (2012) Joints, Springs and Beams, Introduction to ANSYS Mechanical Part 2, ANSYS, Inc.

[7] Bhaveshkumar P Patel1 and J M Prajapati (2012), Static analysis of mini hydraulic backhoe excavator attachment using FEA approach, *International Journal of Mechanical Engineering and Robotics Research*, Vol. 1, No. 3, October 2012, pp. 163-175.

AUTHOR BIOGRAPHY

Author:	Mr. Kantapit Meetam
Degree:	Master of Engineering
Date of Graduation:	6th June 2017
Date of Birth:	2th February 1990
Place of Birth:	Trang, Thailand

Undergraduate and Graduate Education:

Master of Engineering in Automotive Engineering,
King Mongkut's Institute of Technology Ladkrabang, Bangkok, 2016

Bachelor degree in Mechanical Engineering,
Prince of Songkla University, Songkhla, 2011

Presentations and Publications:

[1] Kantapit Meetam, Preechar Karin, Chi-na Benyajati, Masaaki Okuma and Thanapol Luckanawat, "Design and Development of Sugarcane Loader Frame Structure", 2015, The 6th TSME International Conference on Mechanical Engineering, December 16-18, 2015, The Regent Cha-Am Beach Resort, Phetchaburi, Thailand.